Universität der Bundeswehr München
Fakultät für Elektrotechnik und Informationstechnik
Institut für Hoch- und Höchstfrequenztechnik

Combined Switched and Phase Aligned Multi-Antenna Diversity System for Signal-Error-Reduction in Mobile Receiving Systems

Raed S. Shatara

Vollständiger Abdruck der von der Fakultät für Elektrotechnik und Informationstechnik der Universität der Bundeswehr München zur Erlangung des akademischen Grades eines

Doktor-Ingenieurs
(Dr.-Ing.)

vorgelegte Dissertation

ACKNOWLEDGMENTS

I would like to thank my Professor Dr.-Ing. habil. Heinz Lindenmeier for giving me the opportunity to pursue my Ph.D. at the University of the Bundeswehr Munich, Germany. I can not thank him enough for his technical guidance and consistent support during the past three years.

I am particularly indebted to my mentor and colleague Jeffrey Marrah for his valuable support. Thank you Jeffrey for your continuous support. I also want to thank all my colleagues working in his elite group at Delphi Delco Electronics Systems for their contributions.

Special recognition is hereby expressed to PD Dr.-Ing. habil. L. Reiter for his valuable assistance and contribution. I also want to thank Apl. Prof. Dr.-Ing. habil. J. Hopf for his help and comments. Credit must also be given to my colleague Dipl-Ing. Gunther Bauer, not only technically but also on a personal level, especially when I first moved to Germany. Thank you Gunther for everything. Appreciation is owed to my other colleagues at the institute.

I want to acknowledge those people who supported my Ph.D. studies abroad. They are: Jeffrey Marrah, Jeffery Jones, Bob Schumacher, Nancy Hartley, Bruce Parkinson, George Selibas, and the rest of Delphi Delco Electronics Systems employees. Thank you for awarding me the Delphi Fellowship that made this research possible.

Thank you Oliver, Markus, and Bernd, my colleagues from the mechanical lab, for building all kinds of sophisticated mechanical units for my hardware and taking pictures. Thank you Ashraf Ramadan for all the technical discussions that we had.

Thank you Rania for your patience, understanding, and support.

Section 2.1 is dedicated to Richard Kennedy who gave me a deep insight into the PAS system. God bless his soul.

Contents

Thesis Summary

Mobile communication is a very broad and exciting field. Nature makes it more difficult for radio engineers to receive mobile radio frequency (RF) signals. The RF signals can experience many obstacles (or interferences) and travel through harsh environment before they arrive at the mobile antenna. Some of these interferences are multi-path interference, co-channel or/and adjacent channel interference, and man made noise. Multi-path means that the mobile antenna receives the RF waves from multiple paths. The various paths are due to obstacles (like buildings, rough terrains, and mountains) that lead to reflection, scattering, and diffraction. The signal combining can be constructive or destructive. During destructive combining, the signal envelope (or amplitude) can experience fades of $30dB$ or more.
For FM mobile communications, the multi-path interference is divided into two categories, short and long delay multi-path. Short delay multi-path is concerned with the rapid fluctuation of the amplitude of the RF signal, where the time delay of the reflected signal is usually less than $5\mu sec$. Short delay multi-path is modelled by Rayleigh distribution. Long delay multi-path is when the reflected signal time delay is greater than $5\mu sec$. In this case, we have to include the FM modulation and the output of the FM detector when analyzing long delayed signals.
FM adjacent channel interference is more severe in the countries that have tight channel separation (i.e. $100kHz$). This phenomenon occurs when some of the spectrum of a strong channel falls within the desired channel, which causes severe audible distortions.
Diversity reception is one method to reduce interference. There are many types of diversity techniques: Space diversity, Polarization diversity, Angle diversity, Frequency diversity, and Time diversity. Space diversity is the one widely used for FM mobile communications because it is simple to implement and does not require additional frequency spectrum [23]. Many papers [2]$-$[5] have been written about diversity reception in the past years in the area of mobile communications to reduce distortions. There are three main systems that were compared by Brennan[5]: scanning diversity, equal gain combiner and maximal ratio combiners.
Scanning diversity is simple to implement and requires no extra receivers. Usually with scanning diversity systems, the selection is based upon the signal level. But the scanning diversity system that was developed at the Bundeswehr university selects the least distorted antenna among N antennas. Equal gain and maximal ratio are combining diversity techniques and they are harder to implement because they require multiple receivers.

In the following pages, a short overview of the thesis is given. Chapter 1 reviews the multi-path transmission phenomenon. Section 1.1 describes the envelope amplitude fluctuations that are modelled by Rayleigh fading distribution. A typical Rayleigh faded signal is shown in Figure 1 where the car is moving in the x-direction. The fast amplitude variations of the signal are evident.

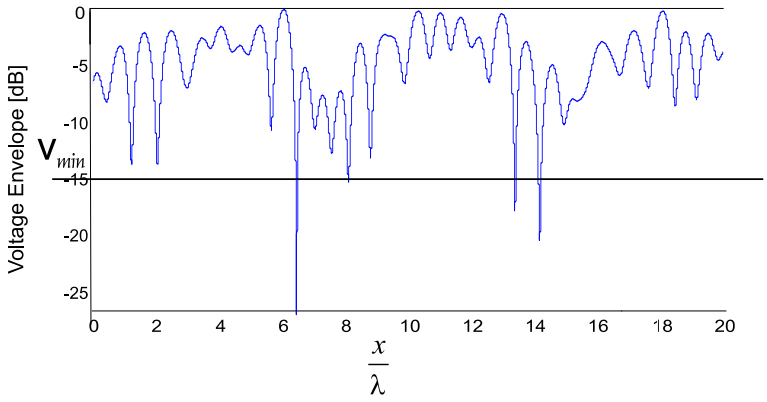

Figure 1: Typical signal Rayleigh fading as the Car moves in the x-direction

Section 1.2.1 (time delay $\tau < 5\mu sec$) describes short delay multi-path and derives Equation 1.6, it is the sum of all incident waves at the mobile antenna, which yields Rayleigh fading field. It also considers the antenna gain pattern. The Doppler frequencies are then calculated by taking the derivative of the phase of the Rayleigh faded antenna signal. Such Doppler frequencies are shown in Figure 2 where the average Doppler frequency for a car moving with a speed of $100km/hr$ is in the range of $9Hz$. The calculation of Doppler frequency is important because we refer to it when analyzing the control loop of a Phasing Antenna System that is described in chapter 2.

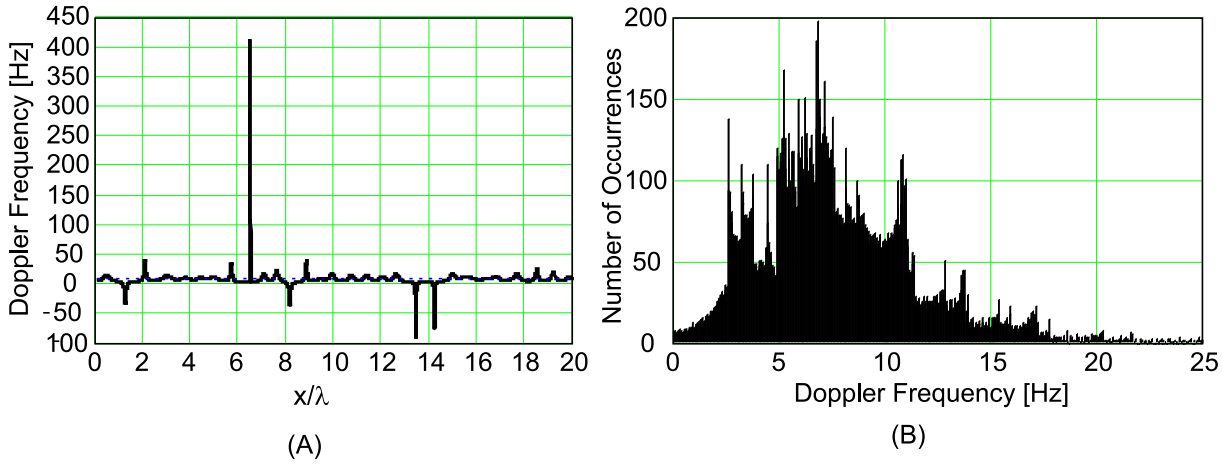

Figure 2: (A) Resulting Doppler frequencies (B) Histogram of the resulting Doppler frequencies

Two signals long delay ($\tau > 5\mu sec$) multi-path model is described in section 1.2.2. The distortion factor, Equation 1.27, is used throughout this thesis for distortion factor calculations. The model displays the affect of long delay on the output signal of an FM demodulator. The output of an ideal FM demodulator, Equation 1.14, has been derived as a function of time delay τ and amplitude ratio $\frac{A_1}{A_o}$ of the two signals. Long delayed signals produce erroneous frequencies that result in evident distortion peaks in the demodulated signal as shown in Figure 3. f_d is the FM frequency deviation and f_m is the modulation frequency. The calculated distortion factor for the signal in Figure 3 is equal to 26.25% with no filtering and 12% with $15kHz$ ideal low-pass filter. This is a severe audible distortion which is not acceptable by HiFi standards.

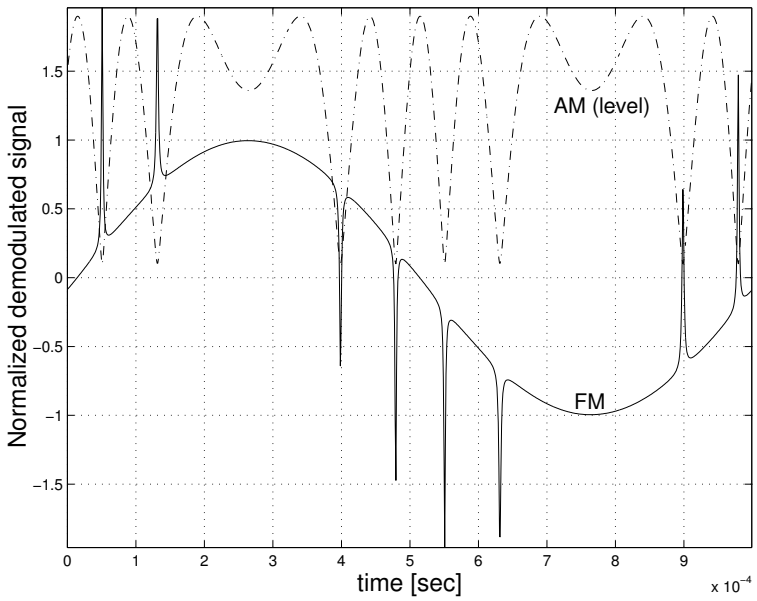

Figure 3: Demodulated FM signal with $A_0 = 1$, $A_1 = 0.9$, $f_m = 1kHz$,$f_d = 75kHz$, $K_D = 1\frac{V}{Hz}$, $\tau_1 = 30\mu sec$

To show the range of the resulting distortions as a function of time delay τ and amplitude ratio $\frac{A_1}{A_o}$ so that we have an idea of the severe effect on the demodulated signals, a three dimensional diagram of the distortions is shown in Figure 4.

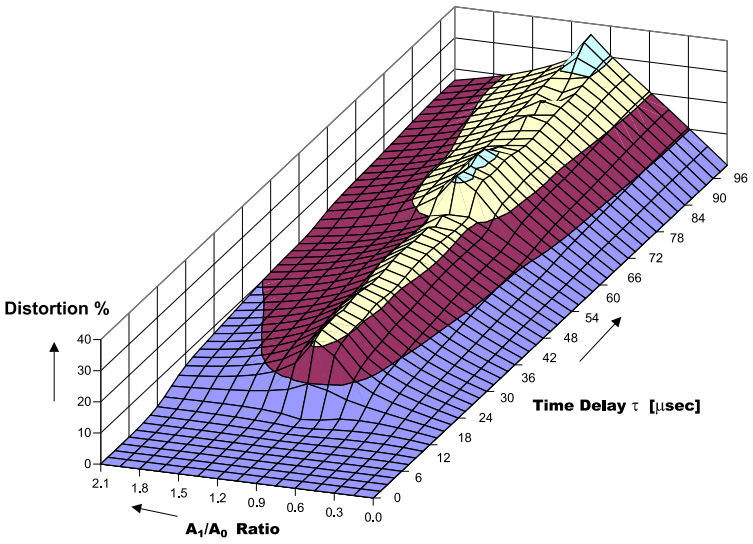

Figure 4: Distortion due to different $\frac{A_1}{A_0}$ ratios and delay times with $f_d = 25kHz$, $f_m = 1kHz$

Chapter 2 describes and analyzes two current diversity systems that are used in modern vehicles. First (Section 2.1), the Phase Alignment System (PAS) is described. It is a two antennas combining system. The antennas are printed for example on the vehicle glass. PAS basic functionality is to automatically adjust the electrical phases of the signals received by the two antennas so that they are combined co-phased. Second, Switching Diversity System (SAS) operates with a very fast distortion detector that selects the least distorted available antenna.

The key idea of the PAS is amplitude modulate (AM) antenna B with ω_r dither signal then added to signal A. When the two antenna signals are not in phase as shown in Figure 2.2(a) (signal B leading signal A), the resulting AM will produce positive phase modulation (PM) at the sum, to which the FM receiver will respond by producing a demodulated output at ω_r proportional to the phase between the two antenna signals A and B. Figure 2.2(b) shows that when signal B lags signal A, the phase modulation produced at the receiver is inverted 180 degrees, as is the demodulated output. To align the two signals in phase we must minimize the resultant phase modulation by minimizing the demodulated signal that is produced by the FM receiver. Figure 2.2(c) shows the two antenna signals are aligned and no resulting phase modulation occurs. An example of a PAS system is shown in Figure 2.5.
The PAS multi-path performance is analyzed in section 2.1.4. The PAS system is designed to combat slow fading signal field (Rayleigh fading). In case of long delay multi-path, if one of the antennas is distorted as the signal shown in Figure 3, the PAS adds the distorted antenna signal to the undistorted antenna signal without any knowledge of the antennas signal conditions. Therefore, the system needs a fast distortion detector so that the PAS knows when and whether to add both antenna signals at a given time. This is the main motivation to implement a new and more sophisticated FM diversity system that can handle both short and long delay multi-path. This thesis suggests a new diversity system called **Scanning Phasing Antenna System (SPAS)** which is a combination of a scanning system and two antenna co-phase combining system. The basic operation of the SPAS is to select, at any instant, the two least distorted out of four antennas for the PAS to combine them in phase.
Section 2.2 provides a short description of the Switched Antenna System (SAS) or Fast Distortion Detector (FDD) [25]. The FDD basically detects, within $20-30\mu sec$, such peaks shown in Figure 3 and searches for the least distorted antenna signal.

Diversity systems performance is evaluated by diversity effectiveness **n** [25]. It is a computation method that provides performance information for a specific diversity system when compared to single antenna performance in the car. Diversity effectiveness **n** is defined as the number of effective uncorrelated antennas for scanning diversity systems. Diversity effectiveness **n** is given by

$$\mathbf{n} = \frac{q_d}{q_s} \tag{1}$$

where $q = 20\log(\frac{1}{P})$ $[dB]$ is defined as the signal quality and P represents the probability of signal-to-distortion ratio not to exceed a certain threshold level in an FM channel. For diversity mode $P_d = P_s^n$ is valid, where subscript d denotes diversity mode and s single antenna mode. Although we compute **n** to evaluate the performance of a selection diversity system at a certain value of P_s, it has been proven by [30] that **n** is independent from P_s. The correlation between the antenna signals results in the fact that **n** is no longer an integer number being found in the area of observation. It has also been shown by [30] that $P_d = P_s^n$ can be used to evaluate the performance of other diversity schemes such as Scanning Phasing Antenna System (SPAS). The diversity effectiveness **n** for the three diversity systems of PAS, SAS, and SPAS were computed in section 3.3.
Automotive technologies of antenna diversity schemes require all antennas to be on one window to reduce cost and warranty claims, and improve styling. Therefore, **n** is computed for the diversity systems under evaluation with all the antennas being placed in one window (see Figure 3.4). The antennas are loaded each either with a standard 50Ω impedance which means that the reflection coefficient Γ is 0, or a high impedance load which indicates that $\Gamma = 1$.

Significant results of diversity effectiveness **n** computation for SPAS, SAS, and PAS are shown in Figure 5 for reflection coefficient $\Gamma = 0$ (50Ω system). It can be seen that the

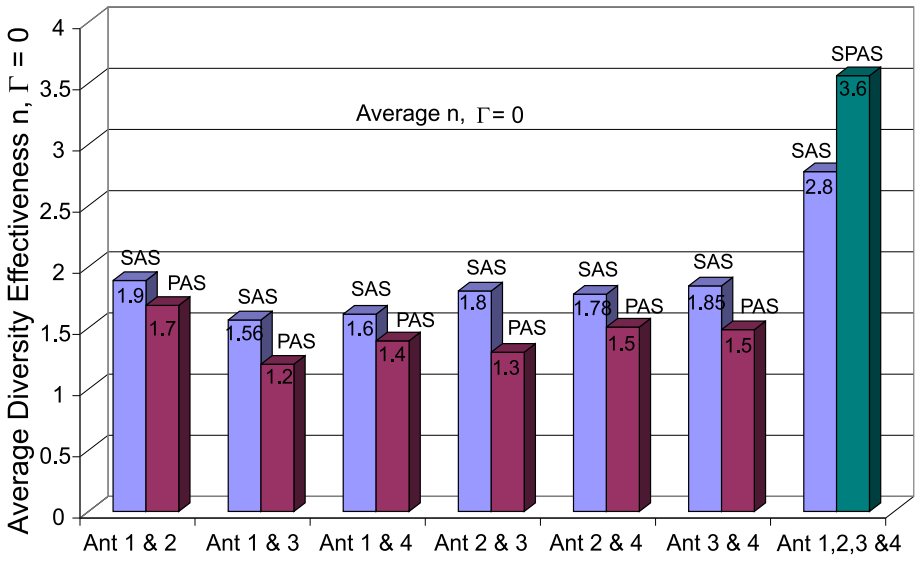

Figure 5: Average **n** for SAS, PAS, and SPAS with $\Gamma = 0$ for all antenna combinations

resulting **n** for 4-antennas SPAS is the highest. It is 0.8 uncorrelated antenna higher than 4-antennas SAS and almost 2 uncorrelated antennas higher than 2-antennas PAS or SAS. The resulting **n** justifies the implementation of the SPAS system.

An example of SPAS hardware and software implementation is described in Chapter 4. The basic operation block diagram of the system is shown in Figure 6. The SPAS consists of two

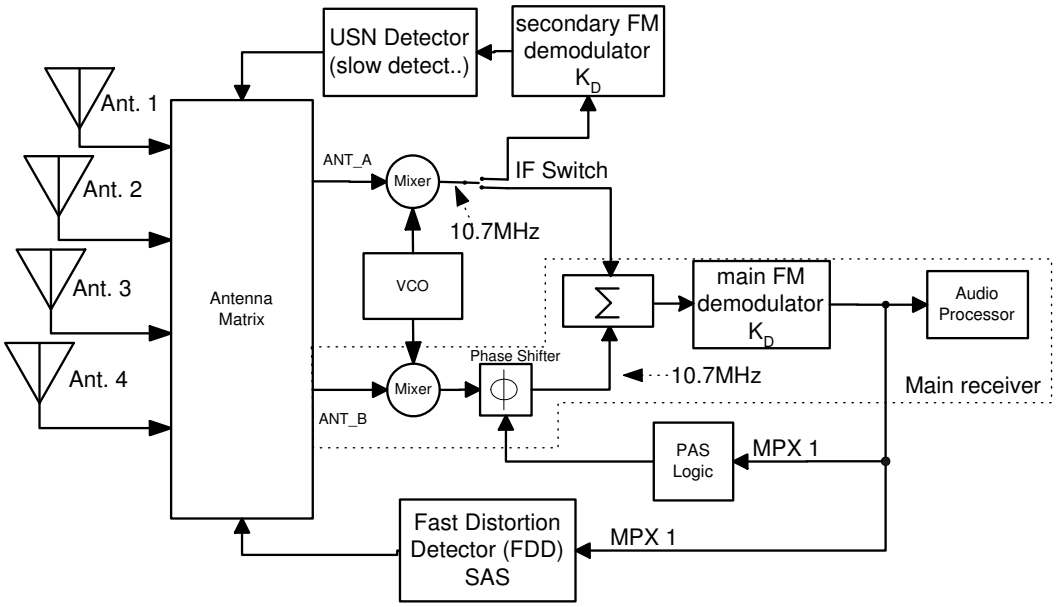

Figure 6: SPAS Simplified Block Diagram

FM tuners (receivers) with one voltage controlled oscillator (VCO) reference, PAS system, SAS system, slow distortion detector called Ultrasonic Noise Detector (USN), and antenna matrix.

The main tuner's FM demodulator output feeds the PAS logic and the SAS blocks. The Intermediate Frequency (IF) switch is connected to the lower part when the system operates in PAS mode. When it is connected to the upper part, the system is merely in USN mode. The antenna matrix has a power splitter for each antenna input signal to be able to provide two isolated paths that are needed for the distortion detectors. There are three modes of operation, USN mode, SAS mode, and PAS mode. They are summarized in the chart that is shown in Figure 7.

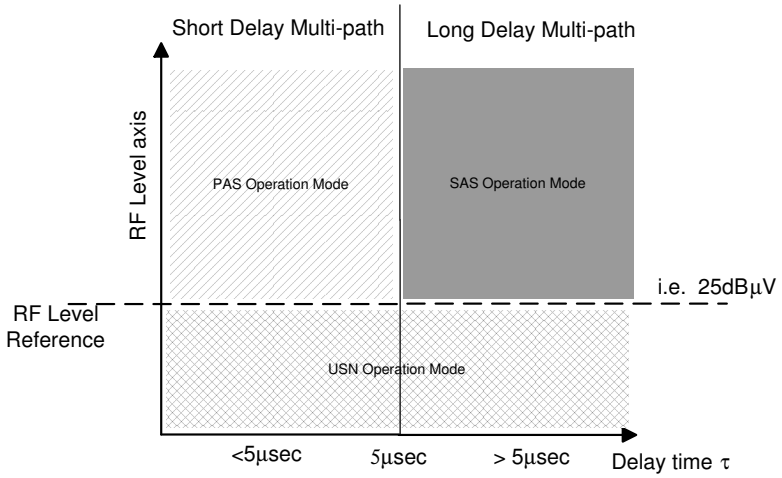

Figure 7: SPAS Modes of Operation

The RF level reference is derived from the main tuner that is connected to ANT_B. It represents the magnitude of the RF input signal. When the RF level is below the reference, the system is merely in USN mode. The main purpose of this mode is to determine by the USN detector the least distorted antenna. The mechanism to do this is described in section 4.12. The USN detector builds a priority list (with the help of a microprocessor) of the antenna distortions. The antenna that has the least USN DC voltage is considered the least distorted.
When the RF level is above the reference, the system can be either in SAS mode or PAS mode, depending on signal conditions. In case of short delay multi-path, the system initially switches from USN mode to SAS mode. When SAS stops on one antenna, considered the least distorted antenna, the USN detector determines the second best antenna before the system goes to PAS mode. In PAS mode, the two antennas are co-phased and the system stays in this mode until SAS detects distortion at the output of the main FM demodulator. Then the system goes back to SAS mode. The USN determines whether the system is in long delay multi-path area (or/and a strong adjacent channel is present) or short delay multi-path. This is explained in detail along with USN measurements in section 4.3.

The need to test FM diversity systems in the lab with captured data from the field is the main motivation for the development of the system described in Chapter 5. Diversity Testing System (DTS) has been developed and realized in this dissertation. It can test up to 4-antenna FM diversity systems. The basic block diagram of the DTS system is shown in Figure 8. The DTS consists of a receiver unit, computer recording/playing unit, and re-modulation unit.

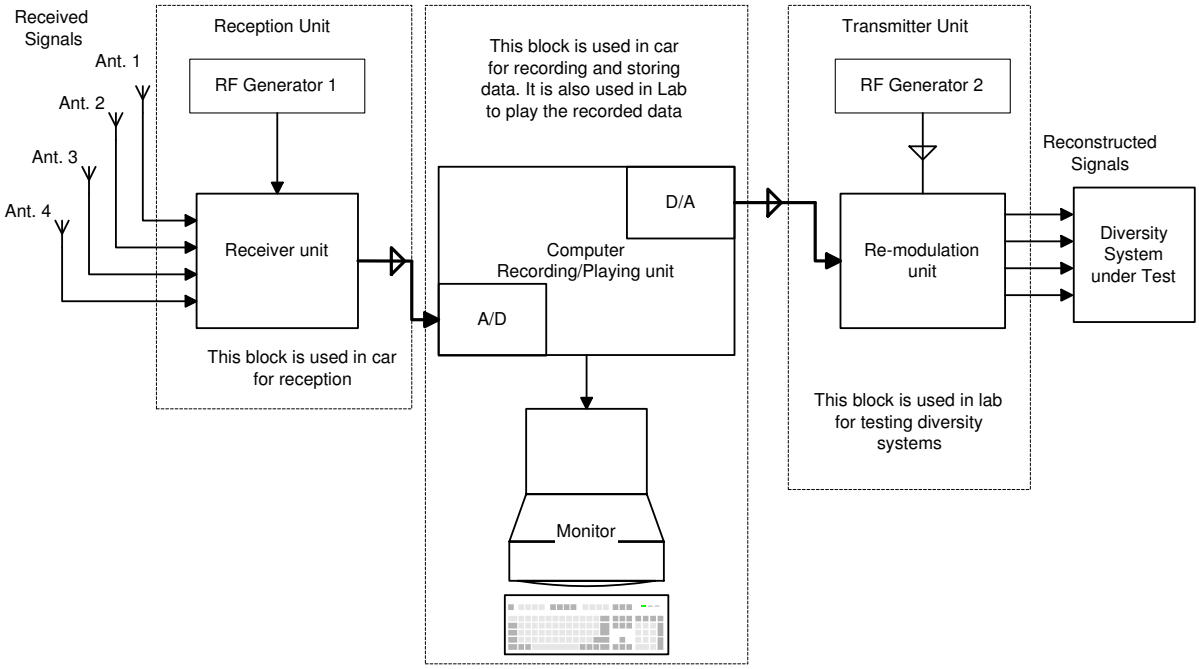

Figure 8: Diversity Testing System (DTS)

The DTS consists of four FM receivers that are synchronized to the same VCO to capture and record the FM signals in the car. The signals are captured by the receiver unit before they are divided to In-phase (I) and Quadrature (Q) components via I/Q demodulators. The I/Q FM baseband signals are digitized via Analog-to-digital (ADC) cards in the computer unit before they are saved on the hard drive. The computer recording/playing unit reproduces the captured I/Q data via Digital-to-analog (DAC) cards and passes it on to the re-modulation unit. The re-modulation unit reproduces the RF antenna signals via four I/Q modulators for the system under test in the lab. The system is capable of capturing Rayleigh faded signals that have maximum fades of $50dB$.
Chapter 5 describes in detail hardware implementation of DTS. The DTS software implementation [35] is not the scope of this thesis.

Finally, the reader may refer to Appendix A for the acronyms used throughout the thesis. Appendix B contains some important variable definitions. Derivation of the effects of the I/Q modulator offsets on the distortion output of an ideal FM demodulator are shown in Appendix C. This information is needed when building the hardware that is described in Chapter 5. Appendix D presents the signal-to-noise measurement of DTS. The DTS has approximately $60dB$ signal-to-noise ratio with $1kHz$ modulation signal and $25kHz$ frequency deviation. The broadcast stations in Europe usually have signal-to-noise ratio of $65dB$. The last Appendix, appendix E, shows the derivation of the PAS FM demodulator output that is presented in section 2.1.2.

Chapter 1

Signal Errors in Mobile Communication Systems

In an ideal wireless communication channel link, the mobile antenna receives the transmitter signal without any distortions or signal alterations. In a realistic communication link, nature makes it more difficult to the moving vehicle to receive radio frequency (RF) signals. Radio designers must work around the difficulties that nature introduces to the communication link. The RF signals experience, in urban environment, changes in amplitude and phase. This results in amplitude fades of $40dB$ or more as the vehicle moves. Further, the RF signal fluctuation rates as the vehicle moves is in the range of 100 to $1000Hz$ [23].
This Chapter reviews the basic concepts of multi-path in FM mobile communications. Section 1.1 reviews Rayleigh distribution function because it is commonly used to characterize short delay or slow fading multi-path in wireless communication links. Section 1.2 discusses short delay multi-path and doppler spread. It includes the equation that characterize Rayleigh fading along with measured antenna patterns. Rayleigh fading is a result of the sum (at antenna input) of multiple signal reflections that occur in big cities and urban areas. Section 1.2.1 shows, by an example, FM short delay multi-path for a typical receiving glass antenna in the vehicle. It includes plots of the resulting Rayleigh amplitude fading, phase fluctuation, and doppler spread.
Section 1.2.2 describes long delay multi-path that usually occurs in mountainous areas. Long delay multi-path occurs when the FM antenna receives delayed signals of $5\mu sec$ or above. Long delay multi-path is analyzed in details along with examples. When an adjacent channel is present, it can have severe effect on the desired channel. Adjacent channel interference is analyzed in section 1.3. Finally, integrated multi-antenna system on one glass of the car is described in section 1.4.

1.1 Rayleigh Fading Distribution

Rayleigh distribution function is commonly used to characterize the FM channel short delay multi-path or slow fading phenomenon of the signal envelope (or amplitude) in mobile communications. If v represents the signal voltage envelope seen by a mobile antenna, then the Rayleigh probability density function (pdf) is

$$p(v) = \frac{v}{\sigma^2} e^{\frac{-v^2}{2\sigma^2}} \tag{1.1}$$

The expected value (or mean) of v is

$$E\{v\} = \sqrt{\tfrac{\pi}{2}} \cdot \sigma$$

and the mean-square is

$$E\{v^2\} = 2\sigma^2$$

where $E(\cdot)$ is the expected value operator.

It is practical to describe Rayleigh pdf with mean-square in the mobile communication field. Substituting the mean-square $E\{v^2\}$ into Equation 1.1 to become

$$p(v) = \frac{2\,v}{\overline{V^2}}\, e^{\frac{-v^2}{\overline{V^2}}} \tag{1.2}$$

where $\overline{V^2}$ is another notation for the mean-square $E\{v^2\}$. Figure 1.1 (A) shows the well known Rayleigh pdf where $\sigma = 1$ and as a result $\overline{V^2} = 2$.

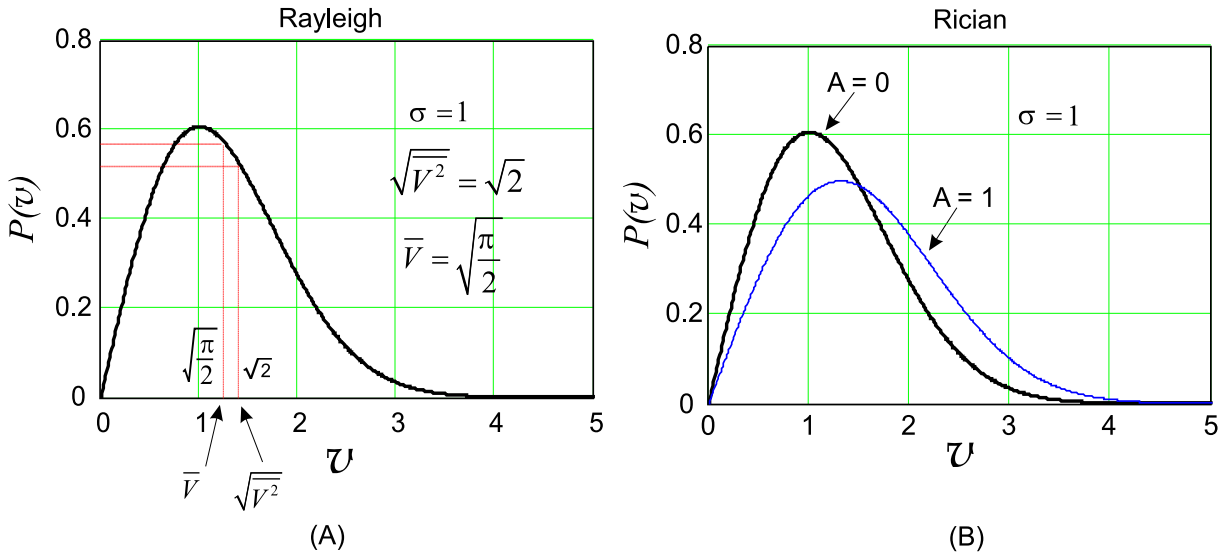

Figure 1.1: (A) Rayleigh probability density function (B) Rician probability density function for $A = 0$ (Rayleigh) and $A = 1$

The probability function $P(v \leq v_s)$, Where v_s is some arbitrary selected voltage level, can be expressed as

$$P(v \leq v_s) = \int_0^{v_s} p(v)\, dv = 1 - e^{\frac{-v_s^2}{\overline{V^2}}} \tag{1.3}$$

When the mobile antenna sees scatterers or reflections that are superimposed on strong direct signal, Rician amplitude distribution is used for the fading envelope. In Rician case, the probability that the voltage level fades or drops below some minimum threshold voltage is less than in a Rayleigh fading field. Therefore, the average Signal-to-Noise Ratio (SNR) of an FM receiver output improves due to the direct signal component. It can be noticed

that Rayleigh density function is a special case of the Rician amplitude distribution. The following represents Rician pdf

$$p(v) = \frac{v}{\sigma^2} e^{\frac{-v^2+A^2}{2\sigma^2}} I_0(\frac{vA}{\sigma^2}) \tag{1.4}$$

where A represents the peak amplitude of the direct signal seen by the mobile antenna and I_0 is the modified zero-order Bessel function of the first kind. It can be seen that when A = 0, the Rician pdf reduces to Rayleigh pdf (See Figure 1.1 (B)). Figures 1.2 (A) and (B) show the plots when $P(v \leq v_s)$ and $P(v > v_s)$ for both Rayleigh and Rician distributions, respectively.

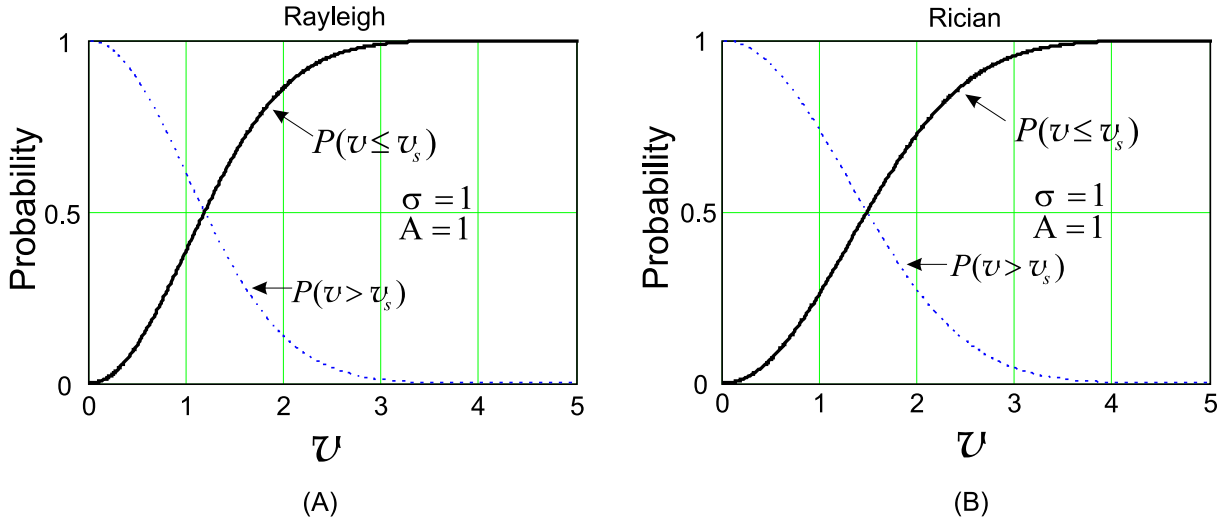

Figure 1.2: Cumulative density functions (Probability) of (A) Rayleigh fading (B) Rician fading

A typical mobile receiver resulting signal from a Rayleigh fading environment is shown in Figure 1.3. Assume the car is moving in constant velocity in the x-direction, the FM receiver would experience fades of $30dB$ or more. The likelihood that the received voltage v is less than a V_{min} is of interest to us (Equation 1.3) when computing diversity effectiveness (Chapter 3). This results in a similar plot of Figure 1.2, wherewith we can predict the percentage of fades that are below V_{min}. When a direct signal A is present, the Rician probability that $v \leq V_{min}$ is less than the Rayleigh probability (as expected) when Figure 1.2 (B) is compared to Figure 1.2 (A).

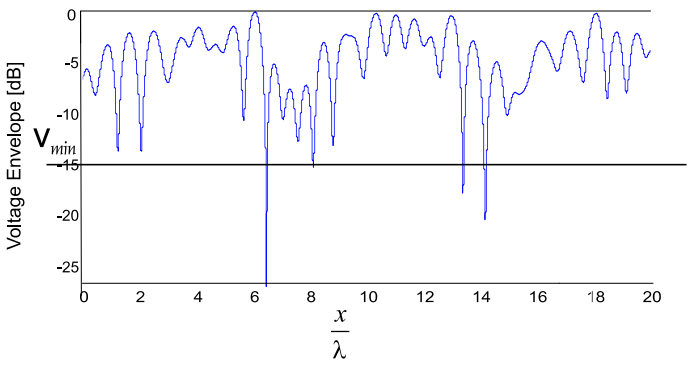

Figure 1.3: Typical Rayleigh Fading as the Car moves in the x-direction

1.2 Multi-path Fading and Doppler

Multi-path fading is a common phenomenon in FM mobile communications. In practice, the electromagnetic waves undergo reflection, scattering and diffraction. The received signal has multiple versions of it due to reflectors, i.e. buildings or mountains. Multi-path fading can be divided into two categories for FM frequency range ($87 - 108$ MHz). First, short delay multi-path (flat and slow fading channel) occur due to random and multiple reflections of waves from high buildings in big cities. This situation is modelled by Rayleigh pdf.

Second, long delay multi-path occur mainly in mountainous areas. This is when the reflected signals have a delay time greater than $5\mu sec$ where the instantaneous frequency of the superimposed delayed waves differ due to the frequency modulation of the signal. Long delay multi-path causes audible distortions when FM demodulated.

1.2.1 Short Delay Multi-path and Doppler

Figure 1.4 illustrates FM short delay multi-path (less than $5\mu sec$) occurrence in the cities. Small scatterers with random amplitude, phase and incident angle sum or superimpose at the received antenna. This can cause destructive or constructive combining. The instantaneous frequency differences that result from the random phase differences of the superimposed waves is very small when compared to the FM modulation frequency deviation. Therefore, the RF frequencies of the scatterers are considered equal in short delay multi-path and we are concerned with the received voltage envelope with respect to a minimum voltage threshold V_{min}. During destructive combining, the signal envelope (or amplitude) can experience fades of $30dB$ or more.

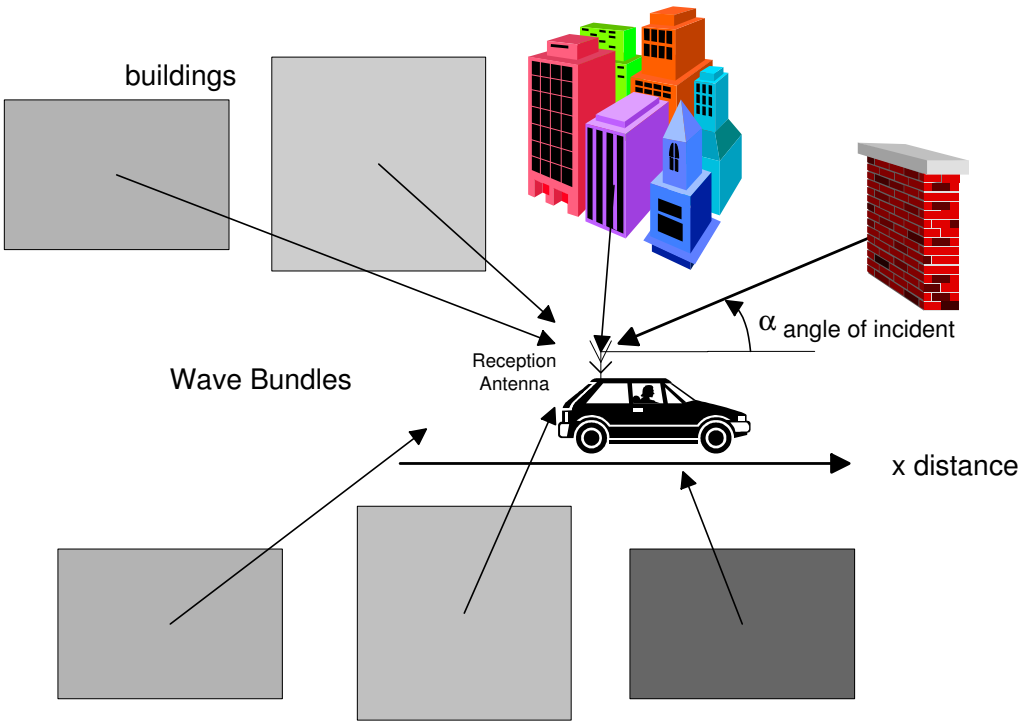

Figure 1.4: Multi-path due to reflected waves from buildings

Figure 1.5 shows the wave front of the electric field **E** and magnetic field **H** travelling in

vector **P** direction. α is the incident angle. The equation that represents the sum of all the incoming waves (scatterers) complex voltages $\underline{V}(x)$ multiplied by a measured antenna pattern is developed next. $\underline{V}(x)$ eventually yields a simulated Rayleigh fading field when having adequate number of waves ($\geq$ 20) and period points. The doppler frequencies are easily calculated by taking the derivative of the phase of $\underline{V}(x)$. Assume that a car moves along a path in the x-direction.

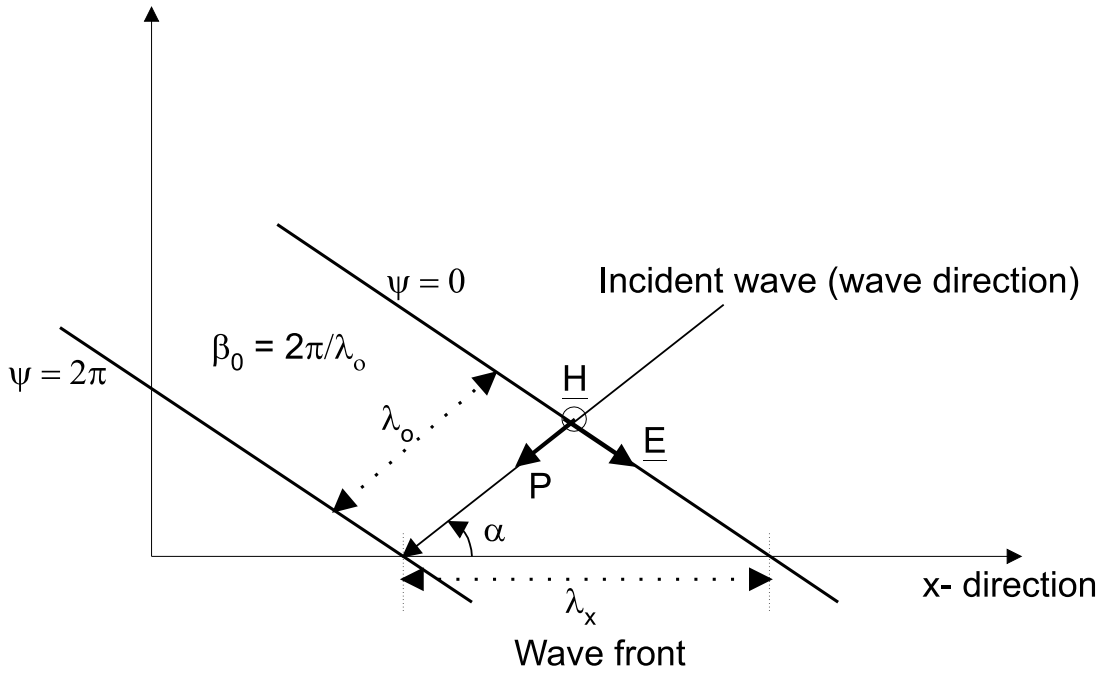

Figure 1.5: Incident Wave Details

The received voltage is the electric field $\underline{E}$ in the x-direction multiplied by the effective antenna length l_{eff} ($\underline{V} = \underline{E} \cdot l_{eff}$). This is defined by

$$\underline{V}_x(x) = V \exp(j\psi) \exp(j\beta_x x) \tag{1.5}$$

where β is the phase constant and it is defined by

$$\beta_o = \frac{2\pi}{\lambda_o}$$

and

$$\beta_x = \frac{2\pi}{\lambda_x}$$

then

$$\beta_x = \frac{2\pi}{\lambda_o} \cos\alpha$$

The resulting signal $\underline{V}(x)$ at the receiving antenna for the case the vehicle and nearby scatterers are moving , can be represented as the sum of direct and reflected waves. It can be expressed as

$$\underline{V}(x) = \sum_{i=1}^{NW} \underline{V}_i \exp(j\frac{2\pi}{\lambda_o} x \cdot \cos\alpha_i) \cdot \underline{C}_i \tag{1.6}$$

where

$$\underline{V}_i = V_i \exp(j\psi_i)$$
$$\underline{C}_i = C_i \exp(j\varphi_i)$$

and

α_i = Random angle of incident [rad]
x = Travelling direction of the Vehicle [m]
λ_o = Wavelength [m]
C_i magnitude of the measured antenna pattern with respect to common reference value
φ_i Angle of the measured antenna pattern with respect to a common phase reference
V_i = Random amplitude of the i-th wave
ψ_i = Random phase of the i-th wave due to different propagation paths
NW = Total number of waves

We will use Equation 1.6 to sum all the waves to simulate Rayleigh field drive. The total travelling distance L is

$$L = (\frac{\Delta x}{\lambda_o}) \cdot n_x \cdot \lambda_o$$

where n_x is total number of x points in one period (Per) as the simulated vehicle travels in the x-direction. Then Δt is

$$\Delta t = \frac{T}{n_x}$$

where T is the total time of the travelling distance and is defined by

$$T = \frac{L}{\nu}$$

where ν is the vehicle speed $[m/s]$.

Once we have the sum of all waves from Equation 1.6, its phase can be calculated. The derivative of the phase of the faded signal is needed to find the Doppler frequencies. We need to write $\underline{V}(x)$ in a different form in order to get the phase component. $\underline{V}(x)$ can be written as

$$\underline{V}(x) = \sum_{i=1}^{NW} \underline{V}_i \underline{C}_i \exp\left[j(\varphi_i + \psi_i - \frac{2\pi}{\lambda_o} x \cdot \cos\alpha_i)\right] \tag{1.7}$$

where

$$\lambda_o = \frac{c_o}{f_c}$$

and c_o is speed of light [m/s], f_c = Carrier Frequency [Hz].

The phase is given by

$$\Phi_t = \arctan\left(\frac{\sum_{i=1}^{NW} V_i C_i \sin(\varphi_i + \psi_i - \frac{2\pi}{\lambda_o}\nu \cdot t \cdot \cos\alpha_i)}{\sum_{i=1}^{NW} V_i C_i \cos(\varphi_i + \psi_i - \frac{2\pi}{\lambda_o}\nu \cdot t \cdot \cos\alpha_i)}\right) \tag{1.8}$$

and the Doppler frequency is defined by

$$f_D = \frac{1}{2\pi} \cdot \frac{\partial \Phi_t}{\partial t} \tag{1.9}$$

The calculation of the Doppler frequencies can be done numerically on a digital computer by using

$$f_{D_t} = \frac{(\Phi_{t+1} - \Phi_t)}{\Delta t} \cdot \frac{1}{2\pi} \tag{1.10}$$

The phase of $\underline{V}(x)$ must be corrected because the arg function gives 2π ambiguities that will cause incorrect calculations of the Doppler frequencies. Therefore the 2π ambiguities must be unwrapped before calculation of the Doppler frequencies. It is important to keep in mind that the Doppler frequency is a function of the car speed. The Doppler frequency in the FM frequency range is given by

$$f_D = \frac{\nu}{\lambda_o} \cdot \cos(\alpha) \tag{1.11}$$

where the maximum doppler is $\frac{\nu}{\lambda_o}$ and doppler bandwidth is $2 \cdot \frac{\nu}{\lambda_o}$.

When the car is moving in the x-direction in a Rayleigh field, a higher Doppler value can occur due to deep fades caused by sharp phase changes. This situation is rare in short delay multi-path and is demonstrated in the next subsection. The RF amplitude with such fades drops way below the minimum threshold voltage which cause the Doppler frequency to be $>> 20Hz$ in the FM range. In this case the input voltage may be close in amplitude to the noise floor of the receiver.

Short Delay Multi-path fading and Doppler in FM Range(87.5-to-108MHz)

This section demonstrates by an example the short delay multi-path for FM. Figure 1.6 shows the vehicle travelling in the x-direction with multiple periods. Each period has a fixed set of generated random wave variables of amplitude, phase and incident angle. The following example is done with one period ($Per = 1$). Let the FM carrier frequency be 100MHz, $\frac{\Delta x}{\lambda_o} = 0.001$ per step, and a vehicle speed ν of 100km/hr or 27.8m/s. When $n_x = 20000$, it can be calculated that $\Delta t = 1.08 \cdot 10^{-4}$ and L = 60 meters. Let V_i be random between 0 and 1, and ψ_i random between 0 and 2π. The total number of waves NW is 20. Total time is 2.16 seconds and the measured gain pattern of antenna 3 in section 1.4 is used.

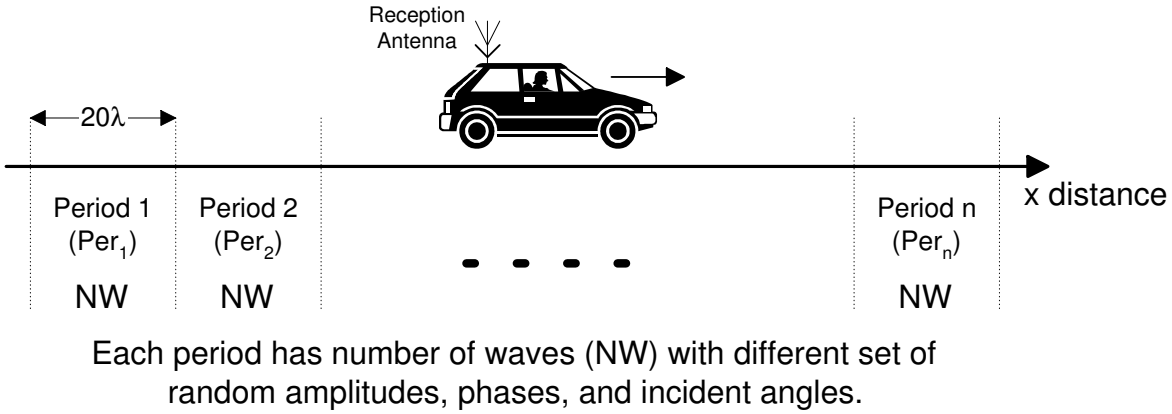

Figure 1.6: Virtual Drive Illustration

The resulting Rayleigh fading for the given example is shown in Figure 1.7. Consider the minimum voltage threshold V_{min} is $-20dB$ as shown in Figure 1.7. When the signal voltage drops below V_{min}, distortion occur in the FM receiver. In other words, the signal voltage can drop into the noise floor of the FM receiver. Therefore, audible distortions or fades occur in a Rayleigh field as the vehicle travels in the x-direction. The distortion duration for the maximum fade for our example is found to be $7msec$.

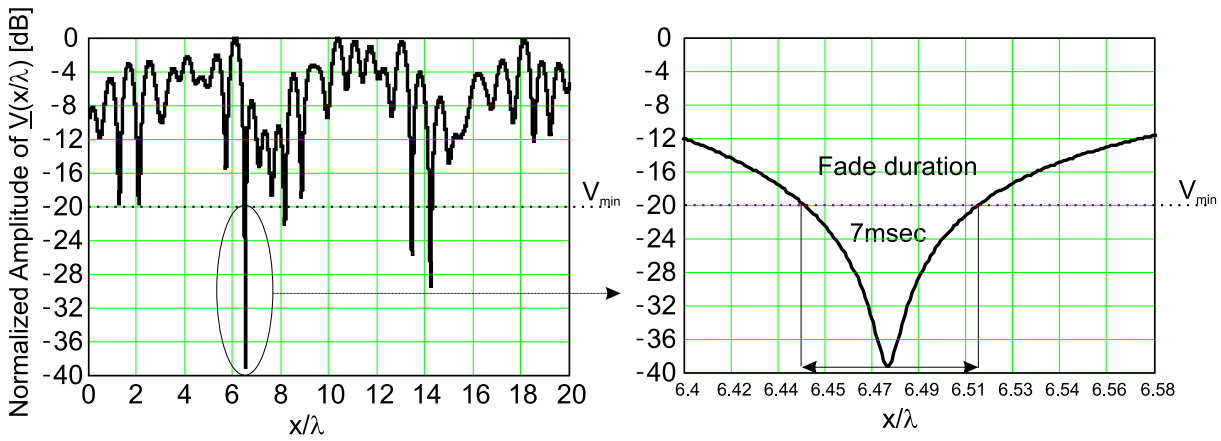

Figure 1.7: Rayleigh fading for Antenna 3 and maximum fade distortion duration

The derivative and corrected derivative for our example are shown in Figure 1.8(A). A scaled amplitude of $\underline{V}(x)$ is plotted in Figure 1.8 (B) for illustration of the relationship between the deep fades and the expected phase ambiguities. The maximum phase derivative occur at maximum fade as expected. The phase and phase derivative are calculated so that we easily calculate the resulting doppler frequency (Equation 1.9).

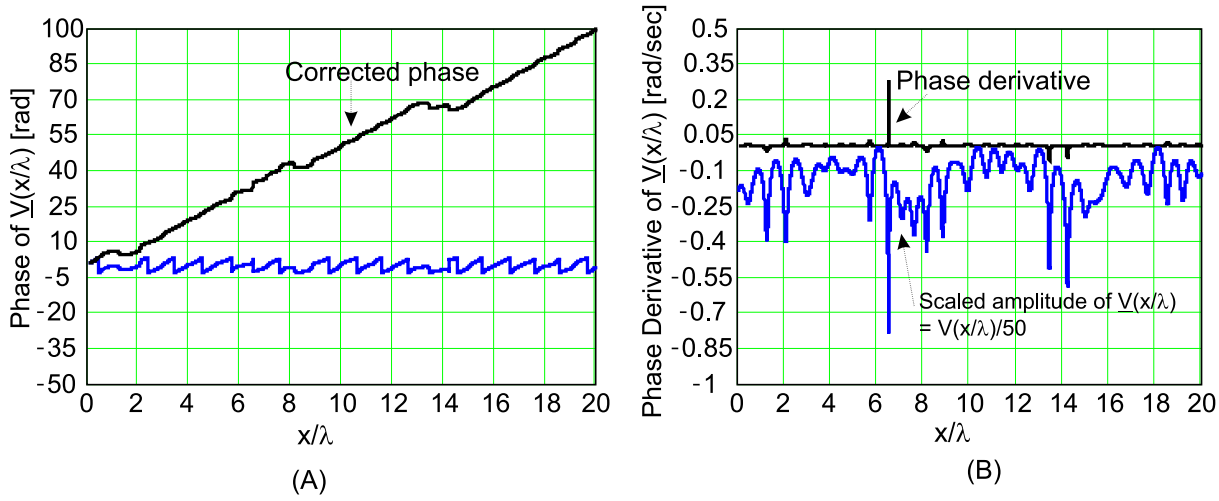

Figure 1.8: (A) Phase of $\underline{V}(\frac{x}{\lambda})$ (B) Phase Derivative of $\underline{V}(\frac{x}{\lambda})$

The resulting Doppler frequencies are shown in Figure 1.9 (A). It can be seen from Figure 1.9 (A) that a wide range of Doppler frequencies occurred in the virtual drive of 2.16 seconds. The maximum is $412Hz$ and the average is $7.3Hz$. If we only have one wave and the incident angle is $0°$, then we calculate a Doppler frequency of $9.25Hz$. The resulting Doppler are not audible in FM frequency range because they contribute very small frequency changes ($< 20Hz$) when compared to the RF frequency ($100MHz$). It is important for us to consider the Doppler frequency when we design a co-phase combining diversity system in section 2.1. Figure 1.9 (B) shows a histogram of the Doppler frequencies. As expected, it can be seen that the Doppler bandwidth in the FM frequency range is about $20Hz$. This is the value that is used to design the 3-dB loop bandwidth of the control loop of the co-phase combining diversity system in section 2.1.

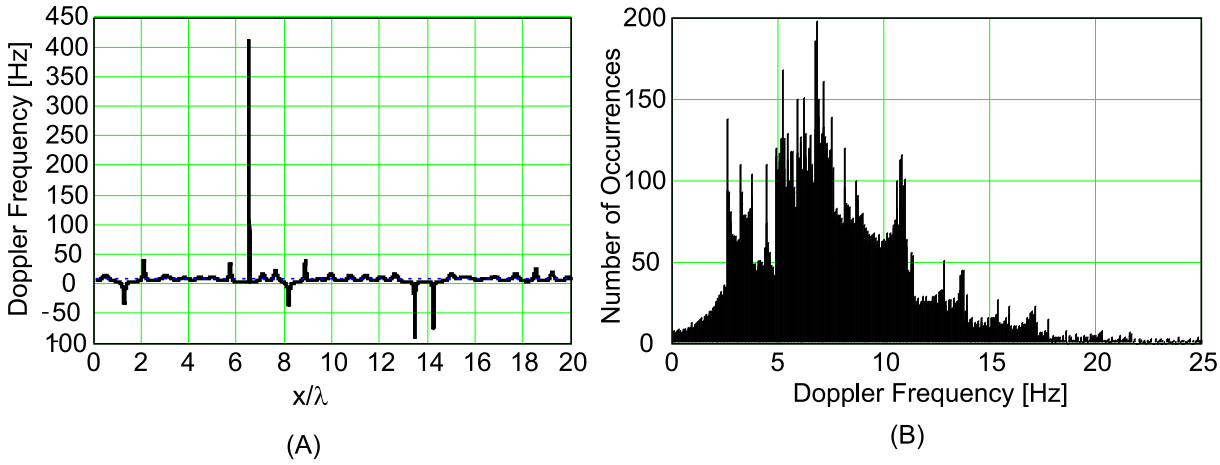

Figure 1.9: (A) Resulting Doppler frequencies (B) Histogram of the resulting Doppler frequencies

1.2.2 Long Delay Multi-path

Long delay Multi-path is common in mountainous areas as seen in Figure 1.10. It results from reflected signals that have a range of 5 - 100 microsecond (μsec) delays [26] [20]. The resulting signal distortions at the output of a FM receiver can reach up to 40%, depending on the amount to time delay, frequency deviation, and amplitude ratio between the signals.

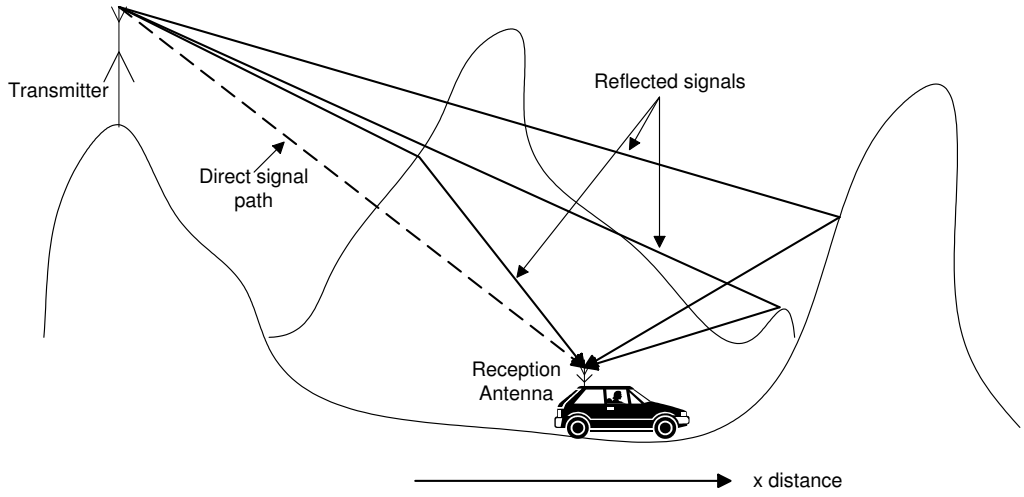

Figure 1.10: Long delay Multi-path due to reflected waves from mountains

Consider the two received voltage amplitudes or envelopes $A_0(t)$ and $A_1(t)$ that are Rayleigh faded as shown in Figure 1.11 (A). In case of long delay multi-path, assume envelope $A_0(t)$ has very small or no time delay when compared to the time delay τ of $A_1(t)$ as shown in Figure 1.11 (B).

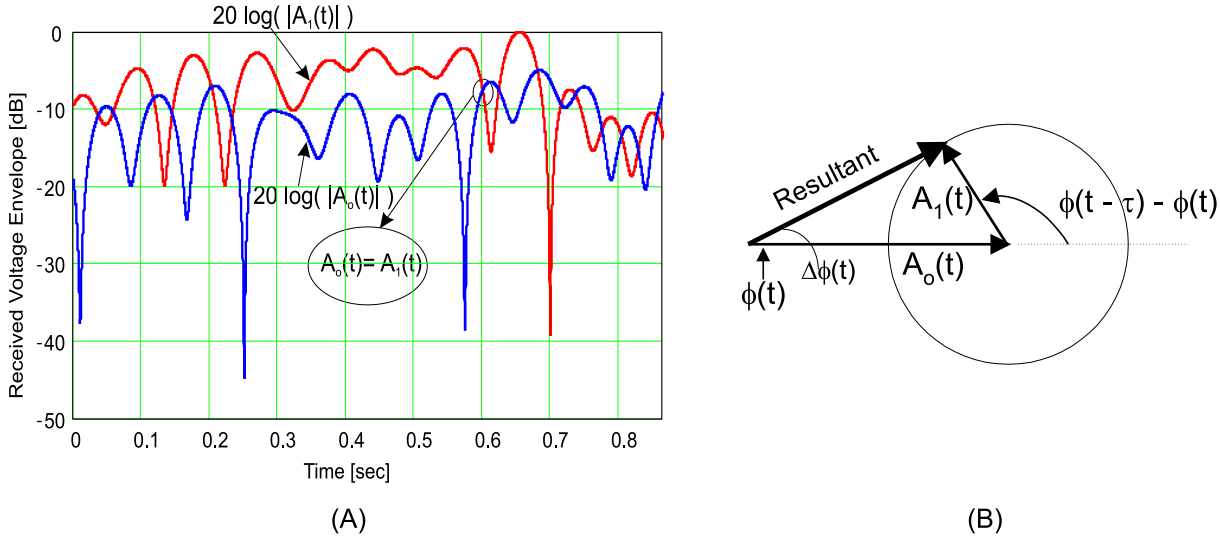

Figure 1.11: (A) Rayleigh faded envelopes (B) Vector representation of two signals with long delay

It is important to examine the resulting erroneous or extra angle deviation $\Delta\phi(t)$ due to time delay τ between the two carrier vector signals in Figure 1.11 (B). Straight forward analysis

of the resulting erroneous angular deviation $\Delta\phi(t)$ of Figure 1.11 (B), leads to the following equation

$$\Delta\phi(t) = \arctan\left(\frac{\frac{A_1}{A_0}\sin(\phi(t-\tau)-\phi(t))}{1+\frac{A_1}{A_0}\cos(\phi(t-\tau)-\phi(t))}\right) \tag{1.12}$$

where we assume A_0 and A_1 are arbitrary fixed amplitudes to simplify the mathematical analysis. The same amplitudes are used later in this section. Equation 1.12 is used in section 2.1.4 when we analyze multi-path performance of a co-phase combining diversity system. As the amplitude ratio $\frac{A_0}{A_1}$ approaches unity and time delay τ is greater than $5\mu sec$ in the above equation, the resulting erroneous angle deviation $\Delta\phi(t)$ increases, which produce highly distorted audible signals when FM demodulated ($\frac{\partial\Delta\phi(t)}{\partial t}$).

We analyze long delay multi-path situation with two signals that are FM modulated with one of them as reference, i.e. zero delay or direct path signal. An FM signal can be described by the following equation

$$V(t) = A_c\cos(\omega_c t + \phi(t)) \tag{1.13}$$

The output of an ideal FM demodulator is

$$D_{FM}(t) = \frac{1}{2\pi}\cdot K_D\cdot\frac{\partial\phi(t)}{\partial t} \tag{1.14}$$

where

K_D = FM Demodulator Constant [V/Hz]
$\omega_c = 2\pi f_c$ Carrier Frequency

For FM, $\phi(t)$ is given by

$$\phi(t) = 2\pi f_d\int^t m(\beta)\,d\beta \tag{1.15}$$

where
f_d = Frequency Deviation [Hz] and $m(\beta)$=Modulating signal (message or information)

To demonstrate the effect of long delay multi-path, suppose we have the two signals of Figure 1.11 (A) at the antenna input

$$V_0(t) = A_0\cos(\omega_c t + \phi(t)) \tag{1.16}$$

and

$$V_1(t) = A_1\cos(\omega_c(t-\tau) + \phi(t-\tau)) \tag{1.17}$$

where τ is the delay time of the second signal, A_0 and A_1 are arbitrary fixed amplitudes. The resulting sum is

$$V_s(t) = V_0(t) + V_1(t) = A_0\cos(\omega_c t + \phi(t)) + A_1\cos(\omega_c t - \omega_c\tau + \phi(t-\tau)) \tag{1.18}$$

Simplifying $V_s(t)$ further, yields the following Equation

$$V_s(t) = A_s\cos(\omega_c t + \gamma(t)) \tag{1.19}$$

where

$$A_s = \sqrt{A_0^2 + A_1^2 + 2A_0A_1\cos(-\omega_c\tau + \phi(t-\tau) - \phi(t))} \tag{1.20}$$

and

$$\gamma(t) = \arctan\left(\frac{A_0\sin(\phi(t)) + A_1\sin(-\omega_c\tau + \phi(t-\tau))}{A_0\cos(\phi(t)) + A_1\cos(-\omega_c\tau + \phi(t-\tau))}\right) \tag{1.21}$$

Equation 1.20 represents the resulting AM modulation and Equation 1.21 represents the phase modulation. The output of the FM demodulator is

$$D_{V_s}(t) = \frac{1}{2\pi}\cdot K_D \cdot \frac{\partial\gamma(t)}{\partial t} \tag{1.22}$$

where

$$\frac{\partial\gamma(t)}{\partial t} = \underbrace{\dot{\phi}(t)}_{desired\,term} + \underbrace{\frac{(\dot{\phi}(t-\tau) - \dot{\phi}(t))\cdot(A_1^2 + A_0A_1\cos(-\omega_c\tau + \phi(t-\tau) - \phi(t)))}{A_0^2 + A_1^2 + 2A_0A_1\cos(-\omega_c\tau + \phi(t-\tau) - \phi(t))}}_{distortion\,term} \tag{1.23}$$

and $\dot{\phi}(t) = \frac{\partial\phi}{\partial t}$.

Now let the FM message be

$$m(t) = \cos(2\pi f_m t) \tag{1.24}$$

where

$$f_m = \text{Modulation Frequency [Hz]}$$

Then we can calculate the following from Equation 1.15

$$\phi(t) = \frac{f_d}{f_m}\sin(2\pi f_m t) \tag{1.25}$$

and

$$\dot{\phi}(t) = 2\pi f_d\cos(2\pi f_m t) \tag{1.26}$$

The distortion term represents the second part of the right side of Equation 1.23. The distortion can be calculated (with FFT) by taking the sum of the resulting rms harmonic amplitudes divided by the sum of resulting rms harmonic amplitudes h_i plus the fundamental. The distortion can be represented by the following

$$Dist = \frac{\sqrt{\sum_{i\geq 1}|h_i|^2}}{\sqrt{\sum_{i\geq 0}|h_i|^2}}\cdot 100\% \tag{1.27}$$

where h_0 represents the rms amplitude of the fundamental signal.

The output from the ideal FM demodulator is shown in Figure 1.12 with $A_0 = 1$, $A_1 = 0.9$, $f_m = 1kHz$,$f_d = 75kHz$, $K_D = 1\frac{V}{Hz}$, and $\tau_1 = 30\mu sec$. The distortion peaks of the recovered signal are evident compared to the undistorted original signal. In addition, the resulting AM modulation is also shown. The calculated distortion factor is equal to 26.25% with no filtering and 12% with $15kHz$ ideal low-pass filter. The harmonic distortion of the recovered signal is shown without the $15kHz$ ideal filter in Figure 1.13.

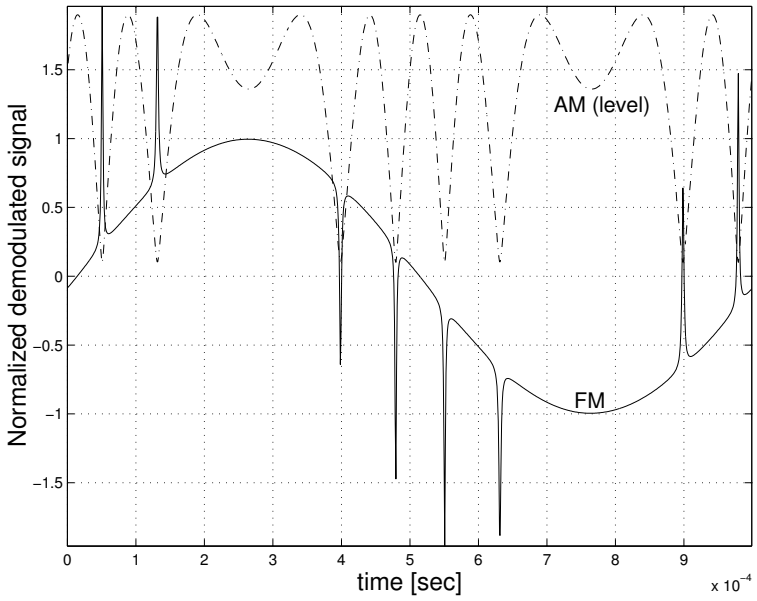

Figure 1.12: Demodulated FM signal with $A_0 = 1$, $A_1 = 0.9$, $f_m = 1kHz$,$f_d = 75kHz$, $K_D = 1\frac{V}{Hz}$, $\tau_1 = 30\mu sec$

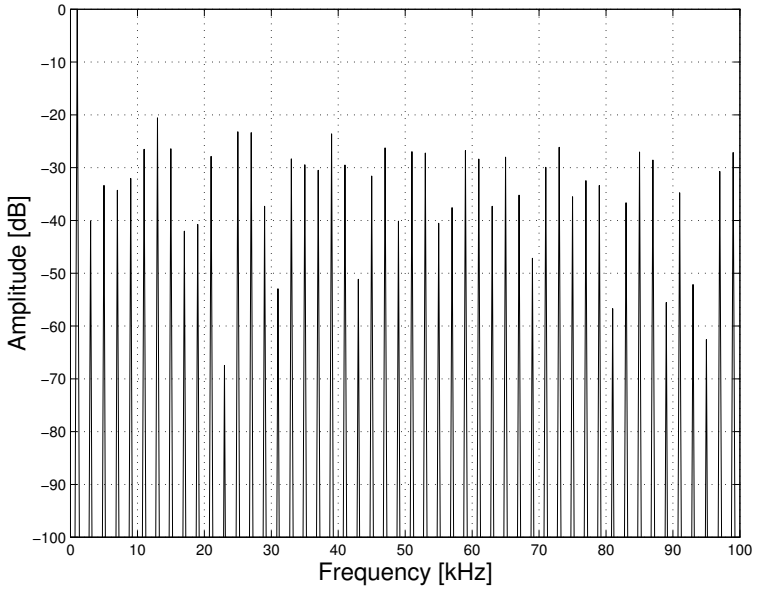

Figure 1.13: Harmonic distortion of the demodulated FM signal

A three dimensional diagram of the distortion factor due to the sum of two signals is shown in Figure 1.14. The distortion factor is calculated with sweeping the ratio of $\frac{A_1}{A_0}$ and the delay difference between the two signals. In addition, the frequency deviation is $25kHz$ and the modulation frequency is $1kHz$. A $15kHz$ ideal low-pass filter after the FM-demodulation is used for the distortion calculation. An amplitude ratio of 0.99 and delay of $100\mu sec$ will result in 37% distortion factor. As time delay τ increases, the two vectors in Figure 1.11 rotates around each other faster. Therefore, the faster they rotate the more erroneous peaks are present at the output of the FM demodulator as shown in Figure 1.12. Therefore, the distortion factor increases as time delay increases. Similarly, as the amplitude ratio $\frac{A_1}{A_0}$ approaches unity, the two vectors cancel each other as they rotate, resulting in high erroneous peaks at the output of the FM demodulator that increase the distortion factor.

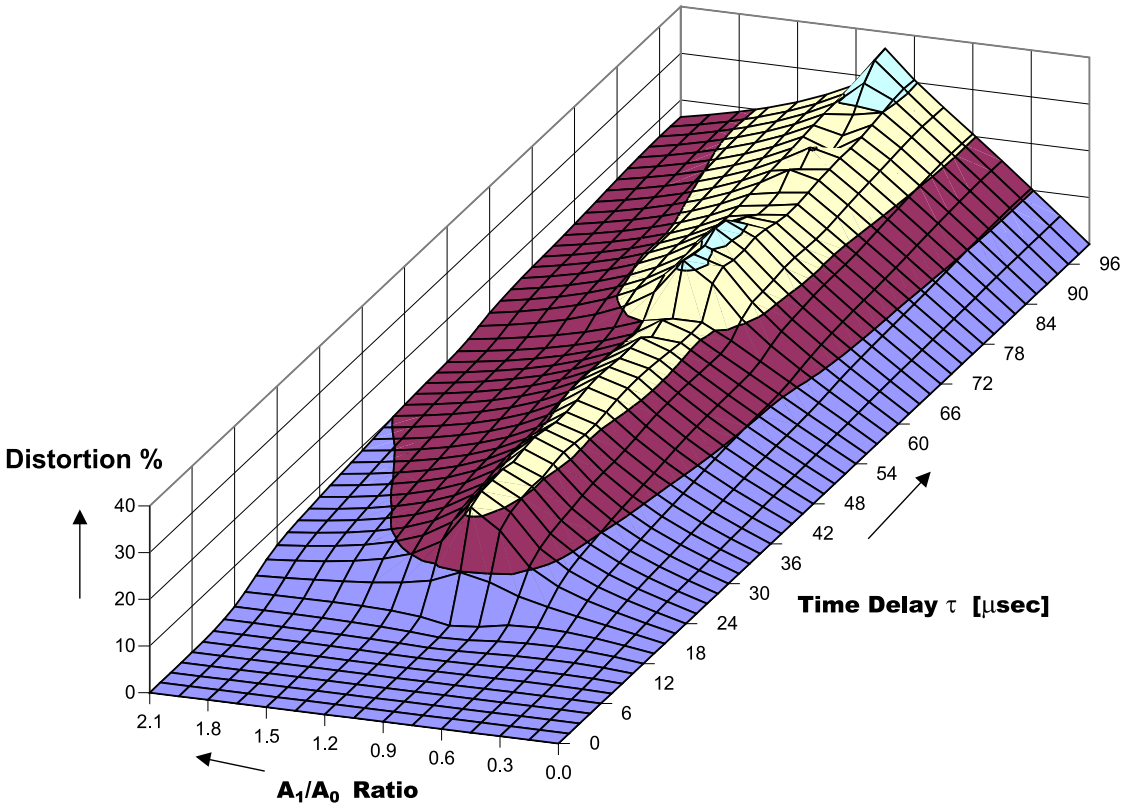

Figure 1.14: Distortion due to different $\frac{A_1}{A_0}$ ratios and delay times with $f_d = 25kHz$, $f_m = 1kHz$

1.3 Adjacent Channel Interference

When a strong adjacent channel is present, some of the undesired adjacent channel spectrum sneaks through and falls in the desired channel bandwidth. This interference can have severe effect on the desired received FM signal. Adjacent channel can be modelled by a simple diagram that is shown in Figure 1.15. f_c represents the carrier of the desired channel and f_{ca} is the adjacent channel carrier frequency. Consider one component with amplitude r of the undesired adjacent channel spectrum. This component is f_a away from the desired carrier f_c and falls within the desired band.

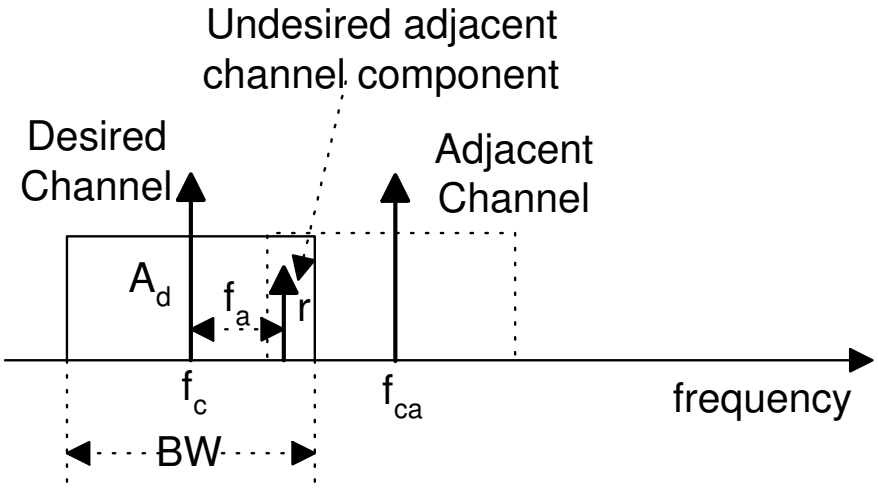

Figure 1.15: Adjacent Channel description diagram

Suppose the desired signal received voltage $V_d(t)$ is

$$V_d(t) = A_d \cos(\omega_c t + \phi(t)) \tag{1.28}$$

and the undesired adjacent channel component voltage $V_u(t)$ is

$$V_u(t) = r \cos(\omega_c t + \omega_a t) \tag{1.29}$$

where the frequency of the undesired signal component is $\frac{1}{2\pi} \cdot \omega_a$, A_d is the amplitude of the desired signal, and r is the amplitude of the undesired signal. $\phi(t)$ is the desired FM information, Equation 1.15. The input to the FM detector is

$$V_c(t) = V_d(t) + V_u(t) = A_d \cos(\omega_c t + \phi(t)) + r \cos(\omega_c t + \omega_a t) \tag{1.30}$$

Simplifying $V_c(t)$ further, yields the following Equation

$$V_c(t) = A_{dr} \cos(\omega_c t + \Upsilon(t)) \tag{1.31}$$

where

$$A_{dr} = \sqrt{A_d^2 + r^2 + 2 \cdot A_d \cdot r \cos(\omega_a t - \phi(t))} \tag{1.32}$$

and the phase is

$$\Upsilon(t) = \arctan\left(\frac{A_d \sin(\phi(t)) + r \sin(\omega_a t)}{A_d \cos(\phi(t)) + r \cos(\omega_a t)}\right) \tag{1.33}$$

The output of the FM demodulator is

$$D_{V_c}(t) = \frac{1}{2\pi} \cdot K_D \cdot \frac{\partial \Upsilon(t)}{\partial t} \tag{1.34}$$

where the derivative of the phase is

$$\frac{\partial \Upsilon(t)}{\partial t} = \underbrace{\dot{\phi}(t)}_{desired\,term} + \underbrace{\frac{(\omega_a - \dot{\phi}(t)) \cdot (r^2 + A_d \cdot r\cos(\omega_a t - \phi(t)\,)\,)}{A_d^2 + r^2 + 2A_d \cdot r\cos(\omega_a t - \phi(t))}}_{distortion\,term} \tag{1.35}$$

To illustrate the effect of an adjacent channel, we use Equation 1.34 to observe the distortions on the desired signal due to the undesired signal component. Consider the FM message signal of Equation 1.15 with modulation frequency $f_m = 1kHz$, frequency deviation $f_d = 25kHz$. Let $f_a = 60kHz$, $A_d = 1$, and $r = 0.5$. The results are shown in Figure 1.16. The desired FM signal is distorted because of the resulting erroneous frequencies that are produced due to the undesired adjacent channel signal. The distortions are more severe as the amplitude r approaches the amplitude of A_d. The distortion factor for the signal in Figure 1.16 (A) is 82% (no filter) and 0.5% when using a simple $15kHz$ low-pass filter.

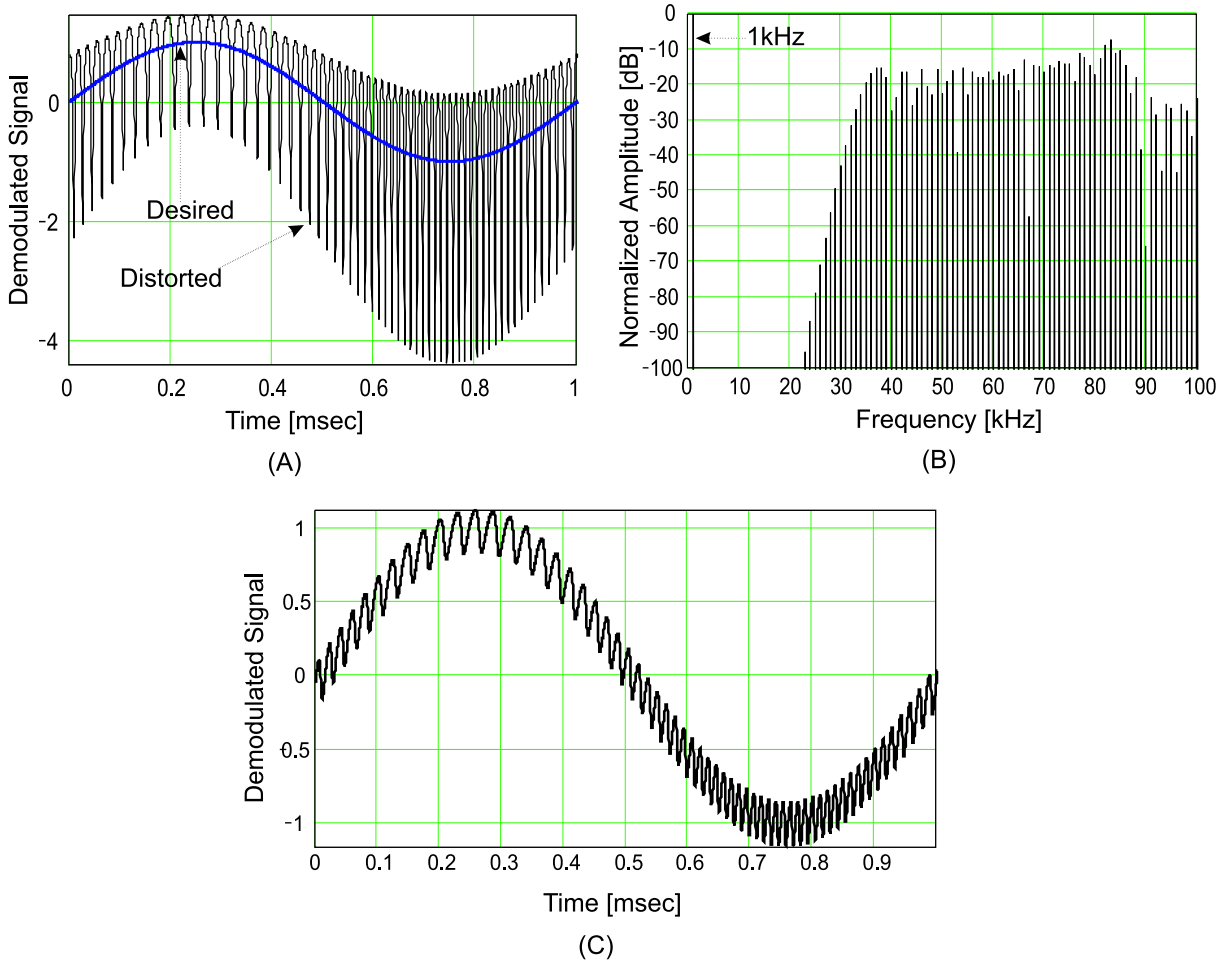

Figure 1.16: (A)FM demodulator desired and distorted outputs (B) Frequency spectrum (C) FM demodulator output, followed by simple RC $15kHz$ low-pass filter

1.4 Multi-Antenna System for Diversity Application

Space diversity systems require that the antennas to be spaced far apart from each other so that they fade independently. Diversity improves signal reception with properly spaced antennas. When using multiple FM antennas in cars, we have limited space to place the antennas. Many automotive manufacturers require that the antennas be placed in the back window. This requirement increases the correlation between the antenna signals but we still can obtain good diversity performance with properly designed antennas. Typical antennas that are designed at the Institute of High Frequency at the University of Bundeswehr Munich are located in the back window (backlite) as shown in Figure 1.17.

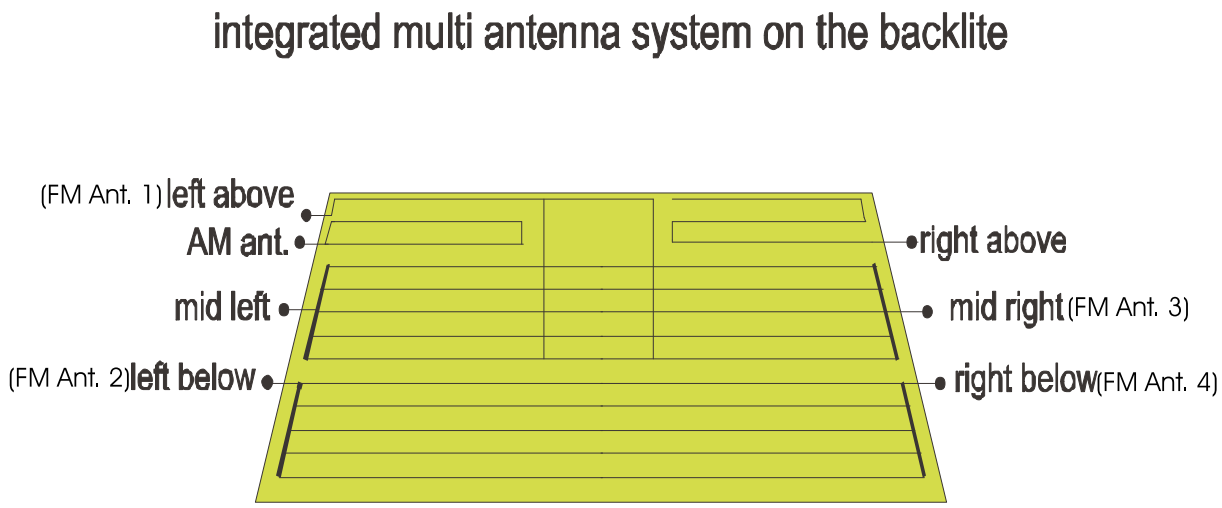

Figure 1.17: Multi antenna system on the backlite

The measured FM antenna pattern magnitude can be represented by the following Equation

$$\underline{C}(\varphi,\theta) = \frac{\underline{V}_{\varphi}(\varphi,\theta)}{\underline{V}_{\varphi\,\max}(\varphi,\theta)} \tag{1.36}$$

where $\underline{V}_{\varphi}(\varphi,\theta)$ = Received Voltage [V]

and

θ is set to be 90°, angle of elevation
$\varphi \in [0° - 360°]$, azimuth angle

The above four FM antennas measured gain patterns are shown in Figure 1.18 and their phases are shown in Figure 1.19. The measurement system that is used to obtain the patterns is shown in Figure 1.20. The system includes the transmitting antenna, the control unit with computer and network analyzer. The measurement is done by rotating the vehicle in 5° (azimuth angle) steps using the turntable and the angle of elevation is fixed to 85°. For more detailed description of the measurement system, please see [24].

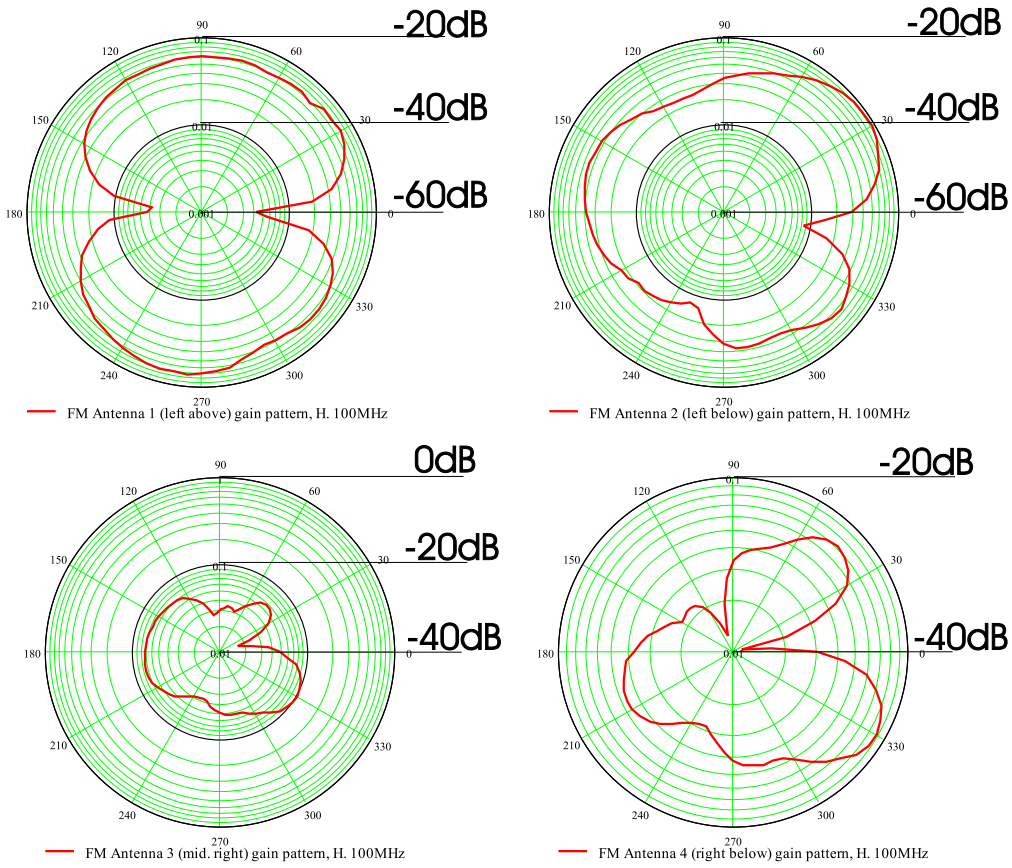

Figure 1.18: Measured Antenna gain patterns of Figure 1.17

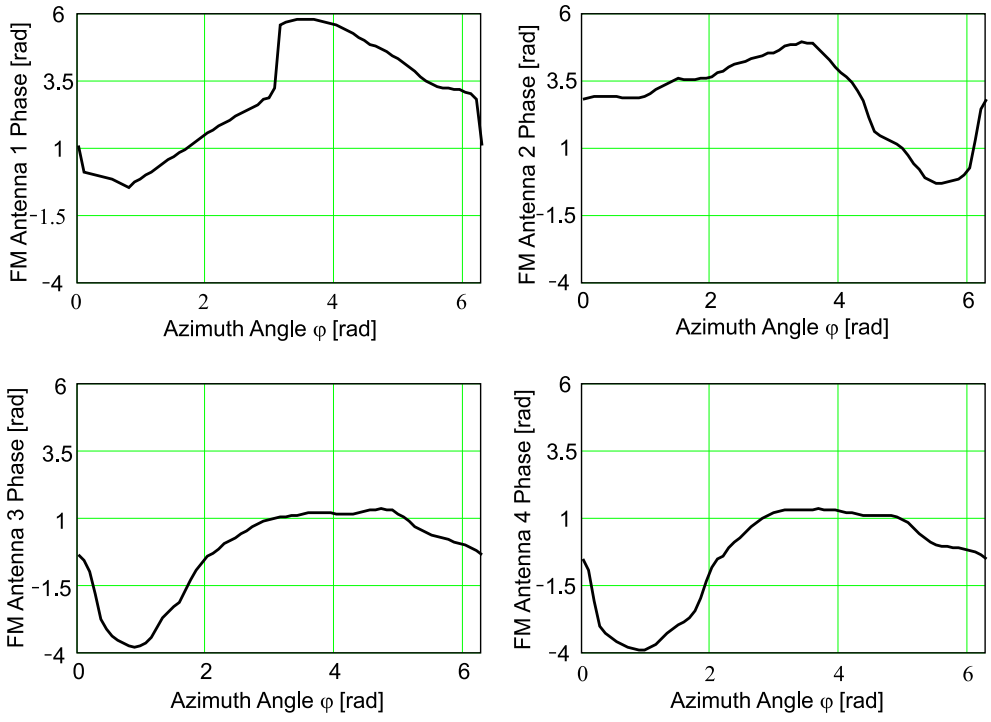

Figure 1.19: Measured Antenna phases of Figure 1.17

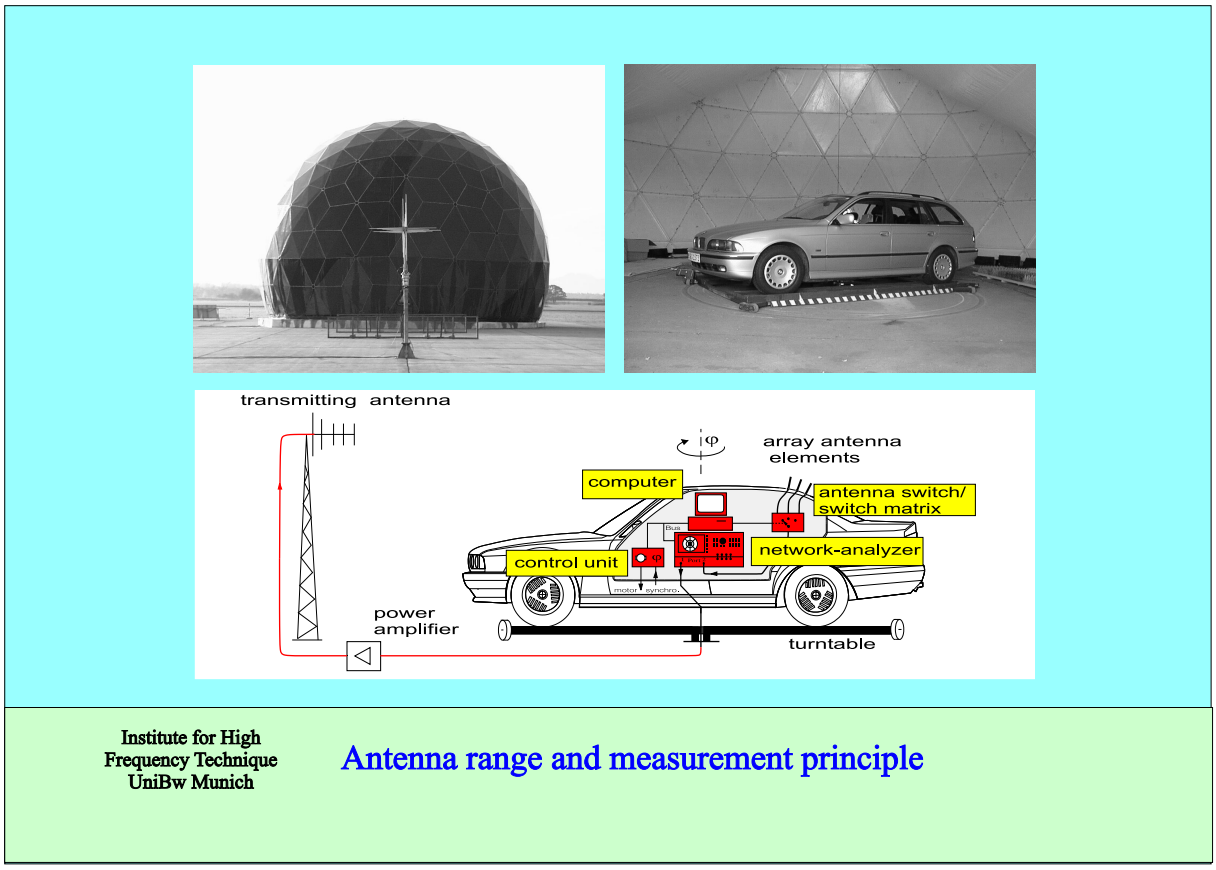

Figure 1.20: Antenna Measurement System

The incoming RF signals to the antennas are summed (or integrated) and weighted by the amplitude and phase of each antenna. If a phase shifter or a recording system (Chapter 5) is placed at the output of each antenna output port, it would not alter the characteristics of the resultant signal at each antenna output. In addition, the interaction between the superimposed waves and the antennas is also not altered. This is an important fact because when a variety of diversity systems are evaluated and compared in Chapter 3, measured antennas are used.

Chapter 2

Diversity Systems in Modern Vehicles

2.1 Phasing Alignment System (PAS)

A two antenna phased array system called Phase Alignment System was implemented based on [6]. The PAS System consists of a standard FM receiver with added circuitry in a separate box [10]. The antennas are printed on the vehicle glass to improve styling, reduce cost, and reduce warranty claims. The system automatically adjusts the electrical phases of the signals received by the array elements so that they may be combined co-phased. This section presents the theory of operation of such a Phase Alignment System (PAS).

2.1.1 PAS Description

Figure 2.1 illustrates the PAS packaging in the car. By properly combining the inputs from an array of multiple glass antennas, the resulting performance can meet or exceed that of the mast antenna. The system in Figure 2.1, is used in some GM vehicles like the Cadillac Seville and Chevrolet Corvette.

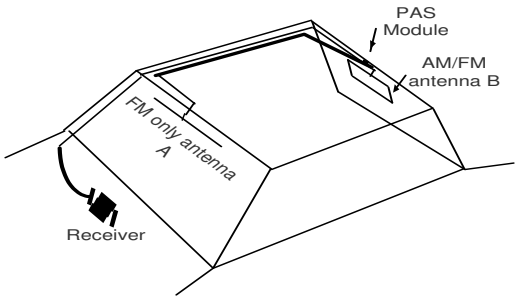

Figure 2.1: PAS packaging in a vehicle

The key idea of the PAS is to align both antenna signals in phase at RF with a standard receiver. To achieve that, for example amplitude modulate (AM) antenna B with ω_r dither signal then add it to signal A.

When the two antennas are not in phase as shown in Figure 2.2(a) (signal B leading signal A), the resulting AM will produce positive phase modulation (PM) at the sum, to which the FM receiver will respond by producing a demodulated output at ω_r proportional to the phase between the two antennas A and B. Figure 2.2(b) shows that when signal B lags signal A, the phase modulation produced at the receiver is inverted 180 degrees, as is the demodulated output. To align the two signals in phase we must minimize the resultant phase modulation by minimizing the demodulated signal that is produced by the FM receiver. Figure 2.2(c) shows the two antennas are aligned and no resulting phase modulation.

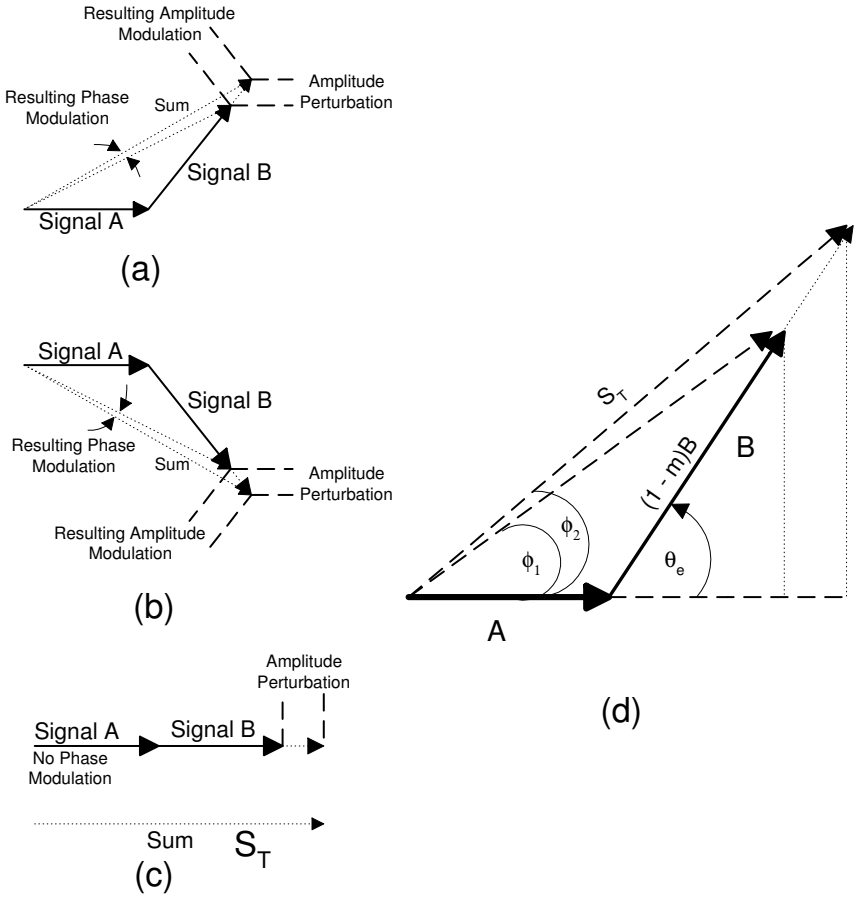

Figure 2.2: PAS vectors representation:(a) Signal B leads signal A, phase mod. and perturbing tone in phase; (b) signal B lags signal A, phase mod. and perturbing tone out of phase; (c) Signals A and B aligned, phase modulation minimized; (d) Vectors geometry analysis.

The placement of the ω_r dither tone is very important because it must not introduce any distortion or audible products to the receiver. It was determined by [9] that the placement must be in quadrature to the L-R baseband modulation, via a PLL to the pilot tone. Figure 2.3 shows the placement of the ω_r, $38kHz$, dither tone in the frequency spectrum. Figure 2.4 shows the resulting phase modulation $\delta \equiv \phi_2 - \phi_1$ as of function of θ_e error angle. The phase modulation is produced as a result of the AM dither tone on antenna B and the sum of both antennas. Refer to Figure 2.2(d) for antenna vector geometry description.

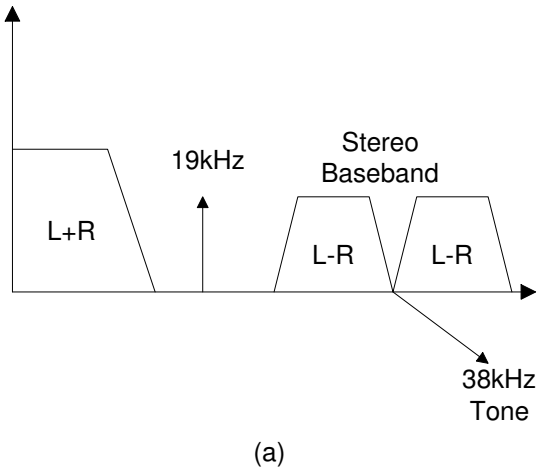

Figure 2.3: Placement of the dither tone

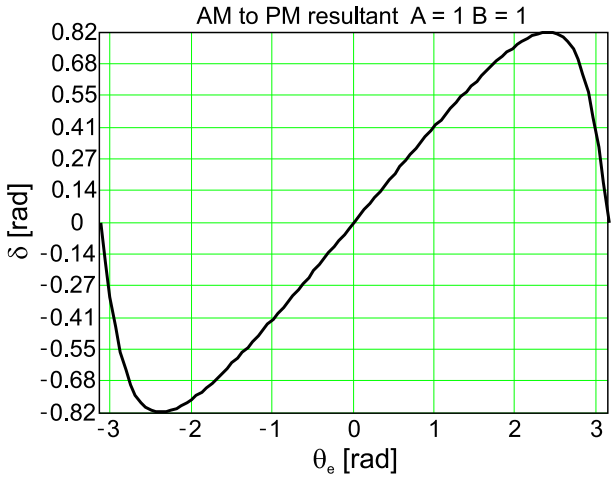

Figure 2.4: Resulting phase deviation(PM), input to an FM receiver.

Figure 2.5 shows the implementation of the PAS. The $38kHz$ dither tone is generated from the $19kHz$ pilot by the 90° PLL and placed in quadrature to the channel information. The resulting dither tone is used to amplitude modulate the incoming RF signal from antenna B in Figure 2.5. The two RF signals, A and B are combined and directed to the FM receiver. Any phase error between the two RF signals will result in phase perturbation of the sum signal. The frequency of this phase perturbation is the same as the $38kHz$ dither tone, and appears at the FM demodulator output. Product detection with the original dither tone results in a DC control voltage used to control the phase shifter. Minimization of the DC voltage (via integrator feedback) will occur when the two signals are phase-aligned.

The receiver has an inherent group delay, which will result in delay of the $38kHz$ dither tone at the FM detector output. In order to maximize the DC error voltage, and therefore maximize the gain of the feedback loop, the two inputs to the product (synchronous) detector or rectifier must have the correct phase relationship. A delay adjustment block is added as shown in Figure 2.5. This adjustment accounts for the inherent delay of the receiver. In addition, the product detector will ignore L-R modulation components because the $38kHz$ from the PLL will be in quadrature with the L-R modulation as shown in Figure 2.6. Assume L-R programming is $\cos(\omega t)$ and the desired $38kHz$ dither tone information is $\sin(\omega_r t)$. Let the input voltage $V_o(t)$ in Figure 2.6 be

$$V_o(t) = V_o \sin(\omega_r t) \tag{2.1}$$

where $\omega_r \equiv 2\pi f_r$ and $f_r \equiv 38kHz$.

$V_o(t)$ is directed to the two mixers and multiplied separately by the signals from the 90° PLL. The 90° PLL generates $\sin(\omega_r t)$ and $-\sin(\omega_r t)$ signals that are 180° out of phase. The resulting voltages V_1 and V_2 are given by

$$V_1 = \frac{1}{2}V_o - \frac{1}{2}\cos(2\omega_r t) \tag{2.2}$$

and

$$V_2 = -\frac{1}{2}V_o + \frac{1}{2}\cos(2\omega_r t) \tag{2.3}$$

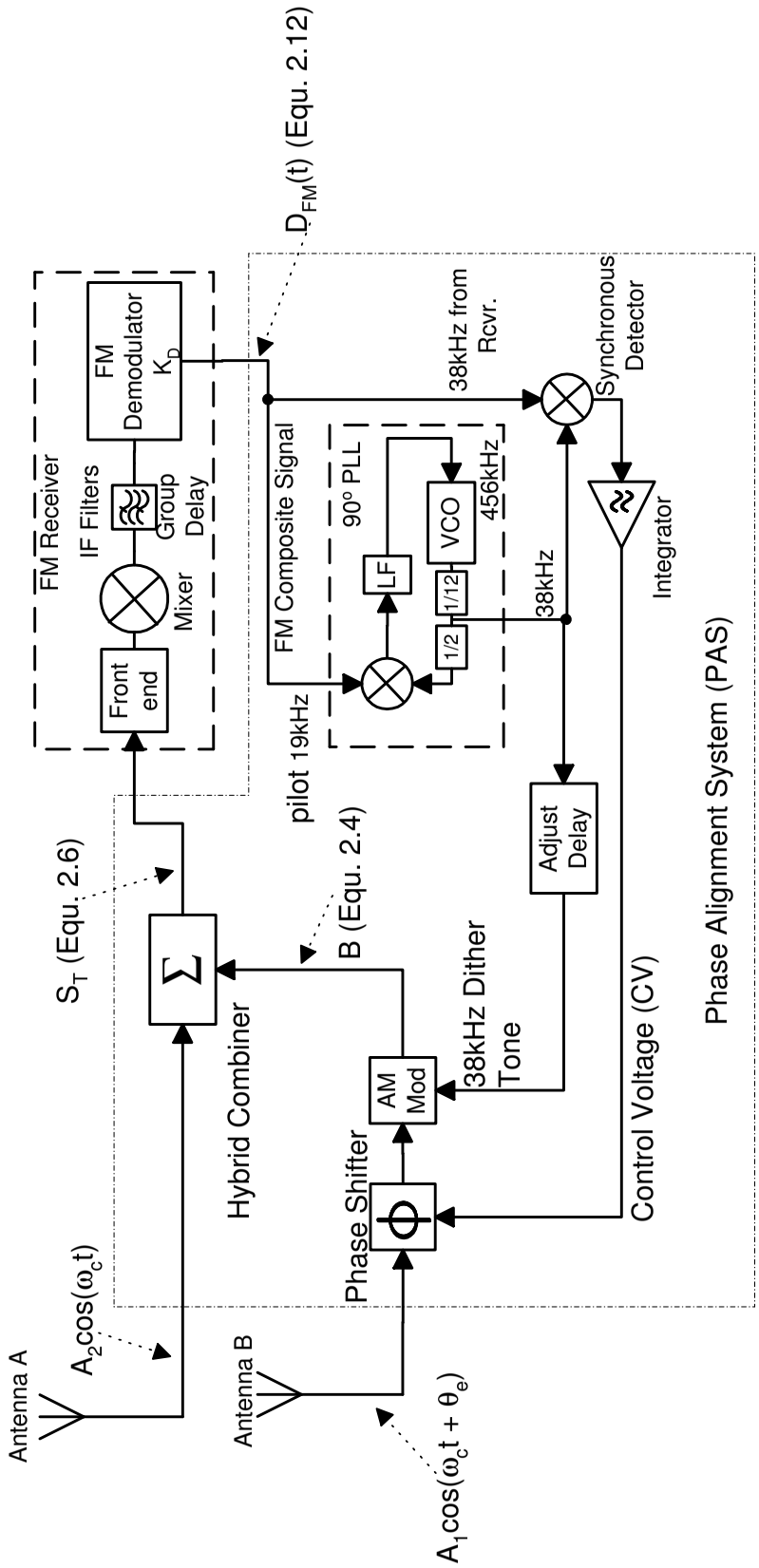

Figure 2.5: Example of a PAS block diagram.

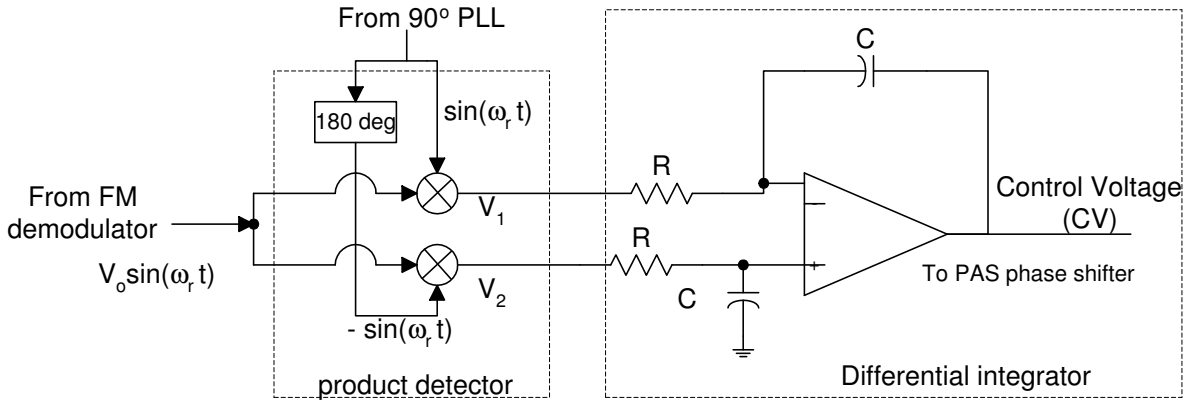

Figure 2.6: PAS product (synchronous) AM detector with 100μs time constant.

The differential integrator filters out the $\sin(2\omega_r t)$ components in both signals V_1 and V_2. The integrator DC output control voltage (CV) in this case is $-V_o$. When the input signal $V_o(t)$ is negative then CV is V_o. The control voltage is used to adjust the phase shifter for antenna B signal input. One section of the PAS phase shifter is shown in Figure 2.7 (A). The response of the phase shifter is shown in Figure 2.7 (B) where 3 sections are needed to achieve 360° phase shift. The integrator has a wrap around circuit that steps the control voltage when it reaches the high or low rail to shift the desired signal by 360 degrees. We

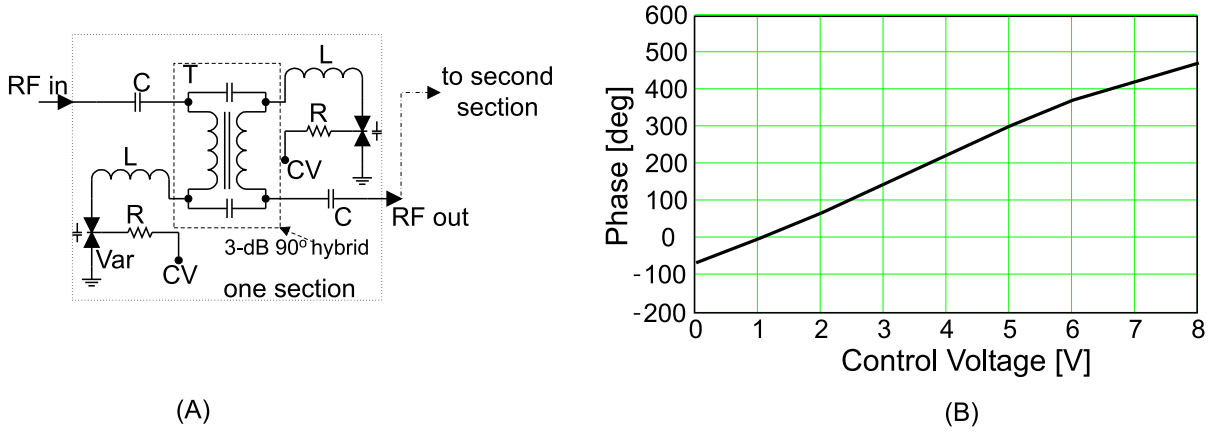

Figure 2.7: (A) One section of PAS phase shifter (B) PAS phase shifter response with 3 sections.

can obtain the slope of the phase shifter, K_p, from Figure 2.7. K_p will be used in the control loop analysis. One might realize the disadvantage of having a phase shifter at RF in the signal path especially in weak signal conditions. Any gain loss in the phase shifter is added directly to the total noise figure of the whole system. This is one of the design trades off in using a single receiver with a phase aligning diversity system. In addition, the phase shifter varactors that are shown in Figure 2.7 (A) can produce non-linear products if a large or strong signal is present (over-load condition). The phase shifter can be protected from over-load condition by adding an Automatic Gain Control (AGC) system ahead of it.

2.1.2 Mathematical Model of the PAS

We assume the reception of a carrier only with no FM modulation to simplify the mathematical analysis of the PAS system. The vectors in Figure 2.2 can be represented by the

following equations

$$B = A_1 \cos(\omega_c t + \theta_e) \cdot (1 + m \cos(\omega_r t)) \tag{2.4}$$

$$A = A_2 \cos(\omega_c t) \tag{2.5}$$

where A_1 and A_2 are the peak amplitudes of the two branches, ω_c is the carrier frequency, θ_e is the angle between the two signal vectors of the antennas, $m = \frac{A_r}{A_1}$ is the AM modulation index percentage, A_r is the AM modulation amplitude, and ω_r is the dither tone frequency, which is modulated in the PAS arrangement.

The sum of A and B will be represented by S_T. S_T will be the input to the FM receiver and will yield the following equation

$$S_T = A_3 \cos(\omega_c t + \phi_3) \tag{2.6}$$

where the total amplitude is

$$A_3 = \sqrt{A_1^2(1 + m \cos(\omega_r t))^2 + A_2^2 + 2A_1 A_2(1 + m \cos(\omega_r t)) \cos(\theta_e)} \tag{2.7}$$

and the resulting phase is

$$\phi_3 = \arctan\left(\frac{(\frac{A_1}{A_2})(1 + m \cos(\omega_r t)) \sin(\theta_e)}{1 + (\frac{A_1}{A_2})(1 + m \cos(\omega_r t)) \cos(\theta_e)}\right) \tag{2.8}$$

The input to the FM receiver S_T will go through the limiter before detection. The output of an ideal FM demodulator is

$$D_{FM}(t) = \frac{1}{2\pi} K_D \frac{\partial \phi_3}{\partial t} \tag{2.9}$$

where K_D is the FM demodulator constant in V/kHz and from Appendix E

$$\frac{\partial \phi_3}{\partial t} = \frac{-(\frac{A_1}{A_2}) \cdot m \cdot \omega_r}{R(t)} \sin(\omega_r t) \sin(\theta_e) \tag{2.10}$$

where

$$R(t) = 1 + 2 \cdot (\frac{A_1}{A_2})(1 + m \cos(\omega_r t)) \cos(\theta_e) + (\frac{A_1}{A_2})^2 (1 + m \cos(\omega_r t))^2 \tag{2.11}$$

Substitute equation 2.10 into equation 2.9 to obtain the output of the ideal FM demodulator

$$D_{FM}(t) = -\frac{1}{2\pi} K_D \frac{(\frac{A_1}{A_2}) \cdot m \cdot \omega_r}{R(t)} \sin(\omega_r t) \sin(\theta_e) \tag{2.12}$$

Equation 2.12 shows that the output of the FM demodulator is a signal of the dither tone frequency. The amplitude is proportional to the sine-function of the error angle θ_e. This tone vanishes only when $\theta_e \equiv 0$ which means that the antenna signals appear phase aligned before they are added in the sum block. The output can be used as the control signal to reduce the phase difference between the two antenna signals as described in the previous section.

2.1.3 PAS Control Loop System Modelling

The closed loop equation of the loop has a low pass filter response and the 3dB-loop bandwidth is dependent on the total gain of the system. It is important to note that this approximation is valid because the poles of the FM detector and PAS' phase shifter are too far away from the dominant integrator pole of the PAS. For that reason we can approximate the phase shifter and FM detector by constant gain factors. Figure 2.8 shows an approximated control loop model of the PAS. The closed loop equation can be easily evaluated, using Figure 2.8,

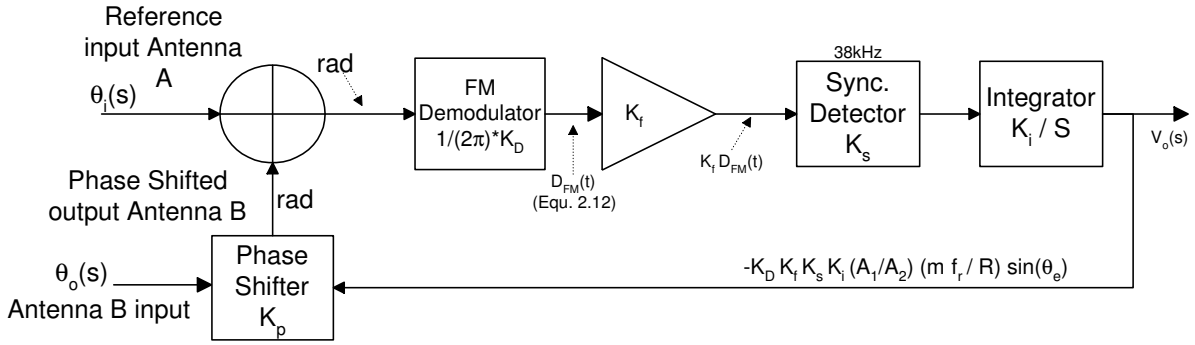

Figure 2.8: PAS control loop block diagram.

to be

$$T(s) = \frac{V_o(s)}{\theta_i(s)} = \frac{a}{s + aK_p} \tag{2.13}$$

where

$$a = K_D K_f K_s K_i \tag{2.14}$$

where K_p is the phase shifter constant in rad/V, K_D is the FM detector constant in V/kHz, K_f is a gain constant, $K_s = \frac{2}{\pi}$ is the synchronous detector constant, $K_i = \frac{1}{RC}$ is the integrator constant, and $s = \jmath\omega$ is the Laplace variable.

The 3dB frequency is

$$f_{3dB} = \frac{aK_p}{2\pi} \quad \text{[Hz]} \tag{2.15}$$

Note that K_s, K_f, K_i, and K_p are internal parameters of the PAS applied blocks.

When a mobile unit travels at a speed of $60mph$, the maximum Doppler shift for a $100MHz$ carrier frequency is calculated to be in the order of $9Hz$ (Equation 1.11). Therefore, the $3-dB$ loop bandwidth should be adjusted to double of maximum Doppler frequency (Doppler bandwidth or case of half wave length). This is shown in Figure 1.9 (B) (Section 1.2.1) which shows a Doppler shift of $20Hz$ in the high end of the spectrum.

The mathematical model is used to show the low pass frequency response and step response of the PAS system in Figures 2.9 and 2.10, respectively. The parameters were chosen so that the $3-dB$ loop bandwidth is $20Hz$ to reject any erroneous frequencies (section 2.1.4) that caused by long delay multi-path or adjacent channel. In addition, the control loop can follow frequency changes due to doppler in case of short delay multi-path. The calculations were done with $K_D = 10mV/kHz$, $K_f = 1.7$, $K_i = 10000Hz$, and $K_p = 1.31rad/sec$.

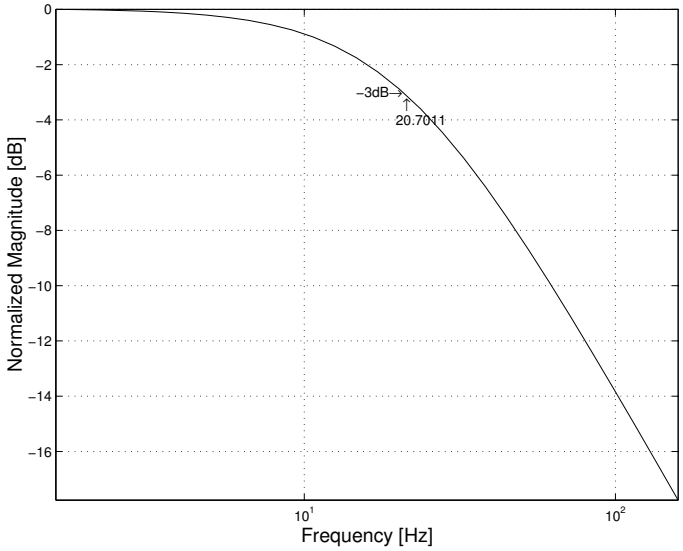

Figure 2.9: PAS Low Pass Frequency Response

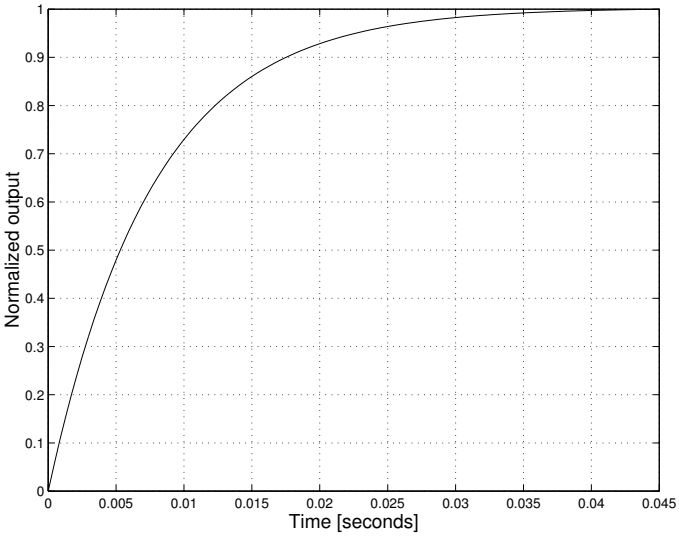

Figure 2.10: PAS Step Response

Figure 2.9shows the $3-dB$ loop bandwidth of about 20.7 Hz for the modelled system. This agrees with the desired frequency response of the actual system.

2.1.4 PAS Multi-path Performance

Short Delay Multi-path:

In order to reduce short delay multi-path fades (Rayleigh fading field), the PAS system was a reliable solution [9] because it reduces the likelihood that the sum signal would fade. Figure 1.11 (A) helps illustrate this point. When the two envelopes are added, it is evident that the fading peaks are reduced. Figure 2.11 shows simplified loop block diagram of the PAS system. Suppose Antenna A incoming signal A_1 is the reference with angle modulation of $\phi_1(t)$. The incoming signal to Antenna B has an angle of $\phi_2(t)$ relative to Antenna A signal. Assume $f_{3dB} = 20Hz$ (as described in the previous section) and the incoming signals has no excess delay ($\dot{\phi}_1(t) \approx \dot{\phi}_2(t)$). When the system initially feeds the FM demodulator with the sum of both antenna signals , the feed back loop system produces a voltage proportional to phase difference between both antenna signals. In this case, the phase shifter voltage adjusts the phase of signal A_2 by $\phi_2(t)$ to align both antennas in phase. The frequency difference, due to Doppler shifts, between the incoming signals is less or equal to $20Hz$. For detailed discussion of short delay multi-path and Doppler, refer to Section 1.2.1.

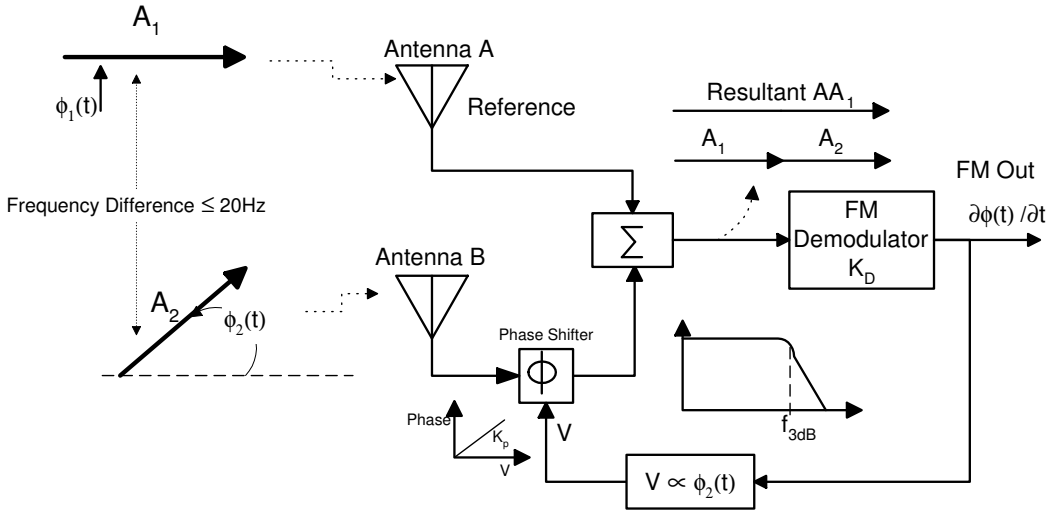

Figure 2.11: Simplified Loop Block Diagram of the PAS System

Long Delay Multi-path:

The PAS System (or any two antennas combining system with slow frequency response, i.e. $f_{3dB} \leq 20Hz$) suffers from phase tracking of the incoming signals when it encounters long delay multi-path (delay time $\tau > 5\mu sec$). This can be illustrated by the analysis of the simplified control loop block diagram of the PAS. We will assume a value for the 3-dB loop bandwidth f_{3dB}, shown in Figure 2.11, then discuss different cases of the incoming antenna signals.

Before we begin analyzing PAS long delay multi-path performance, it is important to examine the resulting erroneous or extra angle deviation $\Delta\phi(t)$ due to time delay τ between two carrier signals (shown in Figure 1.11 (B)). Straight forward analysis of the resulting erroneous angular deviation $\Delta\phi(t)$ leads to Equation 1.12.

It is displayed here again for convenience

$$\Delta\phi(t) = \arctan\left(\frac{\frac{A_1}{A_o}\sin(\phi(t-\tau)-\phi(t))}{1+\frac{A_1}{A_o}\cos(\phi(t-\tau)-\phi(t))}\right)$$

where A_o and A_1 are arbitrary fixed amplitudes.

When two envelopes of Figure 1.11 (A) are equal at one point (as shown with the circled part) and one of them has excess time delay, the resulting erroneous angle deviation is high. This produces highly distorted audible signal when FM demodulated as shown in Figure 1.12. A 3-D plot of the maximum resulting erroneous angle deviation as a function of τ and $\frac{A_1}{A_o}$ is shown in Figure 2.12 to help illustrate the point. Equation 1.25 is used for $\phi(t)$ with frequency deviation $f_d = 75kHz$ and modulation frequency $f_m = 1kHz$. Figure 2.13 shows the frequency spectrum of $\Delta\phi(t)$ for $\tau = 30\mu sec$ and amplitude ratio $\frac{A_1}{A_o} = 0.9$. The feedback loop in the PAS system responds to change in phase difference between the added signals. Therefore, we are concerned with the frequency spectrum of $\Delta\phi(t)$ because we want to relate it to the 3-dB loop bandwidth of the PAS system.

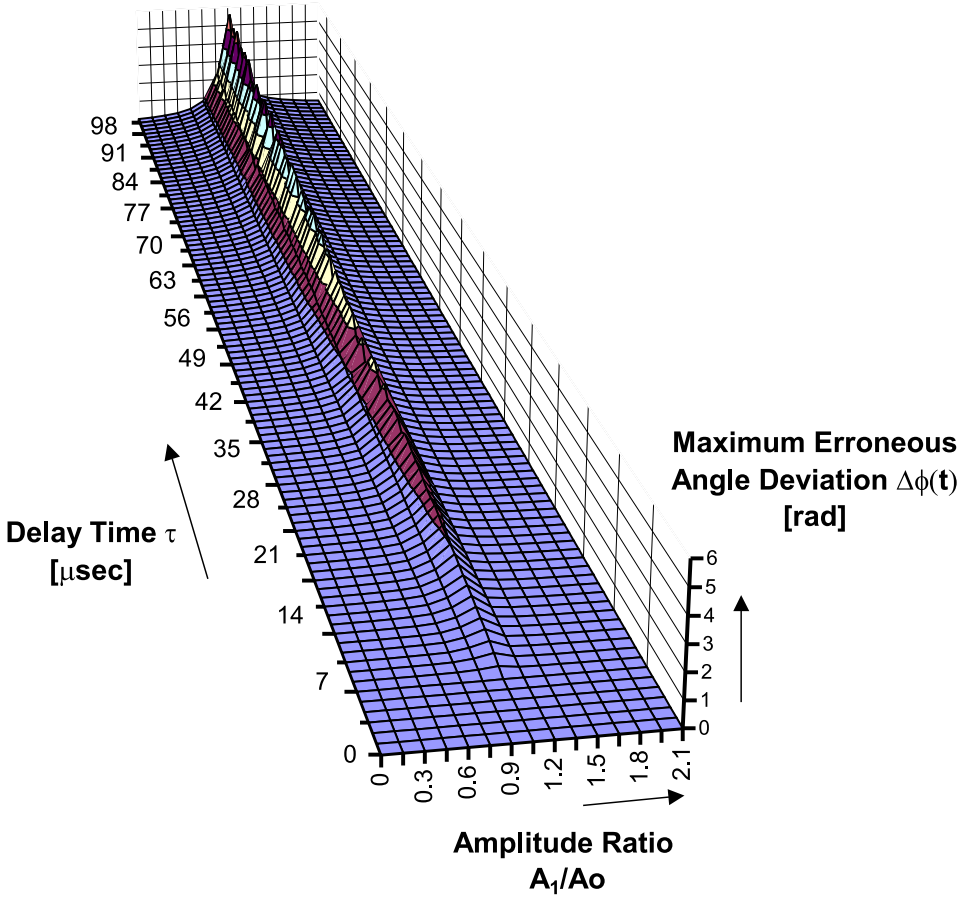

Figure 2.12: Maximum Erroneous Angular Deviation $\Delta\phi(t)$ as a function of τ and $\frac{A_1}{A_o}$. Parameters: $f_d = 75kHz$ and $f_m = 1kHz$

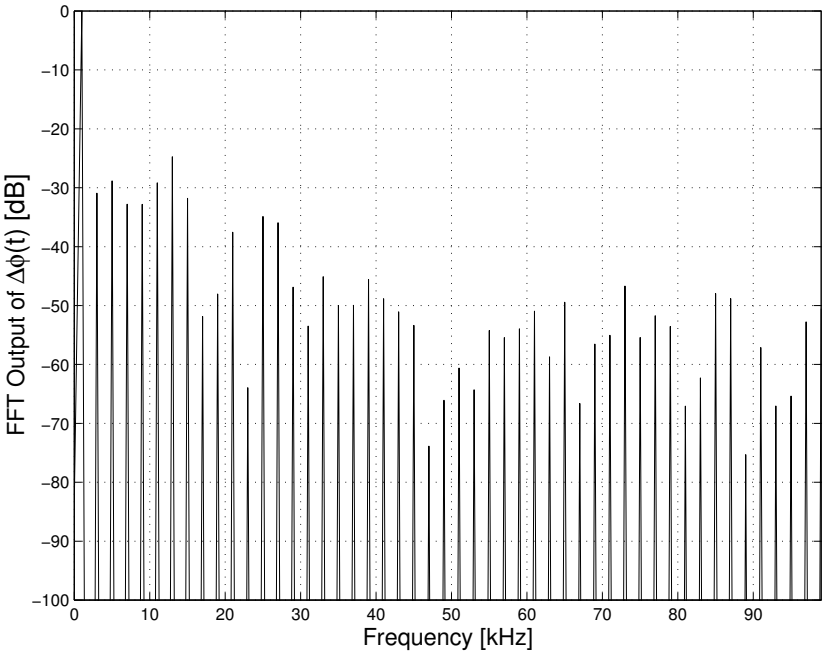

Figure 2.13: Spectrum of the Resulting Erroneous Angular Deviation $\Delta\phi(t)$. Parameters: $f_m = 1kHz$, $f_d = 75kHz$, $\tau = 30\mu sec$, $\frac{A_1}{A_o} = 0.9$

Now let us begin to analyze the signal combining system (PAS) with different incoming signal scenarios.

Figure 2.14 (a) and (b) show simplified PAS block diagrams with input signal vectors of two cases 1 and 2, respectively. The two cases are described below. The block diagram shows a simplified control loop of the PAS with the resulting signal vector after the summer. Antenna A signal considered the reference because it is not phase shifted. The control loop reacts to phase changes between the two antenna signals. Therefore, the input voltage to the phase shifter is proportional to the phase difference between the two antenna signals. The low-pass filter diagram indicates the f_{3dB} loop bandwidth frequency. *assume* $f_{3dB} = \infty$ in Figure 2.14.

Case 1:

The incoming signal to Antenna A has distortion due to $\Delta\phi(t)$ and the input signal of antenna B is not distorted, therefore the input signal to the phase shifter is not distorted. In this case, the loop will adjust the phase of signal A_2 to align it with the resultant signal AA_1. The total sum is increased in amplitude but phase aligned at the erroneous angle $\Delta\phi(t)$. Therefore, the total signal has same distortions as the erroneous signal of AA_1 and are fully audible due to $\Delta\phi(t)$ (Equation 1.12), when FM demodulated. In this case, the system enforces the distortions received with one antenna onto the undistorted antenna signal.

Case 2:

Antenna B receives a direct plus delayed signal, whereas Antenna A receives direct signal only. Due to the infinite 3-dB loop bandwidth, the system is able to compensate for $\Delta\phi(t)$. The resultant AA_1 will be aligned with A_2 in phase after the summer. The FM demodulator output will have the desired undistorted information.

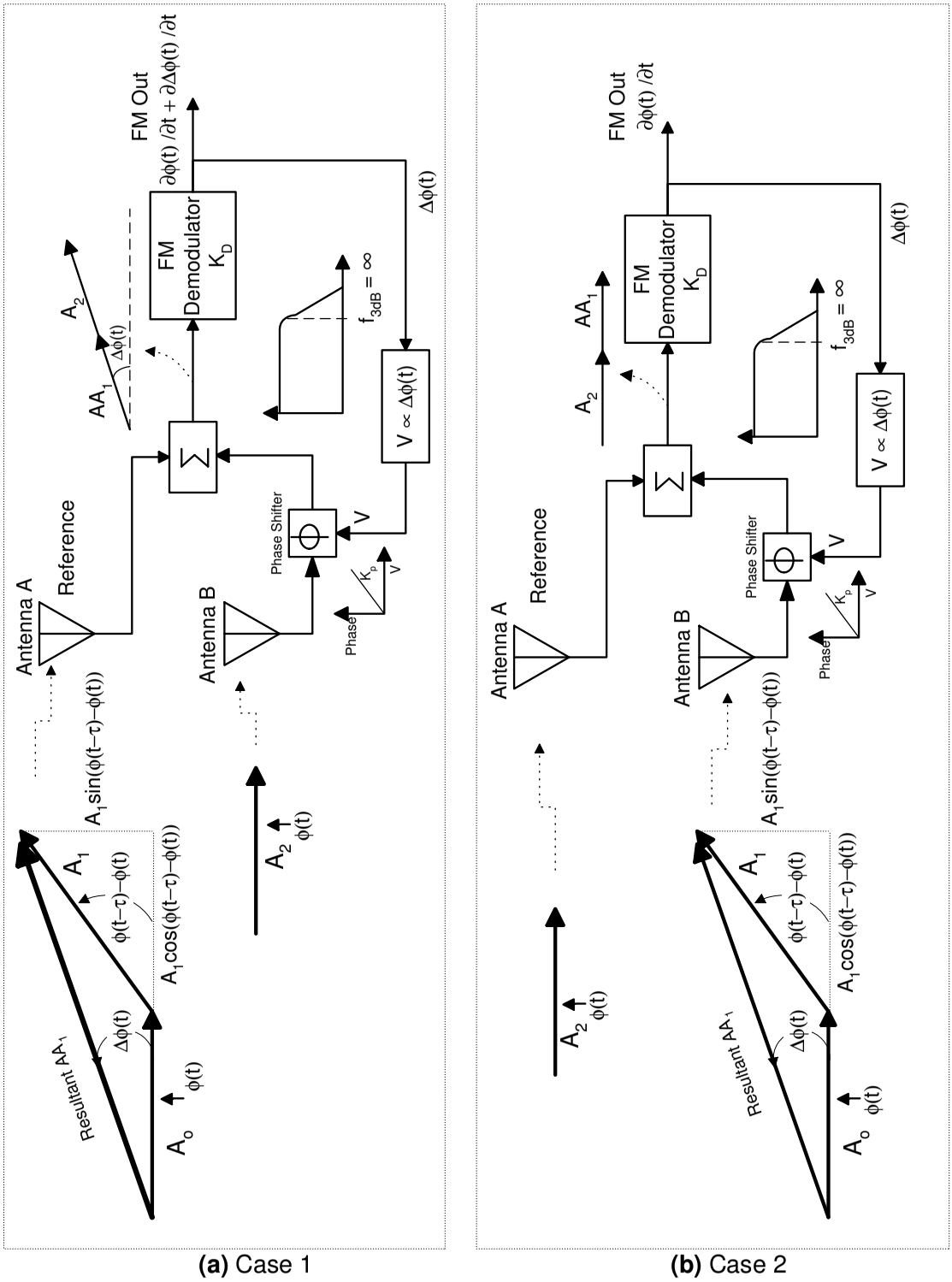

Figure 2.14: Two cases of signal receptions with $f_{3dB} = \infty$

Figure 2.15 is the same as Figure 2.14 but *assumes* $f_{3dB} = 20Hz$.

Case 1:

Antenna A receives the distorted resultant AA_1 and Antenna B receives the direct signal A_2. $\Delta\phi(t)$ is rotating very fast and it has very high frequency spectrum compared to the frequency response of the system. Therefore, the system can not align the two signals in exact phase. Nevertheless, A_2 is added at random phase (shown at the output of the summer) to the distorted resultant AA_1 which results in less distorted signal. In this case, the FM demodulator output will be distorted due to $\Delta\phi(t)$.

Case 2:

Antenna B receives the distorted resultant AA_1 and Antenna A receives the direct signal A_2. $\Delta\phi(t)$ is rotating very fast as in case 1. The frequency difference between the resultant received by Antenna A and the signal of Antenna B is still very high ($>> 20Hz$). Therefore, the feed back system would not be able to align the two signals in phase. In this case, the loop has little effect on the phase of resultant AA_1. Therefore, it passes through the phase shifter almost unchanged and simply adds to A_2. In result, the FM demodulator output will be distorted due to $\Delta\phi(t)$.

Conclusion:

The PAS system is designed to combat slow fading signal field (Rayleigh fading). In case of long delay multi-path, if one of the antennas is distorted, the PAS adds the distorted antenna to the undistorted antenna without any knowledge of the antennas signal conditions. Therefore, the system needs a fast distortion detector so that the PAS knows when and whether to add both antenna signals at a given time. This is the main motivation to implement a new and more sophisticated FM diversity system that can handle both short and long delay multi-path. This new system has been designed and realized in the present dissertation. It is described in Chapter 4.

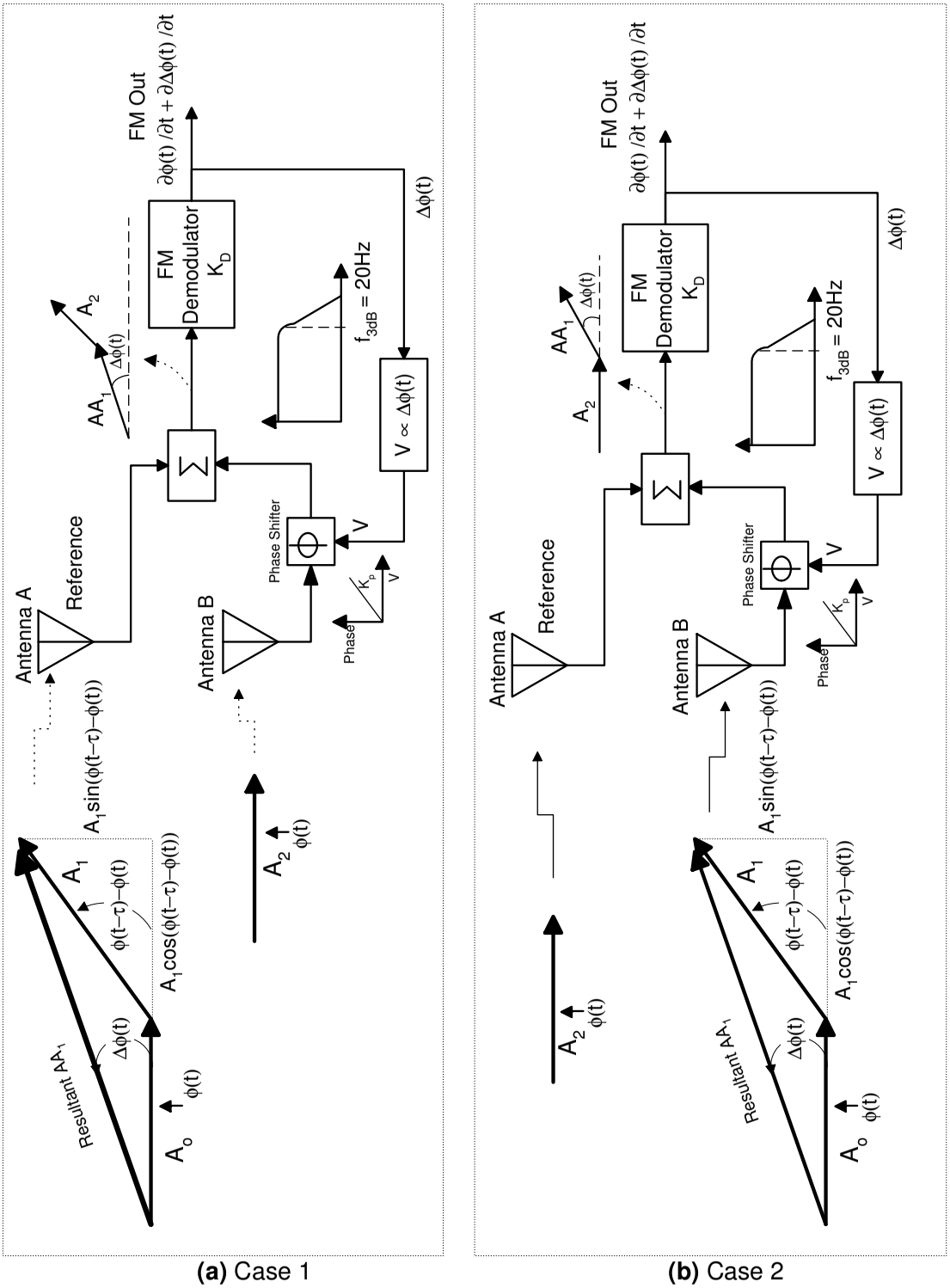

Figure 2.15: Two cases of signal receptions with $f_{3dB} = 20Hz$

The required hardware setup in the lab to verify the two cases of Figure 2.15 is shown in Figure 2.16 and is described in the following. The input Audio Frequency (AF) signal f_m is directed to the AF long delay device which provides a long delay range 5-200μsec. The time delay can be done at the audio frequency because the angle between the RF carriers (FM frequency range) hardly has an affect on the resulting distortion from long delay [20]. Suppose that the two RF carriers are summed up at an angle of 90° at $100MHz$, then the associated time delay between them is $2.5nSec$ which is very small compared to long delay multi-path standards (typically above $5\mu sec$ delay). The Ref signal is the audio input to external modulation input of RF generator 1 and the Delayed audio is the input to RF generator 2. Both RF generators have the same oscillator signal so that the generated RF signals have the same phase reference. RF generator 1 provides undistorted reference signal and RF generator 2 provides the distorted signal. RF generator 1 signal is divided by the power splitter. One output is $20dB$ attenuated and goes straight to antenna A input. The other power splitter output is also $20dB$ attenuated and adds with the $20dB$ attenuated RF generator 2 signal to provide antenna B input. The attenuators are used as isolators between the signals. The input of the receiver is connected to the PAS output. The direct FM demodulator output and the control voltage of the PAS are monitored with a digital scope.

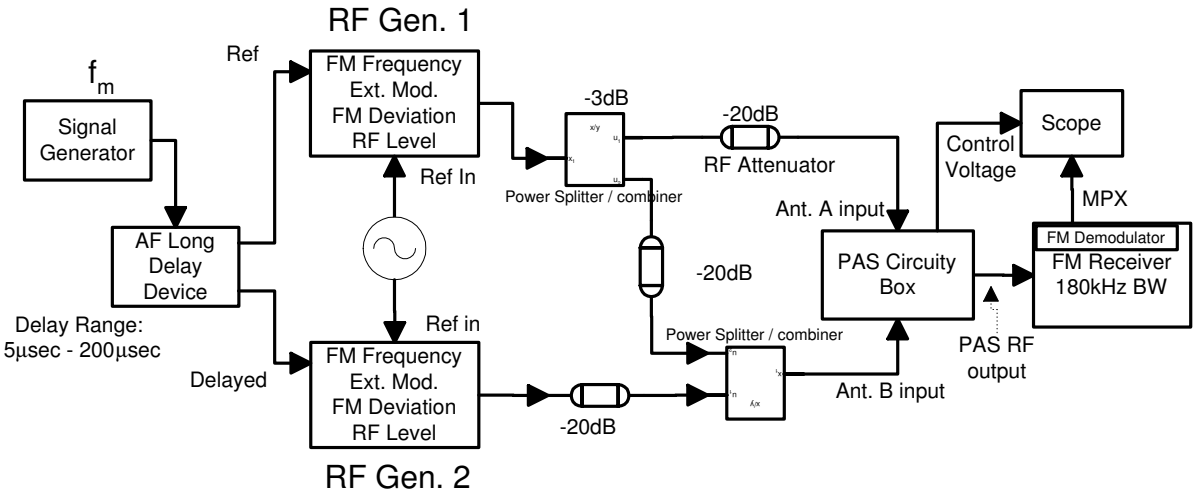

Figure 2.16: Hardware Setup to Test PAS Performance in Long Delay Multi-path

The parameters used are: Time delay $\tau = 30\mu sec$, frequency deviation $f_d = 75kHz$, modulation frequency $f_m = 1kHz$, amplitude ratio $\frac{A_1}{A_o} = 0.9$. Both RF generators are tuned to $90.5MHz$ with $-50dBm$ RF level. The FM receiver has a bandwidth of $180kHz$.

Figure 2.17 shows the FM demodulator output of the resulting signal AA_1 of Antenna A only (no signal on Antenna B and PAS is off). This is done so we can compare the distortions of a single receiver to the resulting distortions with the PAS system. In this case, the distortion peaks are evident and cause audible distortions. Figure 2.18 shows the FM demodulated output of Antenna B only(no signal on Antenna A and PAS is off). The FM output has no distortions. Figure 2.19 shows the demodulated output of the incoming signals in Case 1 ($f_{3dB} = 20Hz$). The distortion peaks are less in amplitude, compared to Figure 2.17, but they are still evident and cause audible distortions. Figure 2.20 shows the demodulated output of the incoming signals in Case 2 ($f_{3dB} = 20Hz$). The FM output is still distorted.

The distortion peaks are different in Figures 1.12 and 2.17 for several reasons. First, the AF long delay device is not exact. Second, the peaks of Figure 2.17 are limited in amplitude due to the IF filter in the FM receiver. Finally, the FM demodulator used to obtain Figure 1.12 is ideal. Whereas the FM receiver in Figure 2.16 uses quadrature FM demodulator.

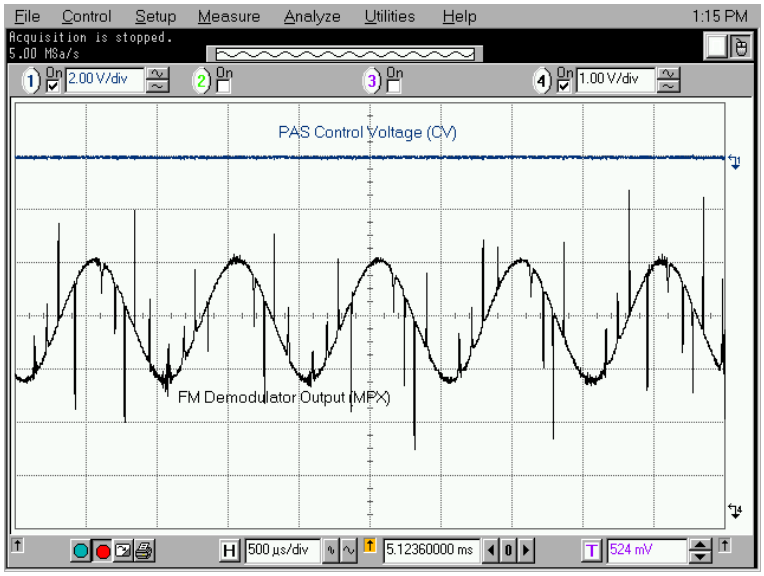

Figure 2.17: FM Demodulated Output of Antenna A Signal only. Parameters: $f_d = 75kHz$, $f_m = 1kHz$, $\tau = 30\mu sec$, $\frac{A_{11}}{A_2} = 0.9$

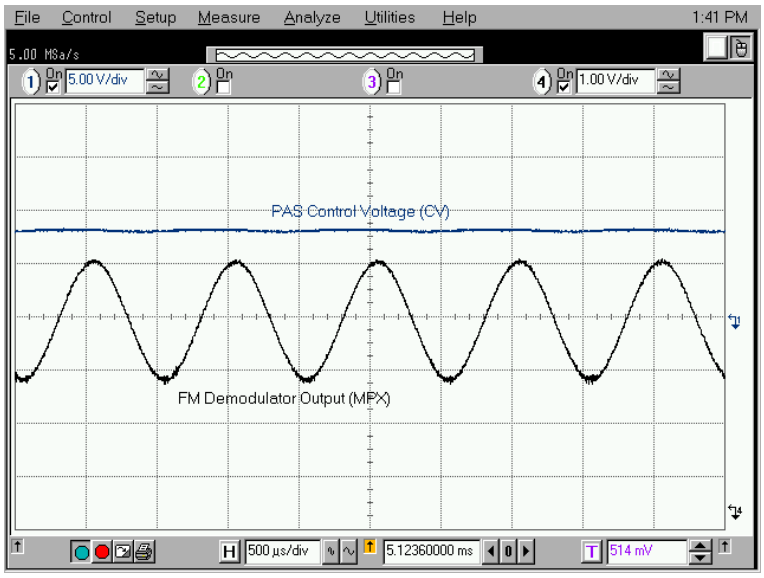

Figure 2.18: FM Demodulated Output of Antenna B Signal only: Parameters: $f_d = 75kHz$, $f_m = 1kHz$

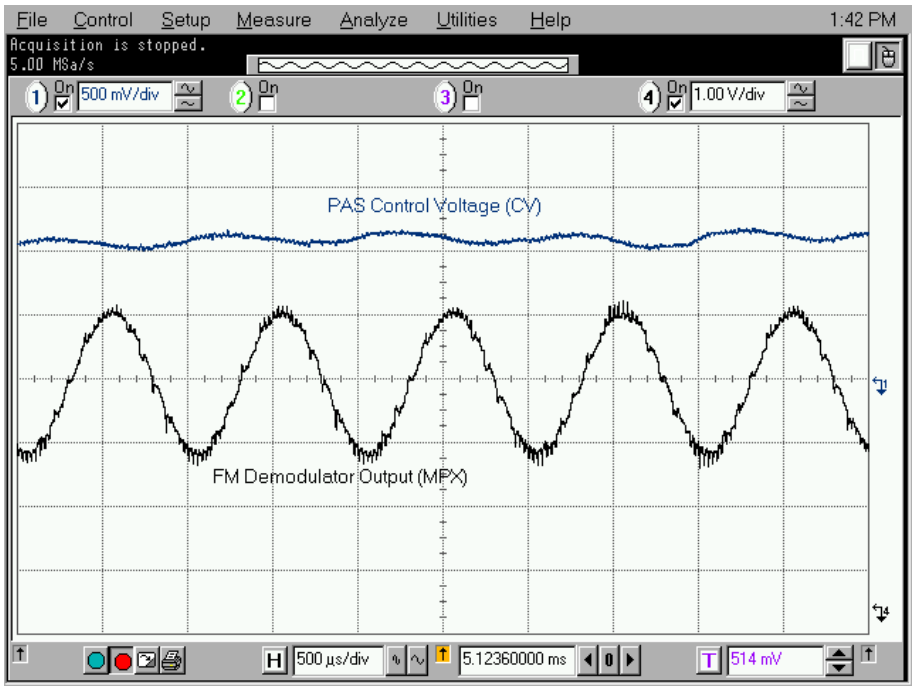

Figure 2.19: FM Demodulated Output of the sum of antennas A and B inside the PAS box (Case 1, $f_{3dB} = 20Hz$). Parameters: $f_d = 75kHz$, $f_m = 1kHz$, $\tau = 30\mu sec$, $\frac{A_{11}}{A_2} = 0.9$

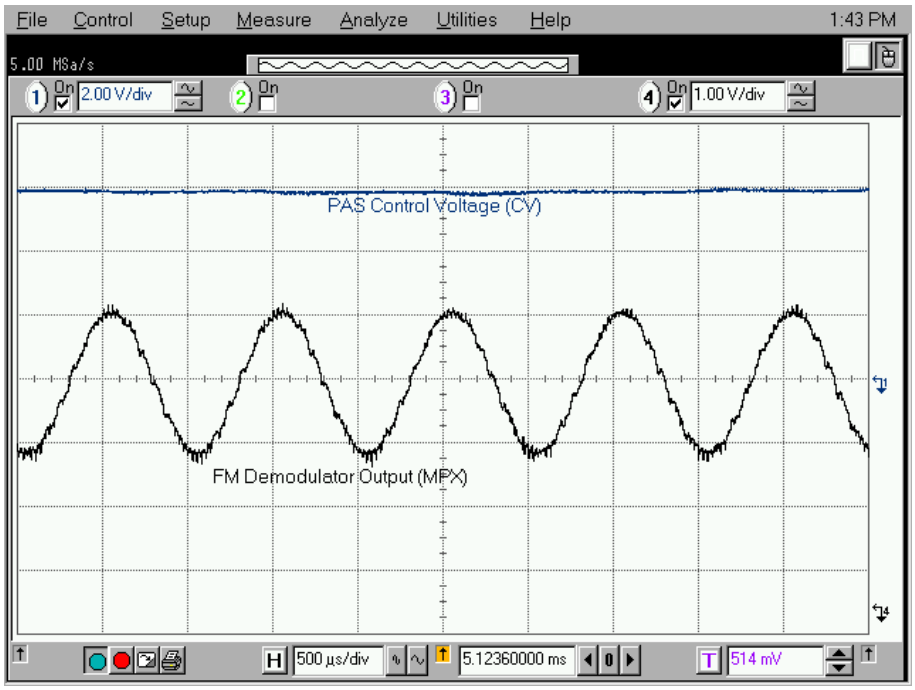

Figure 2.20: FM Demodulated Output of the sum of antennas A and B inside the PAS box (Case 2, $f_{3dB} = 20Hz$). Parameters: $f_d = 75kHz$, $f_m = 1kHz$, $\tau = 30\mu sec$, $\frac{A_{11}}{A_2} = 0.9$

2.2 Switched Antenna System (SAS)

In Chapter 1, we discussed both long and short delay multi-path propagations. In case of short delay, the RF carrier experiences amplitude minima as shown in Figure 1.7. In long delay multi-path, the erroneous phase deviation causes erroneous pulses in the FM demodulated signal along with deep amplitude minima in the RF carrier as shown in Figure 2.21.

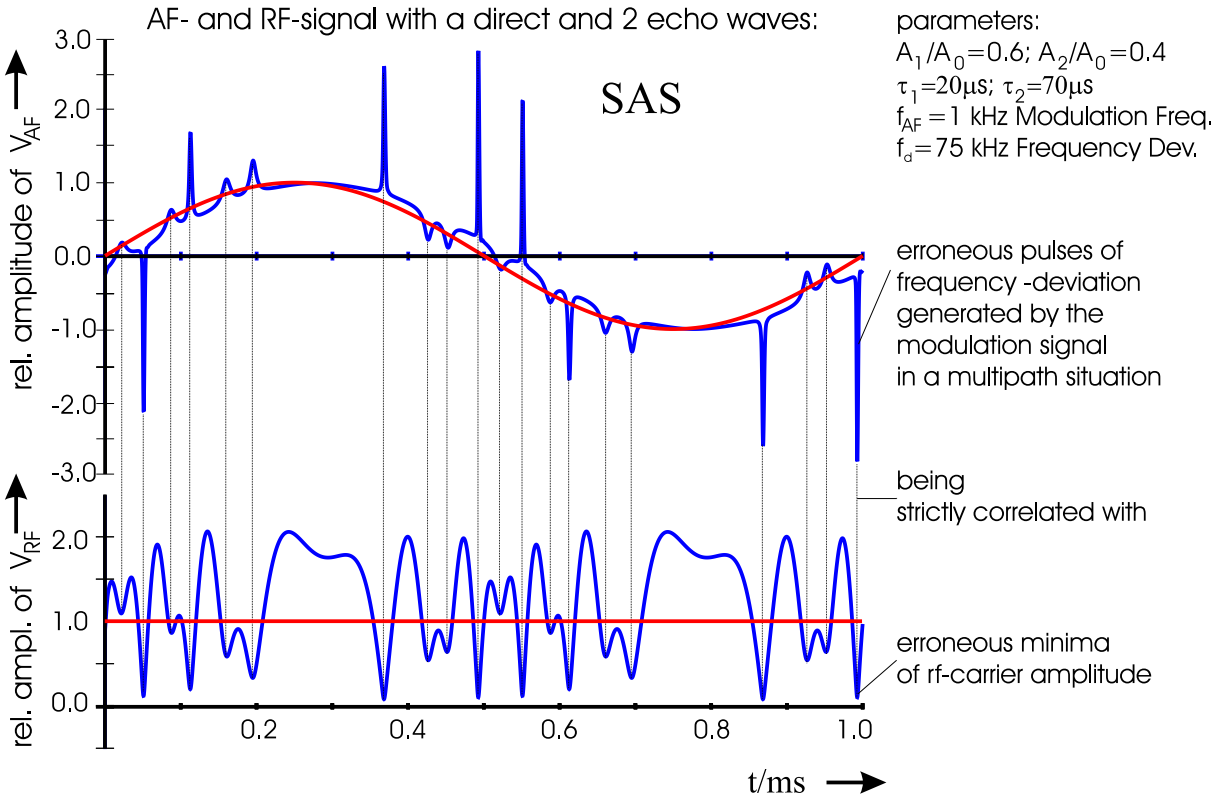

Figure 2.21: Long Delay Multi-path and its effect on FM-signal [25]

The correlation between the erroneous pulses and the amplitude minima is an excellent and fast indication for distortion [26]. Switching Antenna System (SAS) recognizes the above mentioned correlation and is called Fast Distortion Detector (FDD). It takes both the FM demodulator and the voltage level (proportional to RF level) outputs from a standard FM receiver as shown in Figure 2.22 [25]. The signals go through non-linear circuits so that the erroneous pulses and amplitude minima are shaped in steepness. The AND (&) circuit indicates the presence of the erroneous pulse in the frequency deviation and amplitude minima in the RF carrier. When this occurs, the binary logic switches to a different antenna without any recognizable delay in search for less distorted antenna.

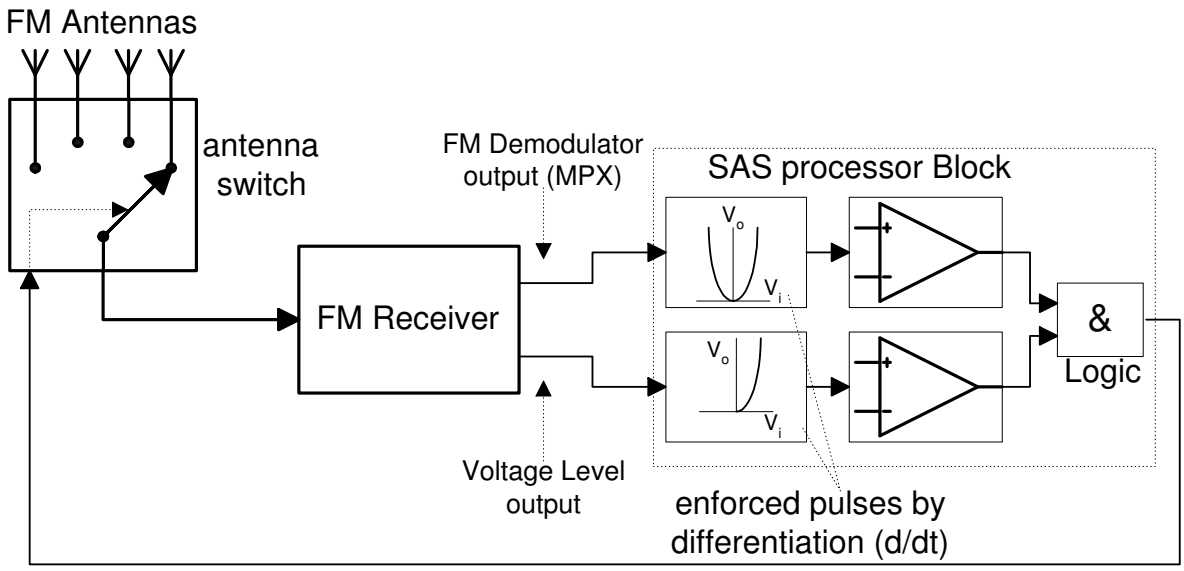

Figure 2.22: Basic circuitry of SAS interfaced with a standard FM receiver

The SAS processor block that is shown in Figure 2.22 has the following features [25]:

• Extremely fast distortion recognition time of approximately $30\mu sec$.

• Adaptive reduction of distortion recognition sensitivity with increasing median distortion rate of all antennas (time constant in the range of seconds).

• Individual floating thresholds for each antenna, depending on the individual median distortion occurrence, generating a floating priority list (time constant in the range of seconds).

Chapter 3

Scanning Phasing Antenna Diversity System and Diversity Effectiveness n

Many papers have been written about diversity effectiveness **n** in recent years [25] [27] [28] [29]. It is a computation method that provides performance information for a specific diversity system when compared to single antenna performance in the car. When computing **n**, the measured antenna gain patterns and the electrical coupling between the antennas are included. Therefore, a close approximation of the FM diversity performance in car is obtained. The next section reviews the basics of **n** computation.

3.1 Computation of n and 4-Ports S-Parameters

Let P represents the probability of signal-to-distortion ratio not to exceed a certain threshold level in an FM channel. For scanning (or selection) diversity, the probability that all channels or antennas have signal-to-distortion less than the threshold is given by the product of the single probabilities of each channel [5]

$$P_d = P_s^N \tag{3.1}$$

where subscript d represents diversity mode and s represents single antenna mode. N is the integer number of the uncorrelated physical antennas or independent, identically distributed antennas (i.i.d.). In the following, the benefit resulting from diversity techniques applied to closely packed antennas on a car is regarded in accordance to [25]. The signal quality is defined as

$$q = 20\log(\frac{1}{P}) \quad [dB] \tag{3.2}$$

The improvement factor i_f due to using diversity rather than single antenna mode is defined by

$$i_f = q_d - q_s \tag{3.3}$$

Simple mathematical manipulations of Equations 3.1 and 3.2 lead to the following equation for the number of uncorrelated antennas

$$N = \frac{q_d}{q_s} \tag{3.4}$$

In practice, we have multiple antennas on one window as shown in Figure 1.17. Such antenna arrangements are not completely uncorrelated. Therefore, equation 3.4 becomes

$$\mathbf{n} = \frac{q_d}{q_s} \tag{3.5}$$

where **diversity effectiveness n** is defined as **the number of effective uncorrelated antennas for scanning diversity systems**. **n** will always be less than N (for selection diversity) in practice and $n = N$ has been shown when the antennas are ideally uncorrelated.

Although we compute **n** to evaluate the performance of a selection diversity system, it has been proven by [30] that **n** is independent from P_s. The correlation between the antenna signals results in the fact that **n** is no longer an integer number being found in the area of observation. It has also been shown by [30] that $P_d = P_s^n$ can be used to evaluate the performance of other diversity schemes such as Scanning Phasing Antenna System (SPAS) that is described in the next section and in more details in chapter 4.

The following simplified steps are to compute **n** and compare the performance of a variety of diversity schemes to a single antenna. Therein, it is shown to be of importance by which impedance the passive antenna structures are loaded at their terminals. This is due to the fact that the load impedances influence the currents on adjacent antenna structures and therewith have an effect on the correlation coefficient of the antenna signals. As a result, different values of the diversity effectiveness **n** are found for different terminations of the antennas.

Step 1: Generate the desired and undesired signals that have spatial Rayleigh field distribution in a virtual drive. This can be done as described in section 1.2.1. Figure 3.1 shows an example of such signals. The undesired signal represents adjacent or co-channel interference.

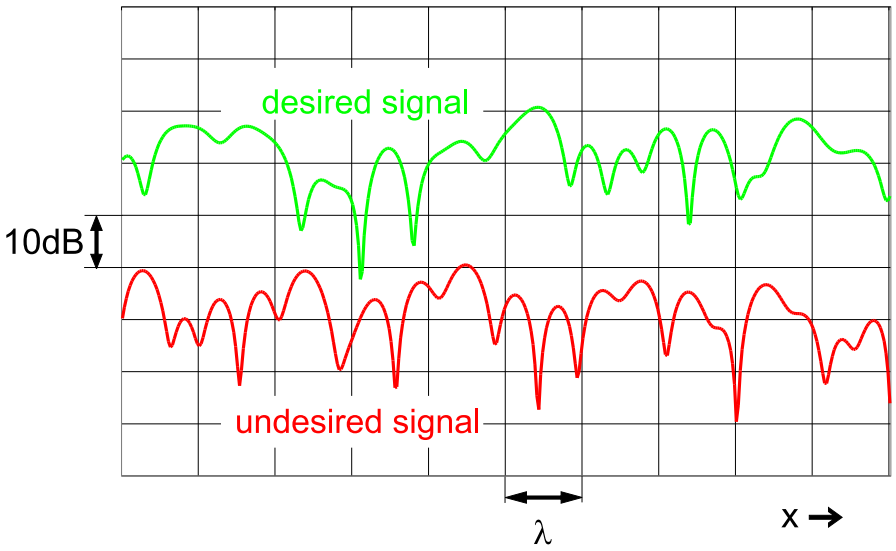

Figure 3.1: Desired and undesired signals used in computing **n** [25]

Step 2: A single antenna signal-to-distortion ratio is simply the difference between the desired and undesired signals in dB as shown in figure 3.2.

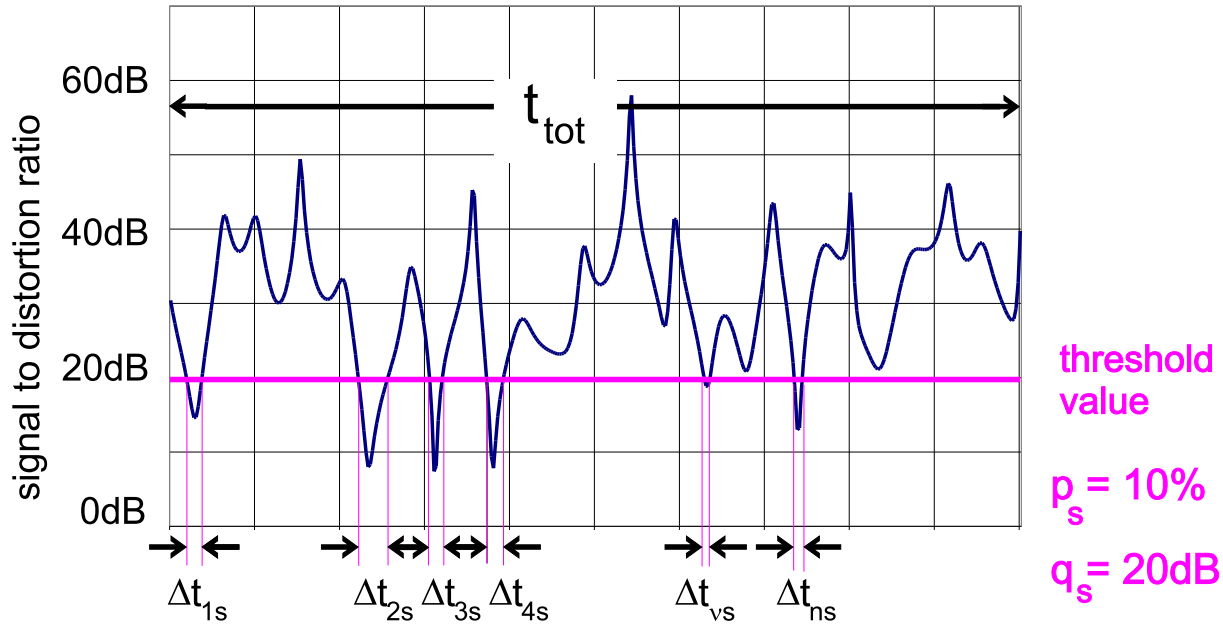

Figure 3.2: Resulting signal-to-distortion ratio of a single antenna [25]

The probability that the signal-to-distortion ratio is less than a given threshold for a single antenna is computed by finding the sum of all time intervals Δt that are below the desired threshold then dividing it by the total time

$$P_s = \frac{\sum_{\nu} \Delta t_{\nu s}}{t_{tot}} \tag{3.6}$$

Step 3: Generate the virtual drive of multiple periods of 20λ to expose the measured antennas to Rayleigh fading field (total of 400λ is adequate for gathering the statistics for the signal quality). Find the resulting signal-to-distortion for the desired diversity schemes, i.e. scanning or combining. Finally, compute the signal quality and **n** for each diversity scheme and compare it to a single antenna.

It is desired to compare the performance of three diversity schemes (PAS, SAS, and SPAS) with all antennas are placed on one window as shown in Figure 1.17. This is done in the next section. Before we compute **n** for each diversity scheme with all possible antenna combinations, we need to analyze 4-ports antenna window network. Figure 3.3 shows 4 antennas represented as 4-ports network. The complex S-parameters matrix (couplings) is given by

$$\underbrace{\begin{bmatrix} \underline{B}_1 \\ \underline{B}_2 \\ \underline{B}_3 \\ \underline{B}_4 \end{bmatrix}}_{[\mathbf{B}]} = \underbrace{\begin{bmatrix} \underline{S}_{11} & \underline{S}_{12} & \underline{S}_{13} & \underline{S}_{14} \\ \underline{S}_{21} & \underline{S}_{22} & \underline{S}_{23} & \underline{S}_{23} \\ \underline{S}_{31} & \underline{S}_{32} & \underline{S}_{33} & \underline{S}_{33} \\ \underline{S}_{41} & \underline{S}_{42} & \underline{S}_{43} & \underline{S}_{44} \end{bmatrix}}_{[\underline{\mathbf{S}}_{\mathbf{p}}]} \cdot \underbrace{\begin{bmatrix} \underline{A}_1 \\ \underline{A}_2 \\ \underline{A}_3 \\ \underline{A}_4 \end{bmatrix}}_{[\mathbf{A}]} \tag{3.7}$$

where $\underline{A}$ is the received complex wave and $\underline{B}$ is the reflected complex wave (underline indicates complex value). The reflection coefficient is defined by

$$\underline{\Gamma} = \frac{\underline{Z}_L - Z_o}{\underline{Z}_L + Z_o} \tag{3.8}$$

where Z_L is the load impedance and Z_o is the characteristic impedance (in this case $Z_o = 50\Omega$).

The received wave $\underline{A}$ is related to the reflected wave $\underline{B}$ by

$$\underline{A} = \underline{\Gamma} \cdot \underline{B} \tag{3.9}$$

The antenna gain diagram for each antenna is measured with a Network Analyzer (NWA) as shown in Figure 3.3, indicated with the dotted lines. For example, when measuring port 2, the NWA P1 generates the transmitted wave A_t and feeds it to the far field test antenna. We measure the antenna response (phase and amplitude) with P2 of the NWA. In this case, all the other antennas are terminated with 50Ω loads. The same procedure is done for the other ports. Refer to section 1.4 for more details.

The antennas gain pattern measurements need to be added to Equation 3.7 so that the system is fully characterized. Equation 3.7 becomes

$$[\underline{\mathbf{B}}] = [\underline{\mathbf{S_p}}] \cdot [\underline{\mathbf{A}}] + \underbrace{\begin{bmatrix} \underline{S}_{t1}(\varphi) \\ \underline{S}_{t2}(\varphi) \\ \underline{S}_{t3}(\varphi) \\ \underline{S}_{t4}(\varphi) \end{bmatrix}}_{[\underline{\mathbf{S}}_{\mathbf{t}}(\varphi)]} \cdot \underline{A}_t \tag{3.10}$$

where $\underline{A}_t = \underline{V}_t \cdot \sqrt{Z_L}$ is the transmitted wave and $\underline{V}_t$ is the transmitted voltage. $\underline{S}_{t1}(\varphi) - \underline{S}_{t4}(\varphi)$ represent the measured gain of each antenna (transmission vector) measured in amplitude and phase as a function of the azimuth angle of the incident wave from the far field antenna shown in Figure 3.3. Substitute Equation 3.9 into 3.10, then

$$[\underline{\mathbf{B}}] = (\underbrace{[\mathbf{I}] - [\underline{\mathbf{S_p}}] \cdot [\mathbf{I}(\boldsymbol{\Gamma})]}_{[\underline{M}]})^{-1} \cdot [\underline{\mathbf{S}}_{\mathbf{t}}(\varphi)] \cdot \underline{A}_t \tag{3.11}$$

where $\mathbf{I}$ is the unity matrix (diagonal matrix) and is defined by

$$[\mathbf{I}] = \begin{bmatrix} 1 & 0 & 0 & 0 \\ 0 & 1 & 0 & 0 \\ 0 & 0 & 1 & 0 \\ 0 & 0 & 0 & 1 \end{bmatrix} \tag{3.12}$$

and the diagonal matrix for the reflection coefficient is

$$[\mathbf{I}(\underline{\boldsymbol{\Gamma}})] = \begin{bmatrix} \underline{\Gamma}_1 & 0 & 0 & 0 \\ 0 & \underline{\Gamma}_2 & 0 & 0 \\ 0 & 0 & \underline{\Gamma}_3 & 0 \\ 0 & 0 & 0 & \underline{\Gamma}_4 \end{bmatrix} \tag{3.13}$$

The resulting voltage at each port is the sum of the received and reflected waves multiplied by square root load impedance

$$\underbrace{\begin{bmatrix} \underline{V}_1(\varphi) \\ \underline{V}_2(\varphi) \\ \underline{V}_3(\varphi) \\ \underline{V}_4(\varphi) \end{bmatrix}}_{[\underline{\mathbf{V}}(\varphi)]} = ([\underline{\mathbf{A}}] + [\underline{\mathbf{B}}]) \cdot \sqrt{Z_L} \tag{3.14}$$

The desired equation is obtained by substituting Equation 3.11 into 3.14

$$[\underline{\mathbf{V}}(\varphi)] = [\underline{\mathbf{M}}]^{-\mathbf{1}} \cdot [\mathbf{I}(\underline{\mathbf{\Gamma}} + \mathbf{1})] \cdot [\underline{\mathbf{S_t}}(\varphi)] \cdot \underline{V_t} \tag{3.15}$$

where

$$[\mathbf{I}(\underline{\mathbf{\Gamma}} + \mathbf{1})] = \begin{bmatrix} 1+\underline{\Gamma}_1 & 0 & 0 & 0 \\ 0 & 1+\underline{\Gamma}_2 & 0 & 0 \\ 0 & 0 & 1+\underline{\Gamma}_3 & 0 \\ 0 & 0 & 0 & 1+\underline{\Gamma}_4 \end{bmatrix} \tag{3.16}$$

Equation 3.15 represents the received voltages at each port of the antenna window. The $[\underline{\mathbf{M}}]$ is a function to the S-parameters matrix $[\underline{\mathbf{S_p}}]$ and reflection coefficient. Both $[\underline{\mathbf{S_p}}]$ and the antenna pattern matrix $[\underline{\mathbf{S_t}}(\varphi)]$ are measured. Therefore, received voltages are computed with a given reflection coefficient. When $\underline{\Gamma} = 0$ or 1, then the antennas are loaded with 50Ω or high impedance (i.e. FET), respectively. When computing $\mathbf{n}$, Equation 3.15 is multiplied by the generated Rayleigh field for each antenna to obtain a realistic signal environment for the diversity system under test. A virtual drive example for FM in Rayleigh fading field is described in section 1.2.1.

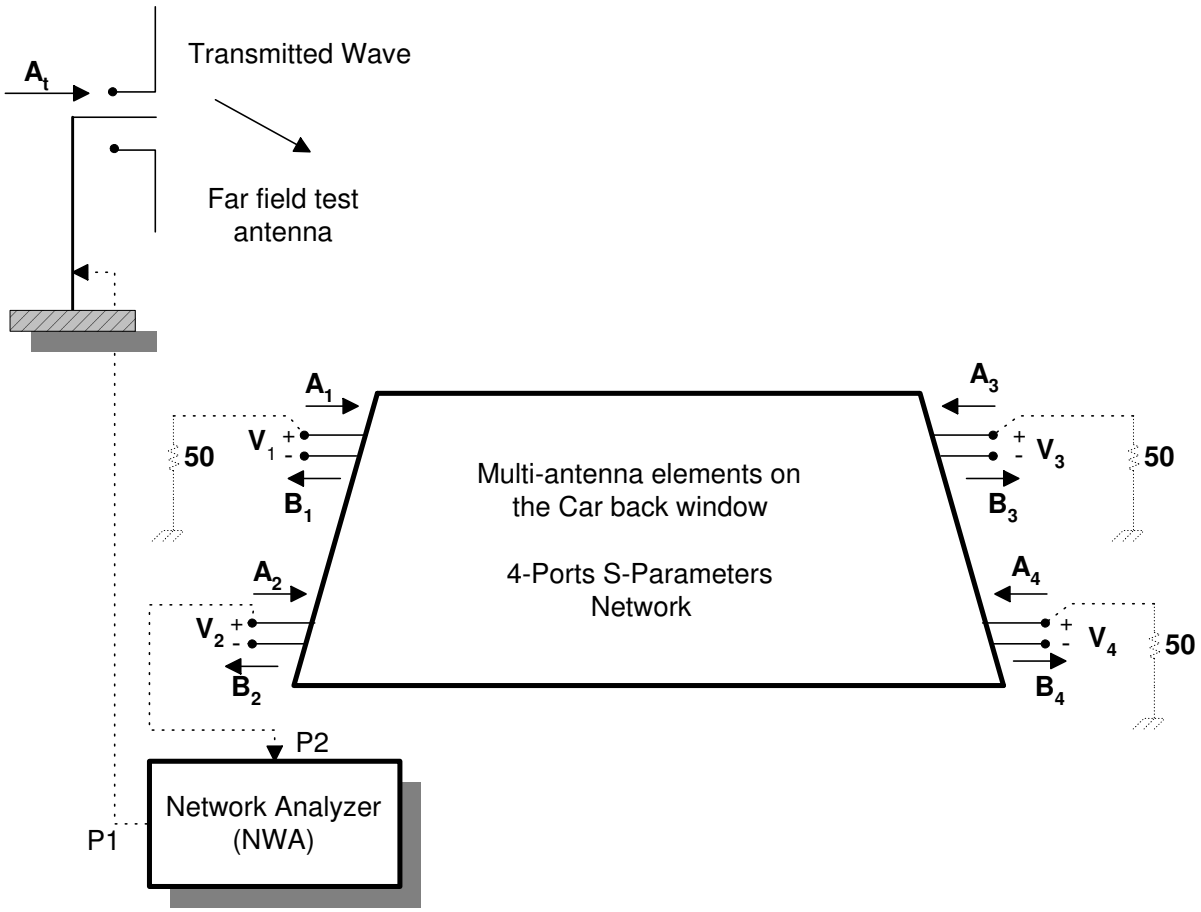

Figure 3.3: Multi-antenna elements as 4-ports network with far field test antenna

3.2 Scanning Phasing Antenna System (SPAS)

The two FM diversity systems (PAS and SAS) that are described in Chapter 2 are used in modern automobiles. The PAS system needs a distortion detector as mentioned in section 2.1.4. In weak signal conditions, SAS tends to increase its switching activity and can not stop on one or desired antenna. It is the aim of the present work to concentrate on the combination of the two systems and investigate its performance and advantages over SAS and PAS. The new system is called Scanning Phasing Antenna System (SPAS) and is described in details in Chapter 4. It selects, at any instant, the two least distorted out of four antennas for the PAS to combine them in phase. The basic operation of the system is shown in Figure 3.4. Each splitter provides two equal signal amplitudes of each antenna for the scanner to examine. Ideally, the scanner that provides ANT_B signal is considered the least distorted among the four antenna signals. ANT_A signal is considered the second least distorted. The distortions can be caused by long delay multi-path, adjacent channel or/and co-channel. Refer to chapter 1 for more details on distortion calculations. ANT_A and ANT_B are co-phased and added by 2-antennas combining system to produce signal-to-noise ratio (SNR) that is higher than the SNR of a single reference antenna. A detailed description of SPAS mechanization and the principle of operation will be presented in the next chapter. The **n** of the SPAS is computed and compared to the **n** of PAS and SAS systems in the next section.

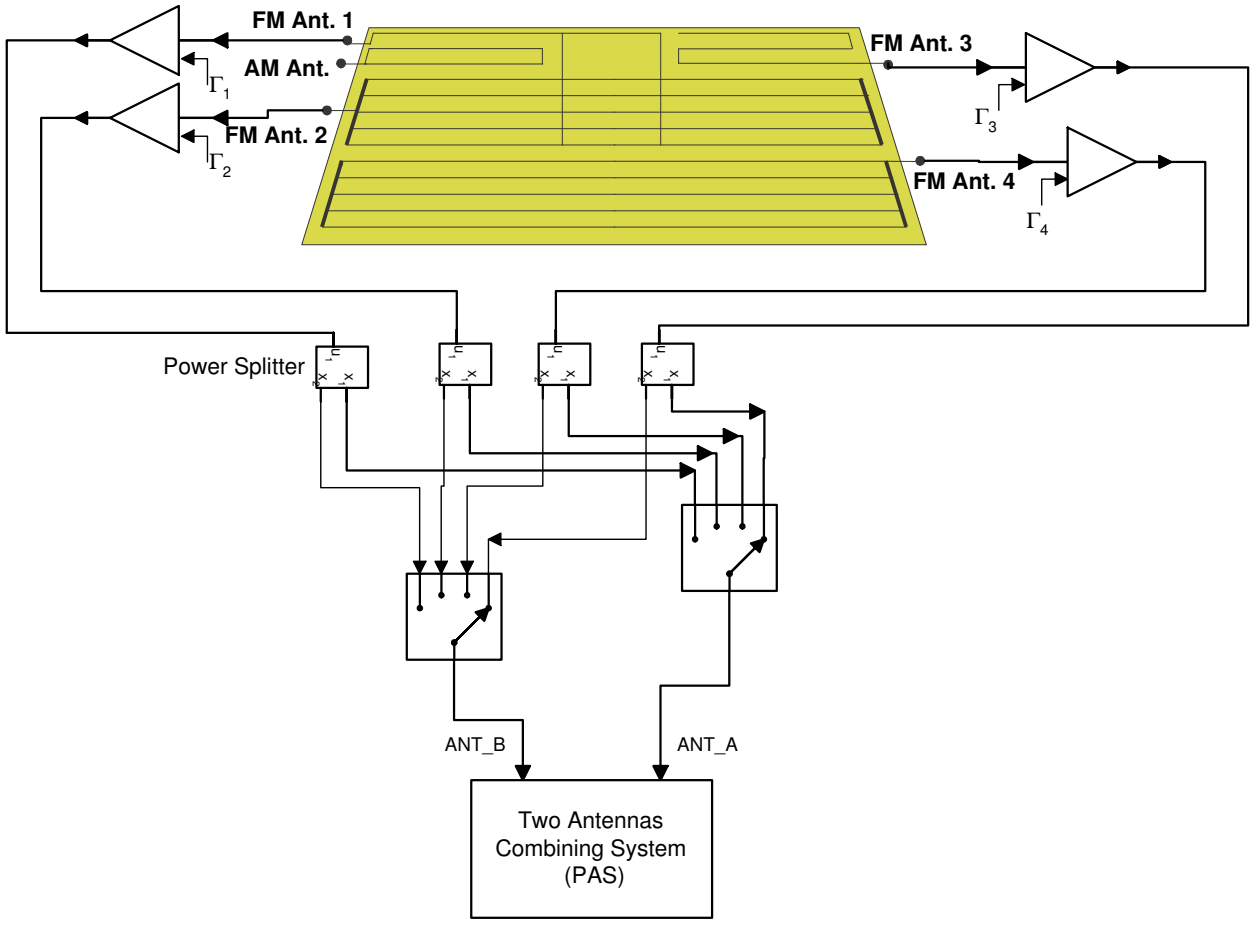

Figure 3.4: Simple Operation of the SPAS

3.3 Diversity Effectiveness n of Three Diversity Systems in Rayleigh Fading Field with Antennas on one Window

The diversity effectiveness **n** is computed for PAS, SAS, and SPAS for all possible antenna combinations. Economic versions of antenna diversity schemes require all antennas to be on one window to reduce cost, reduce warranty claims, and improve styling. Such antennas are shown in Figure 3.4 and their measured gain patterns (horizontal polarization at $100MHz$) are shown in Figure 3.5.

Rayleigh virtual drive is done the same way as in section 1.2.1 for 20λ with the following parameters: $\frac{\Delta x}{\lambda_o} = 0.01$, number of points in one period $n_x = 2000$, number of periods $Per = 40$, and number of waves $NW = 50$.
All computations are done every $2MHz$ from 76 to $108MHz$ and with the reflection coefficient $\Gamma = 0$ (50Ω), $\Gamma = 1$ (high input impedance FET).

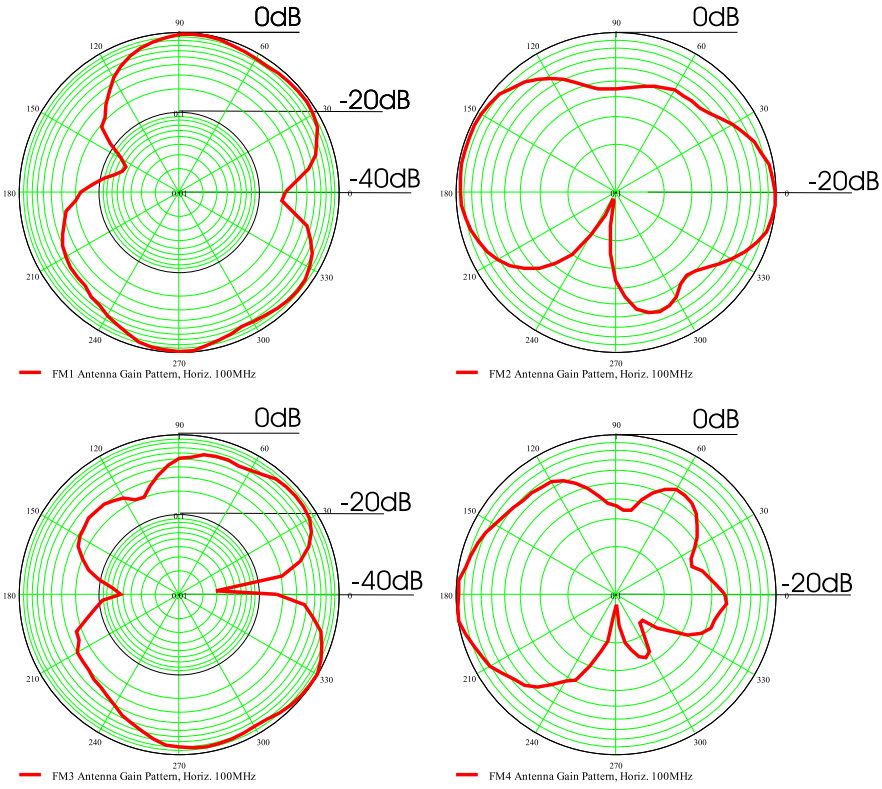

Figure 3.5: Measured Antenna Gain Patterns for the Window of Figure 3.4. Horizontal Polarization at $100MHz$, $\Gamma_1 - \Gamma_4 = 0$

All possible antenna combinations were considered for **n** calculations. Figures 3.6 (A) and 3.6 (B) show the computed diversity effectiveness **n** for the above mentioned diversity systems for reflection coefficient Γ of 0 and 1, respectively. The data shows that the 4-antennas SPAS, for both cases of $\Gamma = 0$ and $\Gamma = 1$, performance is better than all the other systems over the FM frequency range (76 to $108MHz$). The maximum **n** in Figure 3.6 (A) is 4.7. This is higher than the physical antenna number due to the fact that the SPAS co-phase the two least distorted antenna signals.

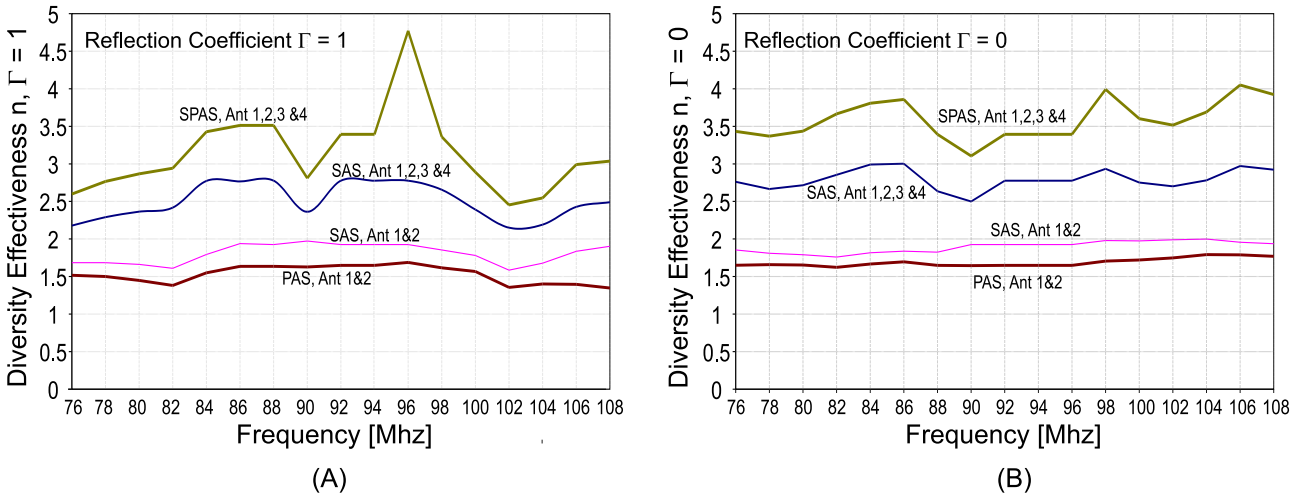

Figure 3.6: Computed **n** for SAS, PAS, and SPAS with (A)$\Gamma = 1$ (B)$\Gamma = 0$

The **n** for the PAS is less than the **n** of the SAS due to the physical size constraints of the car window. A 2-antennas co-phasing system, such as the PAS, needs the antennas to be spaced sufficiently far apart, at least half-wavelength (0.5λ). This is a major necessity so that the antennas are somewhat uncorrelated, meaning that they fade independently. The correlation coefficient $\rho_r(d)$ of two antenna signals where the antennas are separated by distance d is defined by [22]

$$\rho_r(d) = {J_o}^2(\beta d) \tag{3.17}$$

where J_o is first kind zero order bessel function and β is phase constant and defined as $\beta = \frac{2\pi}{\lambda}$. $\lambda = 3m$ for $100MHz$ carrier frequency.
The first null of the correlation coefficient occurs at 0.38λ for uniform angular distribution of incident waves as shown in Figure 3.7. The measured first null of the correlation coefficient in suburban areas is 0.8λ [22]. This may be due to the non-uniform angular distribution of the incident waves.

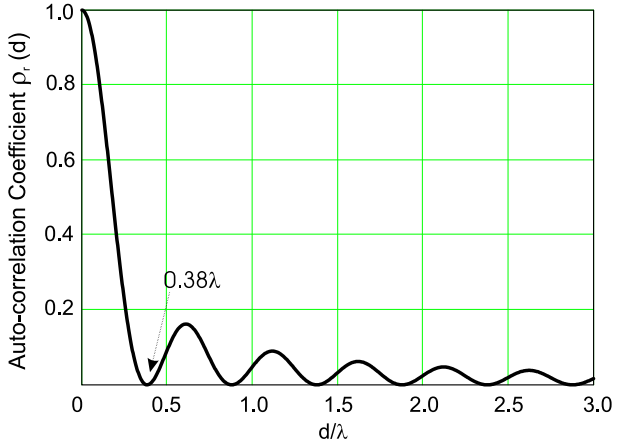

Figure 3.7: Autocorrelation Coefficient $\rho_r(d)$ vs. distance for uniform angle distribution [22]

The **n** of 4-antennas SAS is always below the one for SPAS. This is expected because the least two distorted antennas are co-phased then added by the SPAS which produce a higher SNR than the SNR of one antenna that is selected by 4-antennas SAS.

The resulting values of average **n** over the entire FM frequency range are displayed in Figures 3.8 and 3.9 for all possible antenna combinations. When the reflection coefficient $\Gamma = 0$, SAS outperforms the PAS for all 2-antennas combinations. The best value of **n** for 2-antennas SAS is 1.9 and for PAS is 1.7 (when $\Gamma = 1$, the best **n** for SAS is 1.8 and 1.5 for PAS). The 4-antennas SAS outperforms both the 2-antennas PAS and SAS systems. Its **n** is 2.8 when $\Gamma = 0$ and 2.5 when $\Gamma = 1$. SPAS outperforms, as expected, all the other systems. Its **n** is higher than the **n** of 2-antennas PAS and SAS by 2 uncorrelated antennas in some cases. This is significant improvement over the 2-antennas systems. In addition, the SPAS has 0.8 antennas more than the 4-antennas SAS when $\Gamma = 0$ and 0.6 antennas when $\Gamma = 1$. In result, the SPAS provides a higher SNR. Furthermore, the switching activity of the of the scanning system within the SPAS is less than the conventional stand alone 4-antennas scanning system. This is due to the fact that SPAS co-phase and combine the two least distorted antenna signals. This adds $3dB$ more to overall SNR on average. Some of the other advantages and functionality of the SPAS are discussed in detail in Chapter 4.

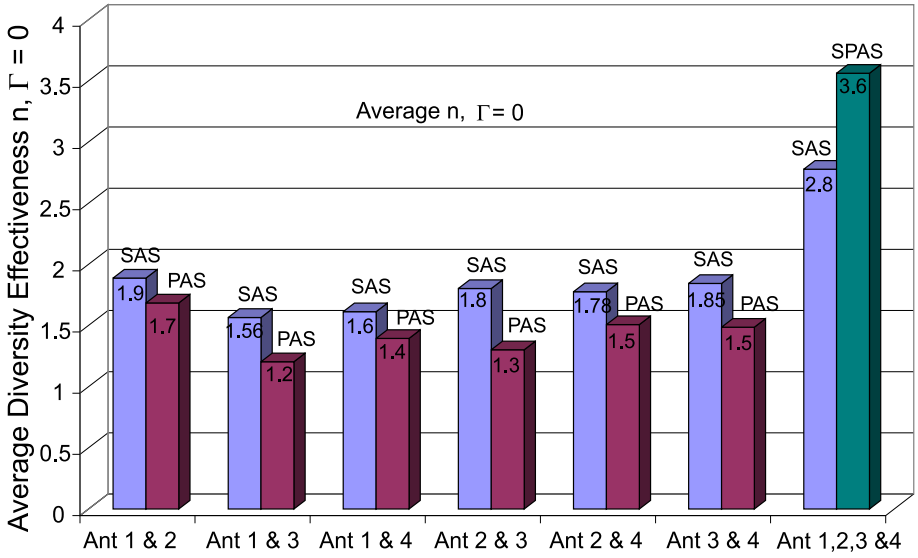

Figure 3.8: Average **n** for SAS, PAS, and SPAS with $\Gamma = 0$ for all antenna combinations

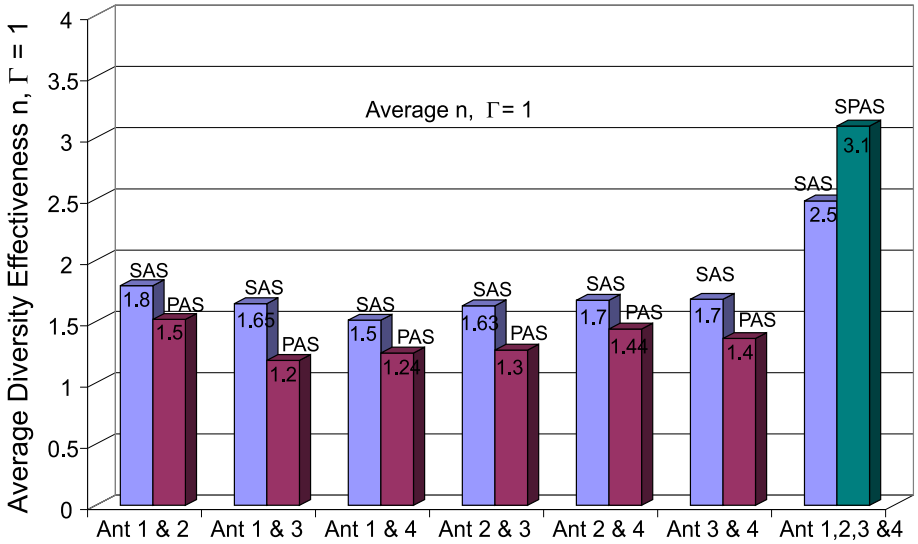

Figure 3.9: Average **n** for SAS, PAS, and SPAS with $\Gamma = 1$ for all antenna combinations

The main advantage in using FM space diversity systems is to increase the reliability of the received signals without increasing the transmitter power. The antennas are usually placed far away from each other so that they fade independently and to obtain an acceptable diversity performance. When using diversity systems in cars, the location of the antennas is usually restricted by reasons given by automotive technologies. In many cases, the antennas must be located in the back window so that they are hidden. This reduces costs and improve styling. Unfortunately, we get higher signal correlation between the antennas in such arrangement. The SPAS is a solution for such antenna arrangement because it has software algorithms that controls the 2-antennas combining system. It informs the combining system (with the help from a fast distortion detector and an ultrasonic noise detector) when it is appropriate to co-phase and add the two antennas. In other words, it guarantees that the combining system would not receive distorted signals (when they are available) to combine. The classic 2-antennas PAS combining system co-phase and add two antennas without any knowledge of the signal conditions (see section 2.1.4). In case that all the antennas are distorted and the fast distortion detector is constantly switching, the SPAS uses a slower distortion detector to search for the least distorted antenna.

Chapter 4

Scanning Phasing Antenna System Implementation

4.1 System Block Diagram Description

The SPAS is an integration of PAS and SAS systems. It consists of two FM receivers, Antenna Matrix, PAS, SAS, and Ultrasonic Noise Detector (USN). The main motivation to implement such a system is to improve the diversity functionality of the PAS and SAS systems. We have concluded in Section 2.1.4 that the PAS has poor performance in long delay multi-path and acceptable performance in Rayleigh fading field (short delay multi-path). Therefore, the PAS needs a fast distortion detector to enhance its overall performance. Figure 4.1 shows a simplified block diagram of the SPAS. The phase shifter is implemented at the Intermediate Frequency (IF) section of the main receiver path (surrounded by the long dashed lines) and it is controlled by the PAS logic block. The IF switch is connected between the IF filter of the second receiver (surrounded by the dotted lines) and the summation block. When the switch is connected to the lower position, the system operates in PAS mode to align both IF signals in phase. When it is connected to the upper position, depending on signal conditions, the system operates in USN or SAS mode. The output of the main FM demodulator MPX1 feeds the FDD (in addition to PAS logic block) so that it reacts when there is distortion on the demodulated sum of the two IF signals.

The SPAS has three modes of operation that are described in section 4.3. The basic and most important operation of SPAS is to combine the two least distorted selected antenna signals out of four. When the RF level is above some reference level and some required signal conditions are met, i.e. short delay multi-path, SAS selects the least distorted antenna signal and USN selects the second least distorted antenna signal for the PAS to combine them. In case of long delay multi-path, the system will be in scan mode if the RF level is above the reference level and in USN mode if below it.

This chapter describes the hardware and software implementations of the SPAS. Section 4.2 describes the USN detector and the Antenna Matrix blocks. PAS and SAS (or FDD) are described in chapter 2. Section 4.3 describes the modes of operation of SPAS. In addition, detailed block diagrams are included for each operation.

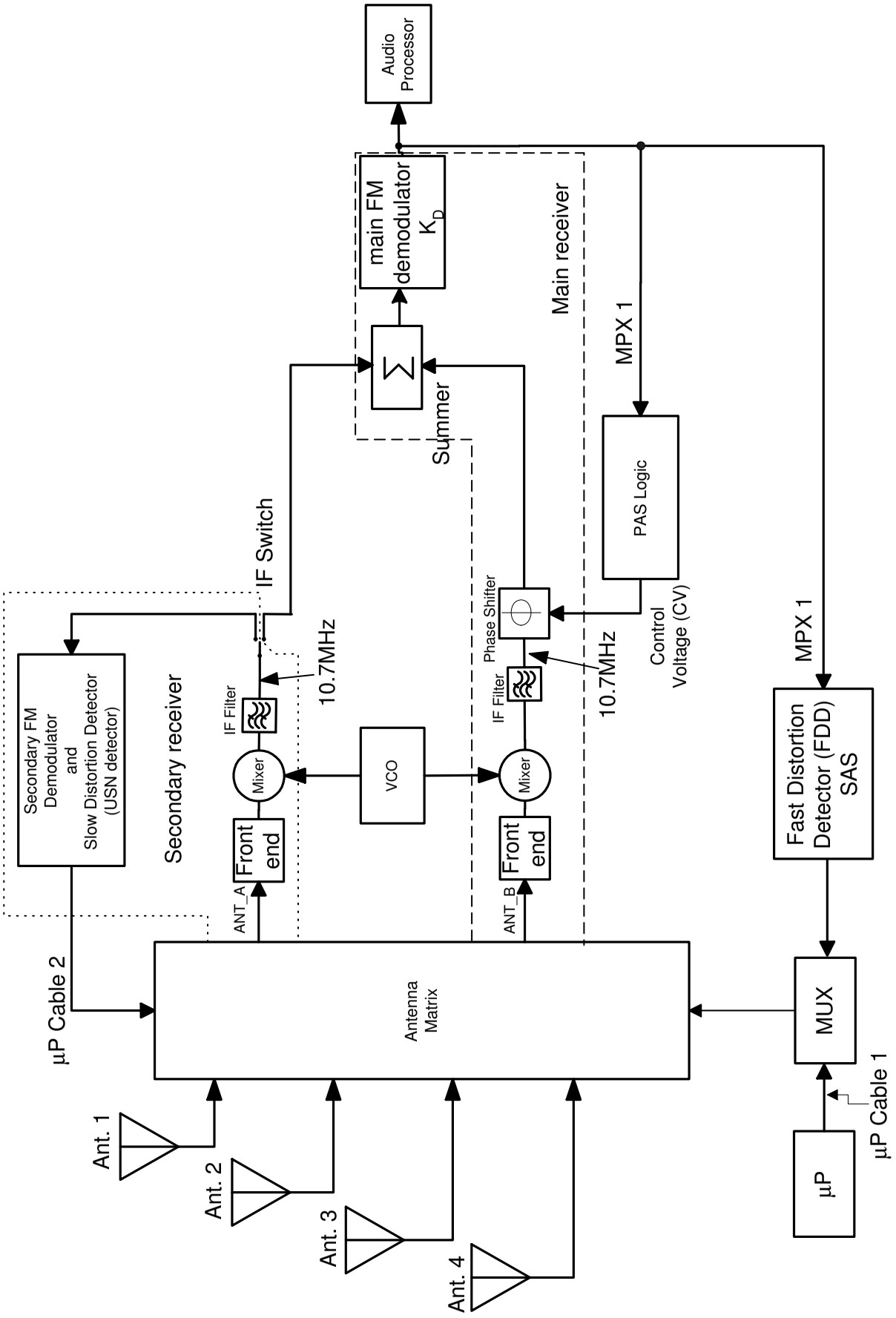

Figure 4.1: SPAS Simplified Block Diagram

4.2 Hardware Implementation

In order to demonstrate the audible signal improvement of SPAS over SAS and PAS systems, a SPAS has been developed and implemented in the present work. The PAS block that was described in Section 2.1 was implemented as a separate unit at the Radio Frequency (RF) where the antennas are connected directly to it. The latter implementation has the advantage to use a single FM receiver. The disadvantage is performance degradation in weak signal areas. Therefore, the PAS block is implemented inside the FM receiver unit at the Intermediate Frequency (IF) $10.7MHz$ section in the SPAS hardware to improve weak signal performance. SAS, USN, and microprocessor (μP) are also implemented inside the FM receiver box. The RF PAS that was described in Chapter 2 has high noise figure due to the phase shifter and additional networks that are in the RF path of the receiver. This noise figure adds directly to the overall noise figure of the system. Therefore, the FM receiver sensitivity is degraded which degrade overall weak signal performance of the system.

The $10.7MHz$ PAS consists of two separate front ends as shown in Figure 4.1. A common VCO drives the two mixers to insure the same phase reference. It would be more difficult to use two separate VCOs because they tend to generate beat frequencies if they are not exactly tuned to the same frequency. A small offset between the VCOs causes undesirable audible distortions at the output of the receiver. A highly sophisticated shielding is required but this is not cost effective. It is desired that both tuners to be on the same board. Therefore, a common VCO is used for both mixers. The PAS logic that is connected to the phase shifter in the main tuner path (surrounded by the long dashed lines) is described in Chapter 2. The output of the main FM demodulator is directed to the PAS logic to provide the information to it to co-phase the two $10.7MHz$ signals.

The SPAS hardware is used to demonstrate the performance improvements over the existing diversity systems both in field and lab.

4.2.1 Antenna Matrix

The Antenna Matrix is designed so that the outputs at ANT_A and ANT_B can be any two combinations of the four antennas at any time. In other words, ANT_A and ANT_B has access to any antenna at any time without loading one another as shown in Figure 4.2. This is achieved by using power splitters to provide isolated outputs. ANT_B output is controlled either by microprocessor Cable 1 or the FDD via the MUX (this will be explained later, section 4.3). ANT_A output is controlled by microprocessor Cable 2. This is mainly used by the secondary tuner to build the antenna priority list with the USN detector as described in Section 4.3.1. The pin diodes would need proper DC path to ground (not shown) in the actual implementation and each diode is microprocessor controlled.

There are four identical power splitters that each provide two isolated 50Ω outputs of each antenna signal as shown in Figure 4.2. The circuitry details of one of the power splitters are also shown.

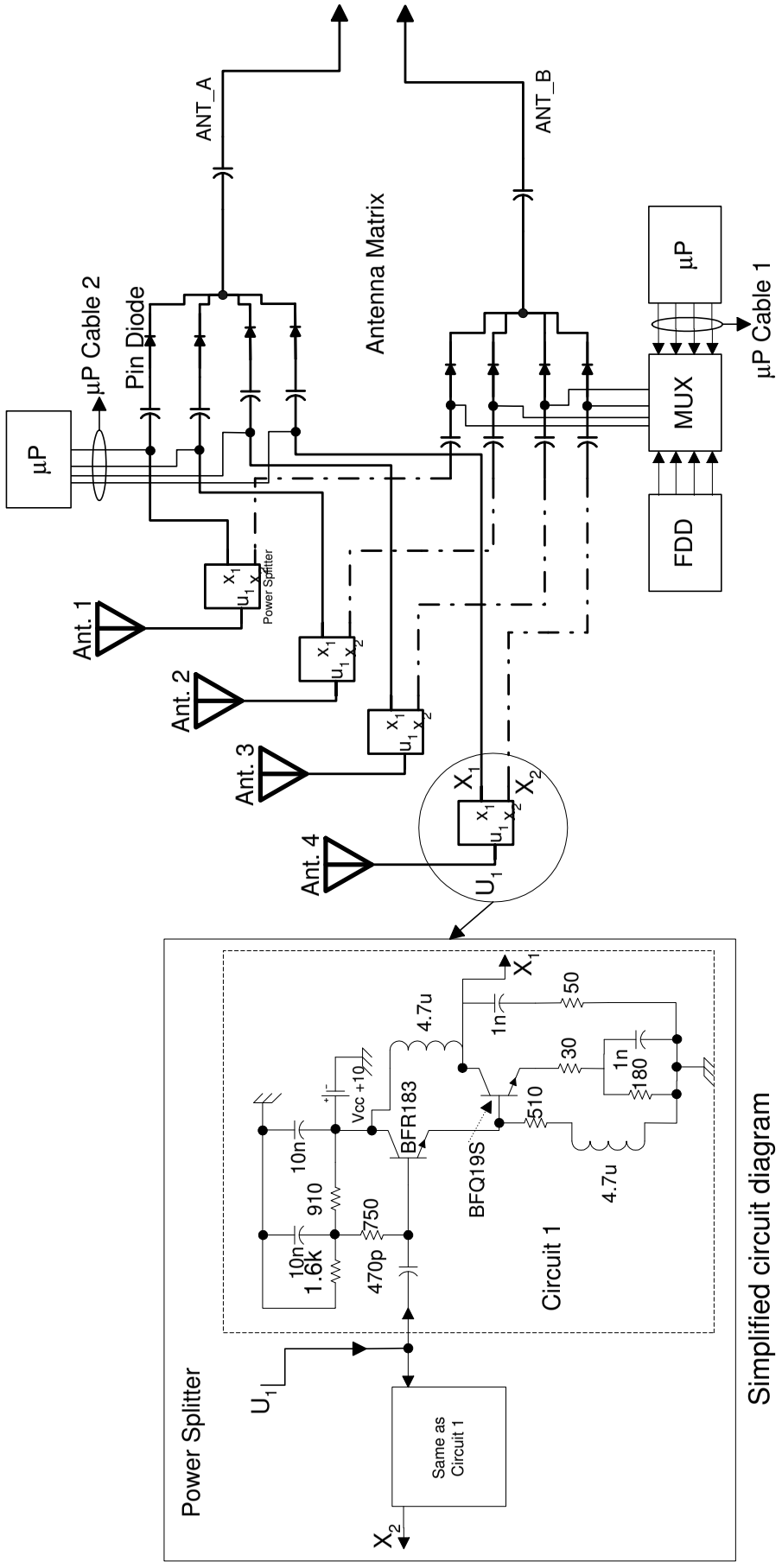

Figure 4.2: Antenna Matrix Simplified Schematic

4.2.2 Ultrasonic Noise Detector (USN)

Refer to Figure 4.1. When the $10.7MHz$ line of the secondary receiver is connected to the upper position of the switch, it feeds the secondary FM demodulator and USN block. In this case, the USN detector is used to build the antenna priority list with respect to distortion in the microprocessor of the received signals. The USN detector is an indicator for long delay multi-path and adjacent channel environments. It detects the resulting demodulated distortion harmonics above $60kHz$. Figures 1.13 and 1.16 (B) show an example of such distortion harmonics. The USN consists of a high pass filter in front of a half-wave rectifier. It produces a DC voltage that is proportional to the demodulated energy above $60kHz$. Figure 4.3 shows a simplified block diagram of the USN interface to an FM receiver and Figure 4.4 shows the measured USN detector's high pass filter frequency response (this is a stand alone measurement, without the FM receiver). It is important to show that the USN detector output correlates to the output distortions of the FM demodulator output in case of long delay multi-path or adjacent channel situation. The resultant input signal to the FM

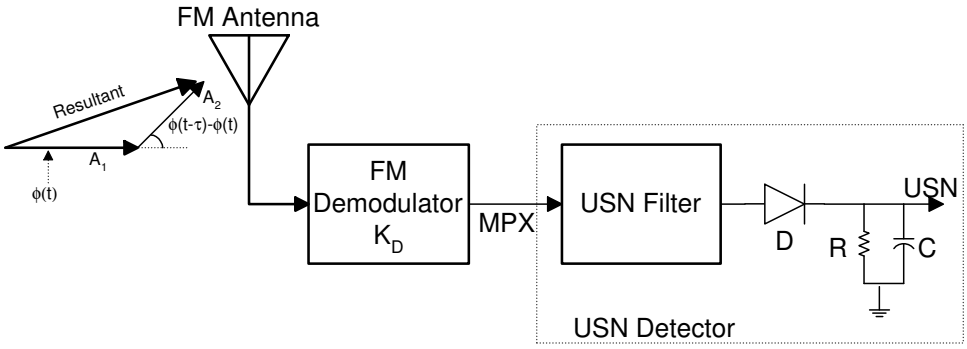

Figure 4.3: USN Detector connected to an FM receiver

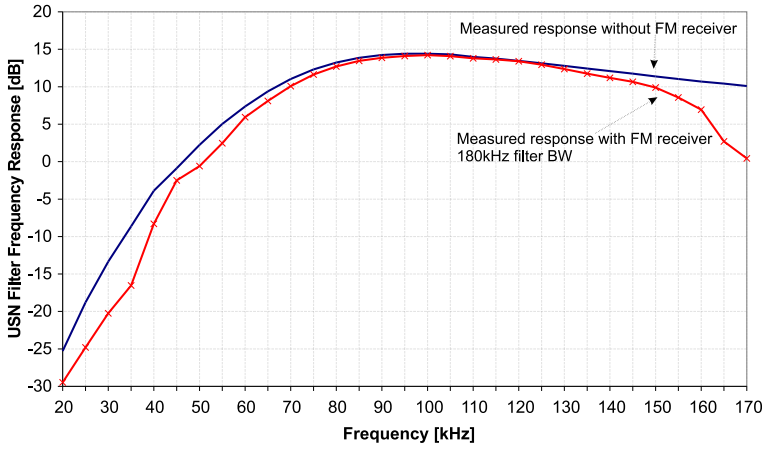

Figure 4.4: Measured USN Filter Frequency Response with and without the FM receiver

antenna shown in Figure 4.3 was analyzed as a function of time delay τ and amplitude ratio $\frac{A_o}{A_1}$ in section 1.2.2. Equation 1.12 represents the resulting erroneous frequencies deviation due to the time delay τ. Suppose that the amplitude ratio $\frac{A_1}{A_2} = 0.9$, $\tau = 40\mu sec$, modulation frequency $f_m = 1kHz$, and frequency deviation $f_d = 50kHz$. The resulting USN filter output and FM demodulator output MPX are shown in Figure 4.5 (A).

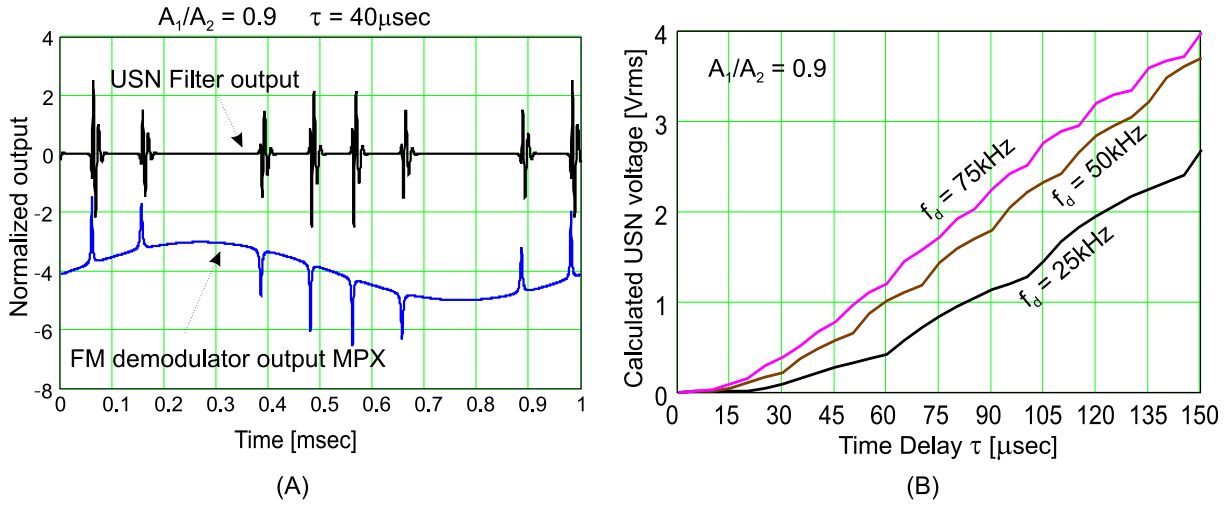

Figure 4.5: (A) Calculated USN Filter and FM Demodulator outputs, $\tau = 40\mu sec$, $\frac{A_1}{A_2} = 0.9$, $f_m = 1kHz$, $f_d = 75kHz$ (B) Calculated USN rms voltage output vs. time delay τ

We can see the strong correlation of the distortion peaks in both signals in Figure 4.5 (A). Therefore, the USN detector correlates with the signal-to-noise of the desired MPX signal. In addition, it indicates, by means of DC voltage, the degree of distortion of an FM antenna. Figure 4.5 (B) shows the calculated USN output voltage (rms) as a function of the time delay τ for three different frequency deviations f_d. It is evident that the USN DC voltage increases as a function of τ due to the erroneous frequencies deviation increase. The necessary hardware setup to measure the USN detector output voltage due to a long delay multi-path signal is shown in Figure 4.6. This is implemented in the laboratory of University of the Bundeswehr Munich – High Frequency Department. The implemented setup has two standard RF signal generators, audio signal generator, two $20dB$ RF signal attenuators, and an audio frequency delay device.

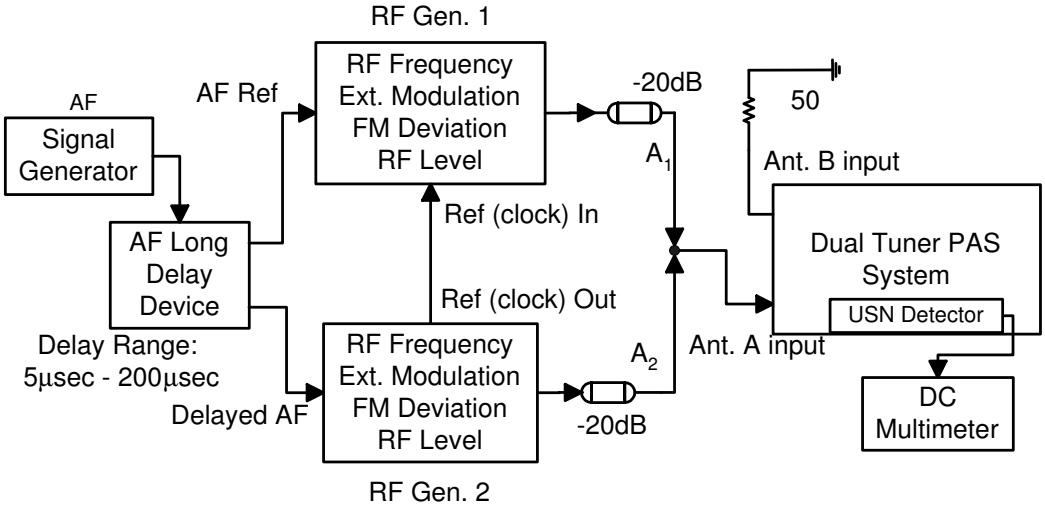

Figure 4.6: Hardware setup for USN measurement

The τ represents the Audio Frequency (AF) modulation time delay between the two RF signals. In this case, the angle between the RF carriers (FM frequency range) hardly has an

affect on the resulting distortion from long delay [20]. This is explained more in details in section 2.1.4, above Figure 2.16. The sum signal of the RF outputs of RF generator 1 and 2 is directed to the input of the FM receiver that has an USN detector. The output DC voltage of the USN detector is obtained as the AF delayed signal varied.
The measured results are shown in Figures 4.7 (A) through (C). A_1 and A_2 represent the RF signal amplitudes (shown as ratios). The USN output voltage increases with the time delay as expected. The more time delay the more erroneous frequencies are produced and therefore higher voltage values. The results in Figure 4.7 are used to determine the necessary USN DC voltage value that is needed in the software algorithms of the SPAS to decide whether the system stays in SAS mode or PAS mode. This is explained further in the next section.

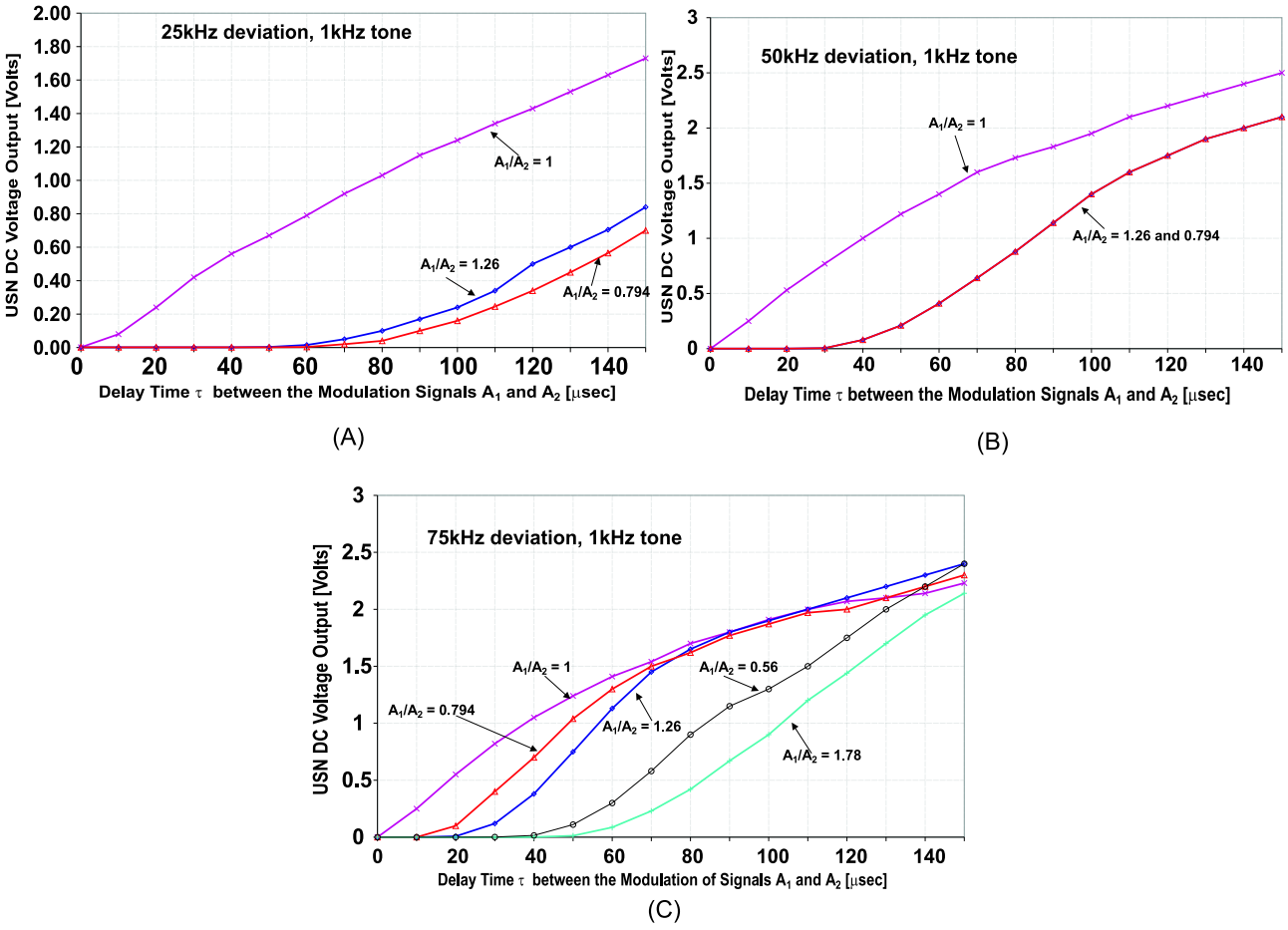

Figure 4.7: Measured USN output rms voltage for $1kHz$ tone and FM Deviation (A)$25kHz$ (B)$50kHz$ (C)$75kHz$

4.3 Modes of Operation

The SPAS modes of operation are summarized in a simple chart as shown in Figure 4.8. In this chart, when the RF level is below a reference level, the system is in USN mode. When the RF level is above the same reference, the USN detector system (software algorithms) decides the required mode of operation, depending on the multi-path signal condition.

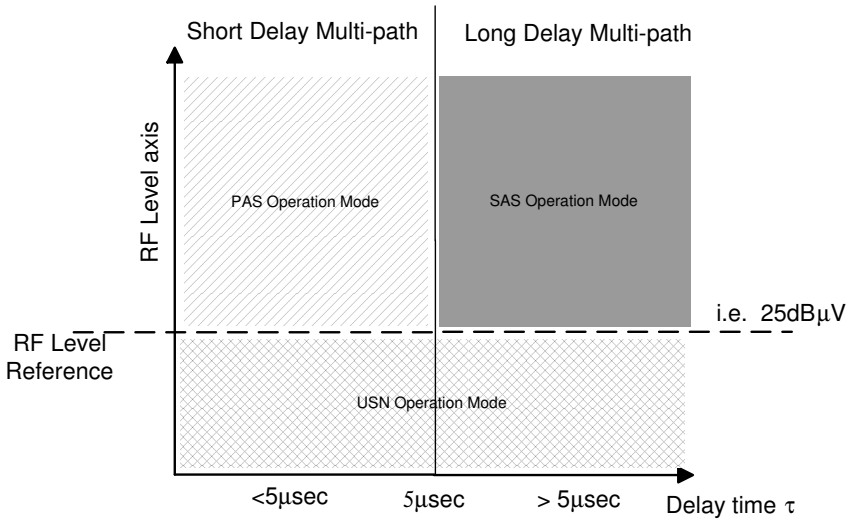

Figure 4.8: SPAS Modes of Operation

When one of the antennas of the PAS system is highly distorted due to long time delay multi-path or adjacent channel interference, and the other antenna is not distorted, the PAS system enforces the distortions of the distorted signal onto the sum signal. Therefore, the FM receiver output is distorted. It is necessary to determine the point of time delay τ that the PAS system starts to degrade the FM receiver distortion output in long delay multi-path. The PAS long delay multi-path performance is discussed in Section 2.1.4. A simple analysis of the situation is shown in Figure 4.9 where Antenna A is distorted and Antenna B is not. The distortion factor is calculated at the output of the $15kHz$ ideal low-pass filter. The noise is assumed to be zero-mean Gaussian distributed white noise (see section 5.3).

The parameters used are: amplitude ratio $\frac{A_1}{A_o}$ is 1, undistorted signal amplitude A_2 is 1, modulation frequency f_m is $1kHz$, Carrier-to-Noise C/N is $60dB$.
The resulting distortions for various FM deviations are also shown in Figure 4.9. It is expected that the distortion increases with time delay τ. It can be seen in Figure 4.9 that when τ is above $5\mu sec$, the distortion factor is higher with the antenna sum of the PAS system. It may be more appropriate to use a single antenna in this case. Therefore, a $5-10\mu sec$ time delay would correspond to approximately $300mV$ USN DC voltage as can be found in Figure 4.7 (C) for $75kHz$ frequency deviation and amplitude ratio $\frac{A_1}{A_2} = 1$ (considered worst case). This is the USN value used in software to decide the mode of operation when the RF level is above the reference level. When SAS selects the least distorted antenna signal, the USN selects the second least distorted antenna signal. If the second least distorted antenna signal has a USN value less than $300mV$ then the system switches to PAS mode to co-phase the two least distorted antenna signals.

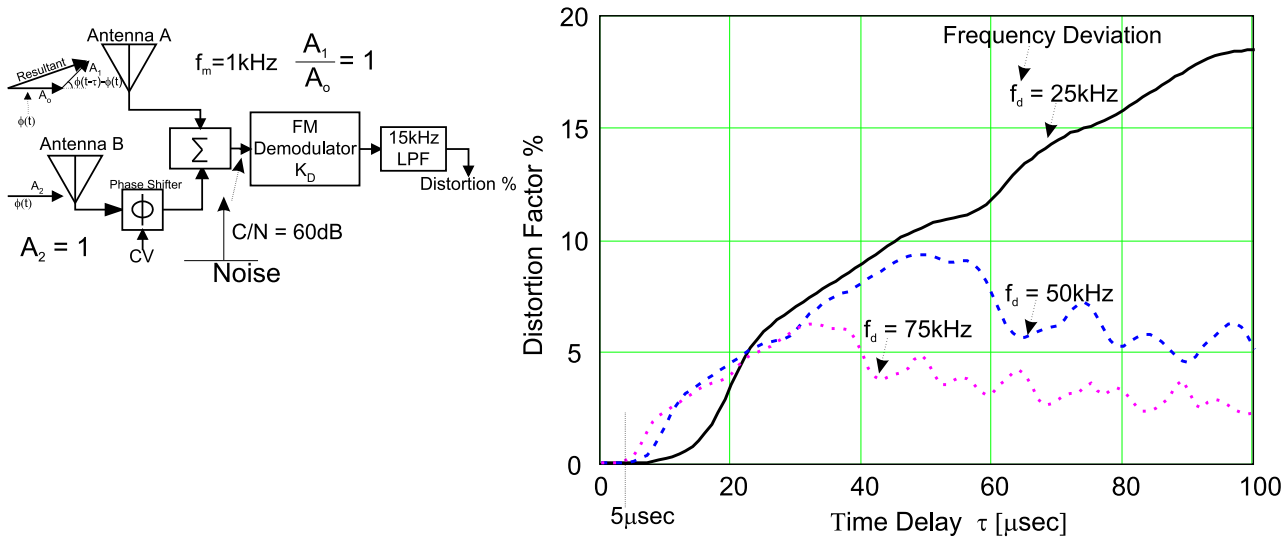

Figure 4.9: Calculated distortion factor of PAS due to long delay multi-path with $15kHz$ LPF

Figure 4.9 shows that the distortion is less as time delay increases for the frequency deviation f_d of $50kHz$ and $75kHz$. This is due to the amplitude increase of the modulation fundamental frequency with the frequency deviation. Whereas the harmonic distortion peaks are limited because of the $15kHz$ low-pass filter. When a $100kHz$ low-pass filter is used with the same above parameters, the distortion factor is similar for all frequency deviation as shown in Figure 4.10.

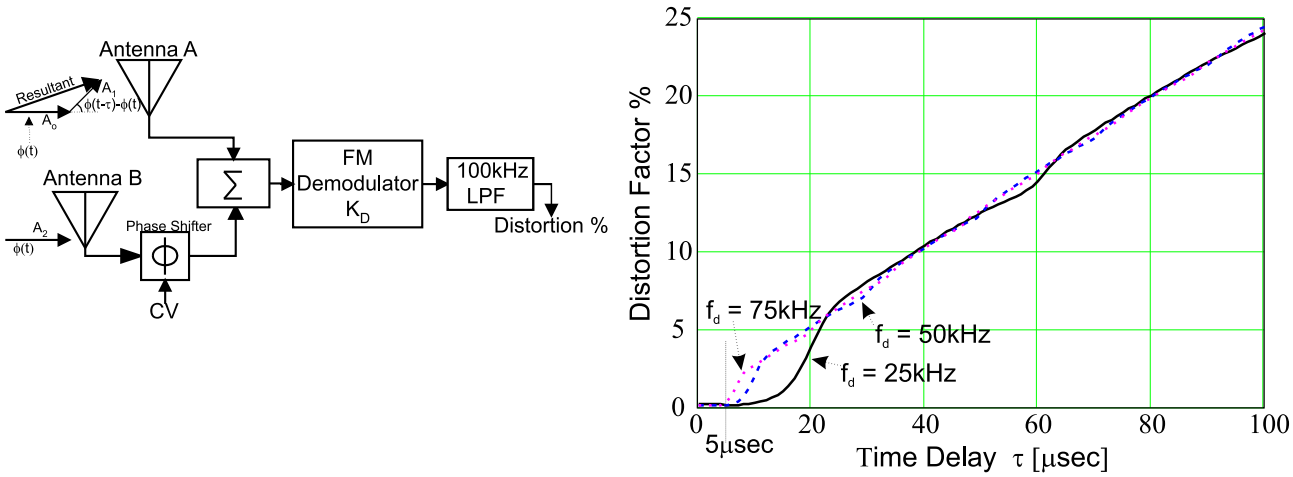

Figure 4.10: Calculated distortion factor of PAS due to long delay multi-path with $100kHz$ LPF

Before we move on to the modes of operation, it is important to determine the time and mechanism needed to switch from SAS mode to PAS mode when the RF level is above the reference level. The PAS control loop system is explained in section 2.1.3. The $3-dB$ loop bandwidth of the PAS closed loop response is about $20Hz$. In other words, the system needs about $50msec$ to lock and co-phase the two antenna signals. The USN response time is about $5msec$ [11] and it requires total time of $20msec$ to evaluate all four antennas. This is an appropriate response time to obtain the antenna signal distortion information. Therefore, the total time needed to PAS to lock and the USN to evaluate the antennas is about $70msec$. Using a timer interrupt of about $100msec$ is appropriate and convenient for

a prototype build in this case. Meaning that the microprocessor software would service the timer interrupt every $100msec$. The interrupt contains the code to determine the appropriate mode of operation based on signal conditions. When SAS selects and stops on one antenna for $500msec$, it indicates that the signal conditions are appropriate for the transition to PAS mode. The PAS should increase the overall SNR of the receiver by $3dB$ when the antenna signals are equal in amplitude. In addition, it increases the level 1 voltage of the main tuner of Figure 4.1. Therefore, the SAS switching activity is reduced. When SAS switching activity is high within $500msec$, it indicates long-delay multi-path or adjacent channel interference. It is appropriate to stay in SAS mode in this case. The system executes the timer interrupt every $100msec$ and checks if SAS is still on the same antenna. If SAS is still on the same antenna for 5 interrupt services, the system switches to PAS mode. When SAS detects distortion at the output of the main FM demodulator (Figure 4.1) in PAS mode and selects another antenna, the system switches back to SAS mode.

4.3.1 USN Operation Mode

The USN operation mode block colored diagram is shown in Figure 4.12. In weak signal areas, the RF level is below the reference as shown in Figure 4.8, whereas the PAS has difficulty locking and SAS is constantly switching. In this case, the system is in the USN mode. In Figure 4.12, the red lines form the demodulated received signal with the main tuner (surrounded with black long dashed lines) and the brown lines describe SAS operating (at the bottom of the figure). SAS is only operating so that its switching status can be monitored by the microprocessor (SAS does not control the Antenna Matrix). The green lines describe the second tuner feeds the USN detector to build priority list in the microprocessor of the received signals (the top part of the figure including the second FM demodulator, USN detector, and the Analog-to-Digital Converter (ADC)). The least distorted antenna signal monitored by the USN detector is turned on by microprocessor Cable 1. The PAS control voltage has a fixed voltage because the PAS logic is turned off. This is indicated by black dotted lines. The blue lines describe the interface to the μP. The Read/Chip Select (RD/CS) is to enable the ADC to read and digitize the USN DC voltage value when needed. Read_USN line is to enable and disable the USN detector as needed.

The main purpose of this mode is to determine the least distorted antenna signal. The mechanism to do that is explained in the following. Figure 4.11 shows the USN detector voltage output for each antenna. Indicated by the green line, Channel 3 at the bottom of the scope screen. Each antenna is evaluated for $5msec$ (time constant of the USN detector) and the best antenna signal is the one with the minimum voltage. The brown line channel 4 at the middle, is one of SAS steering logic outputs which controls Antenna 3 in this case. SAS is switching and can not decide which antenna signal to select. The light green line, channel 1 at the top, is the PAS control voltage and it has fixed value in this mode. The USN detector will also be used to determine the second best antenna signal in the PAS operation mode. This will be described in Section 4.3.3.

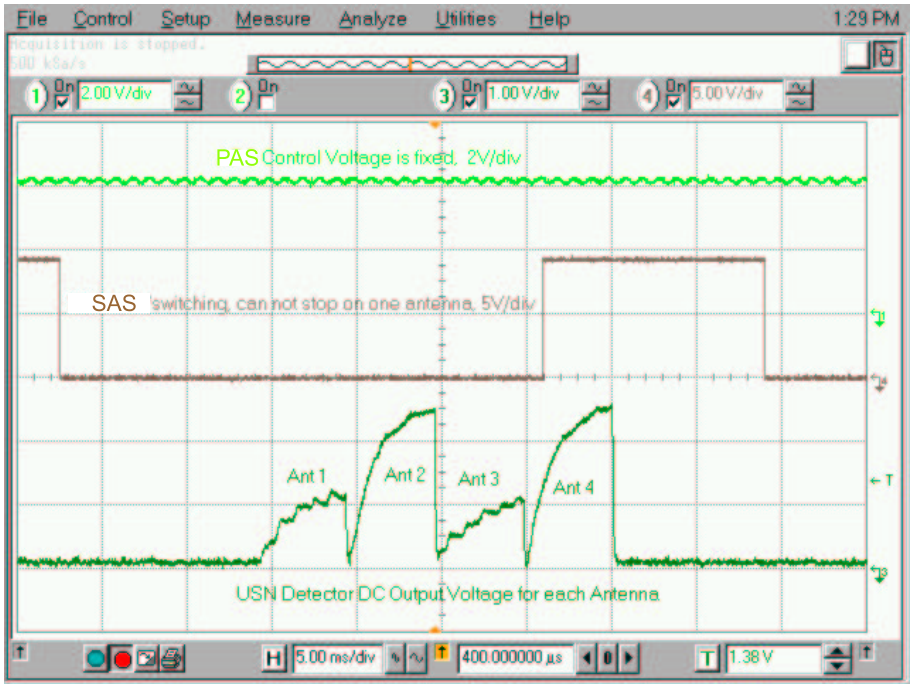

Figure 4.11: USN Output Voltage for each Antenna

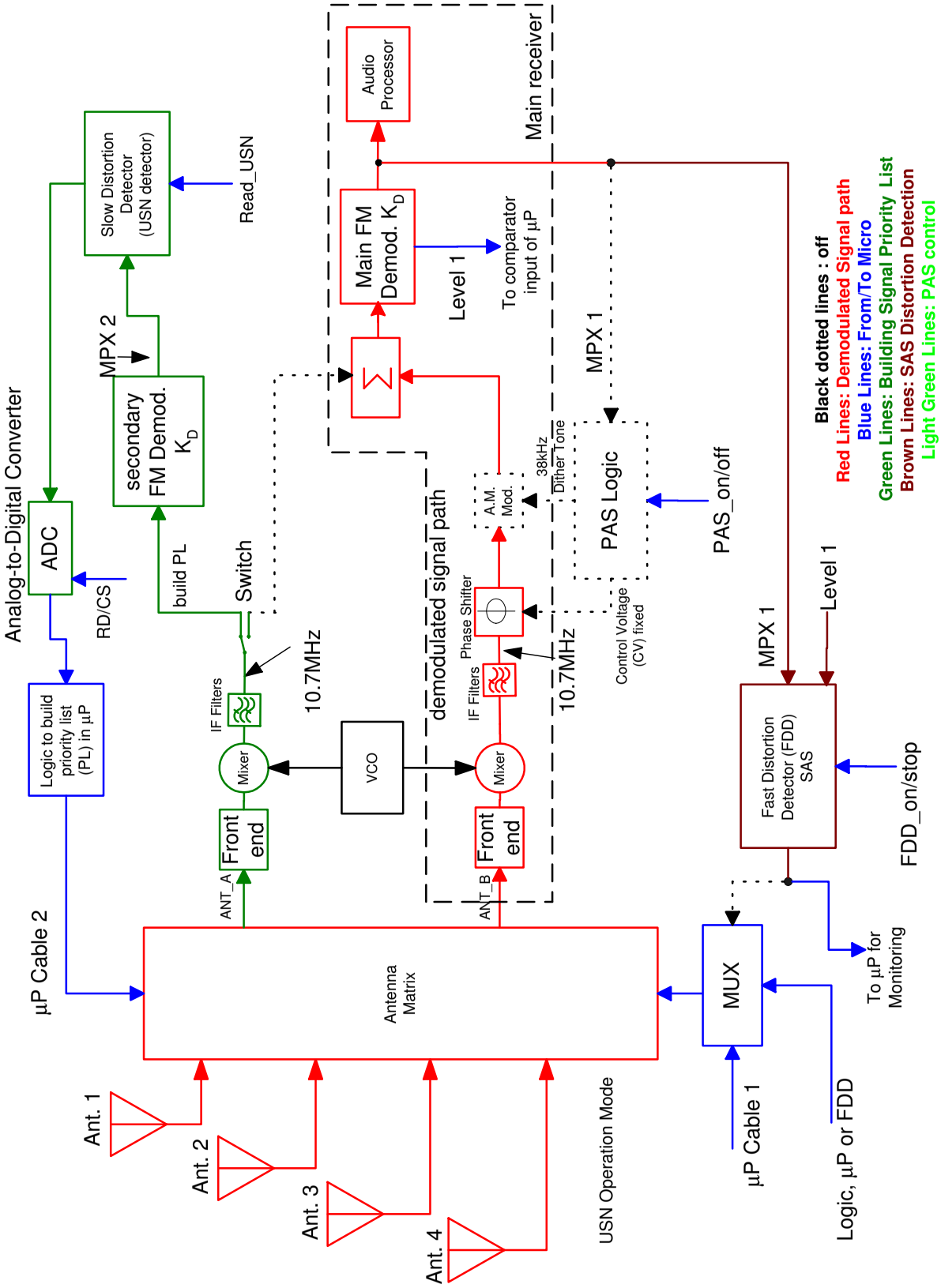

Figure 4.12: USN Operation Mode Block Diagram

4.3.2 SAS Operation Mode

The SAS operation mode block diagram is shown in Figure 4.14. SAS switching activity is always monitored by the microprocessor. The moment the RF level exceeds the reference level, the system switches to SAS mode. In this case, SAS controls the Antenna Matrix as indicated by the brown lines (at the bottom of the figure). In case of long delay multi-path or adjacent channel, which is indicated by the USN detector, the system stays in SAS mode. SAS has to stop on the same antenna for at least $500msec$ before the system switches to PAS mode. The demodulated signal path is again described by the red lines (surrounded with black long dashed lines). The green lines describe the USN detector evaluating each antenna signal distortion (the top part of the figure including the secondary FM demodulator, USN detector, and the ADC). The PAS logic block is off in this mode so that the control voltage is fixed.

Figure 4.13 shows the system operating in SAS mode where SAS selected Antenna 3 as the best antenna signal (channel 4 brown line at the middle of the scope screen). The PAS control voltage indicated by the light green line, channel 1 at the top, still has a fixed value. The USN detector voltage output for each antenna indicated by the green line, Channel 3 at the bottom. In this case, three out of four antenna signals have USN distortion value above $300mV$. The system will stay in SAS mode. The USN value of $300mV$ is chosen based on the results from the beginning of this section. The latter is the decision criterion whether the system stays in SAS mode or not. The software algorithms uses this USN value of $300mV$ and the system has performed well in both field and lab.

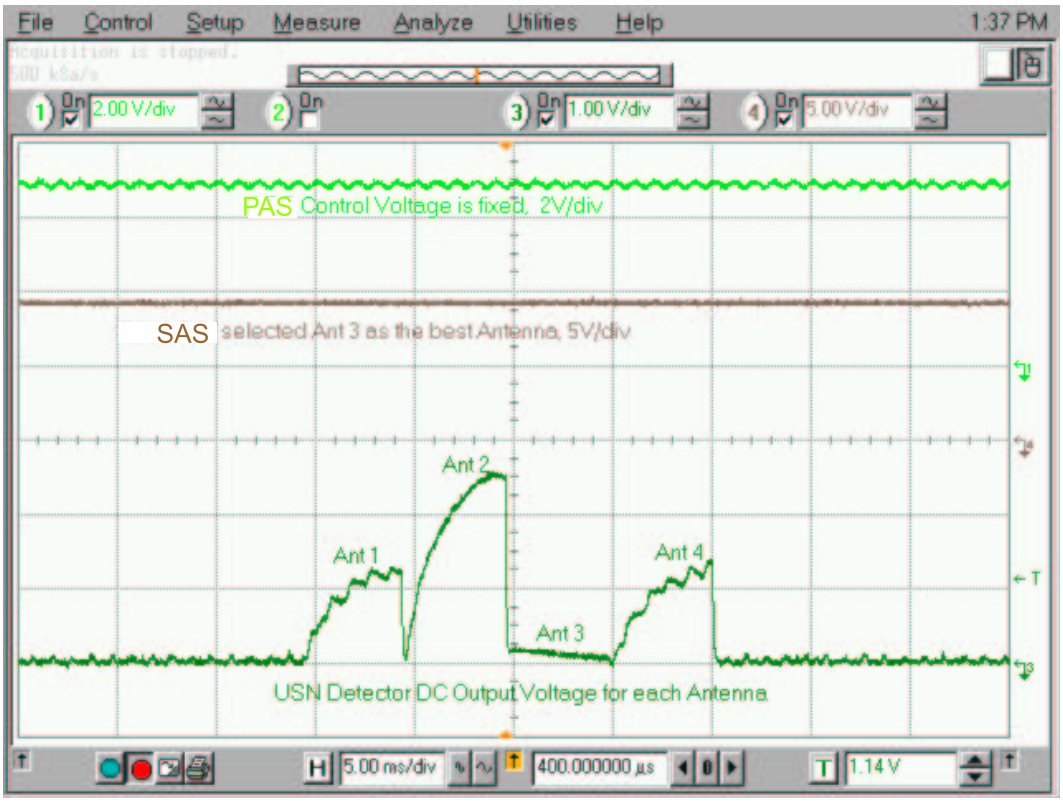

Figure 4.13: SAS selected Antenna 3 as the best Antenna

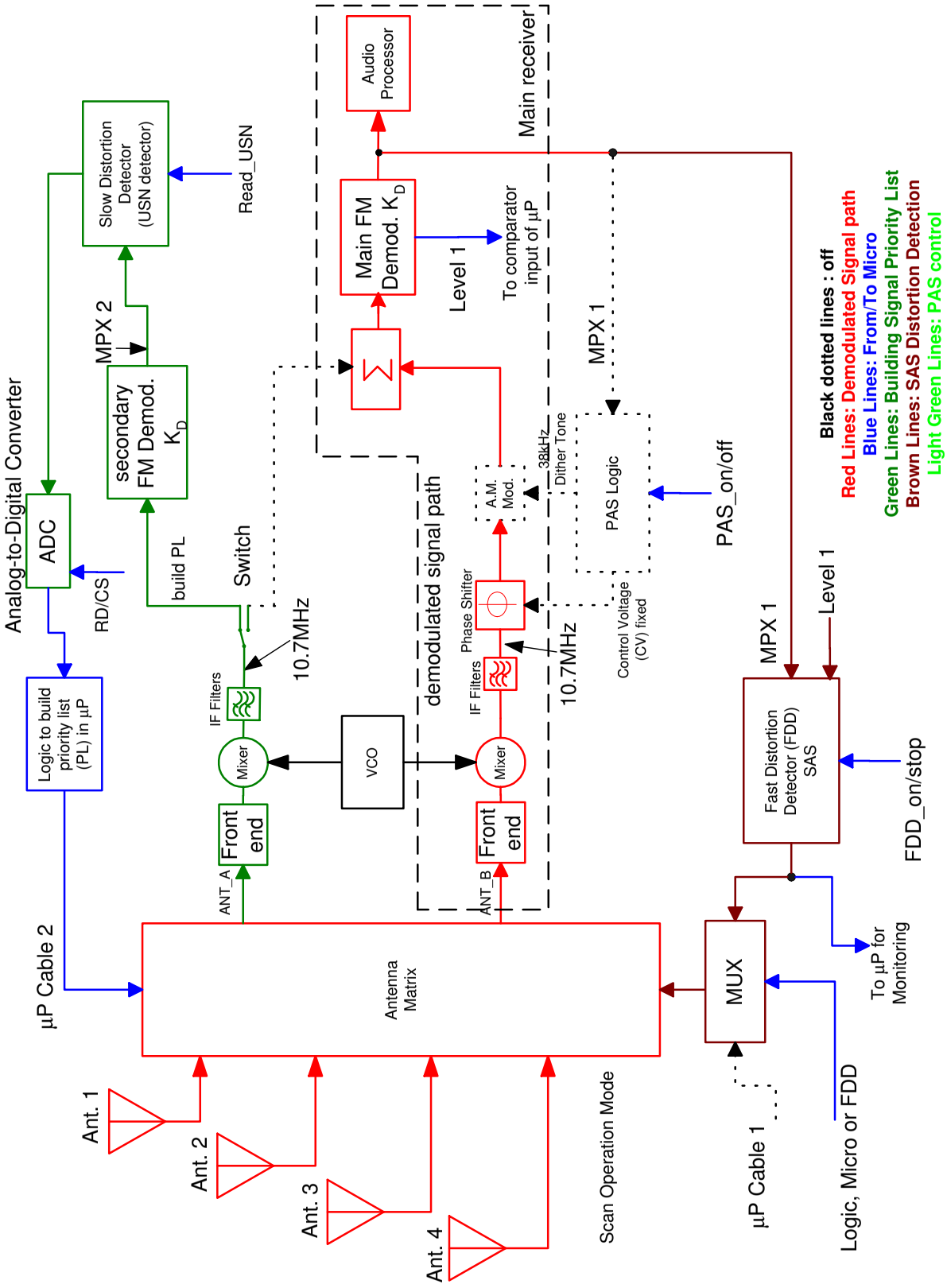

Figure 4.14: SAS Operation Mode Block Diagram

4.3.3 PAS Operation Mode

The PAS operation mode block diagram is shown in Figure 4.17. When the RF level is above the reference level as indicated in Figure 4.8, the system switches to SAS mode at first. When SAS switching activity slows down and stops on the same antenna (considered the best antenna signal) for at least $500msec$, the USN detector determines the second best antenna signal. The USN value of the second best antenna signal has to be less than $300mV$ for the system to switch to PAS mode. In this case, the red lines describe the demodulated signal path which the sum of both ANT_A and ANT_B (surrounded with black long dashed lines). If the USN distortion value is equal or above $300mV$ in reference to Figure 4.7 (C), the system will stay in SAS mode. Every time SAS switches to a new antenna (while in PAS mode), the system switches back to SAS mode and wait for SAS to stop on one antenna. The light green lines describe the PAS control loop. The black dotted lines indicate that the USN and microprocessor cable 1 are off.

Figure 4.15 shows the system at the point before it switches to PAS Mode. SAS selected Antenna 3 as the best antenna signal (The brown line, channel 4 at the middle). The PAS control voltage, indicated by channel 1 light green line, still has a fixed value at this moment. The USN detector voltage output for each antenna signal indicated by the Green line, Channel 3 at the bottom. In this case, Antenna 1 and Antenna 3 have USN distortion values less than $300mV$. Antenna 1 is considered the second best antenna signal. The system is ready to operate in PAS mode.

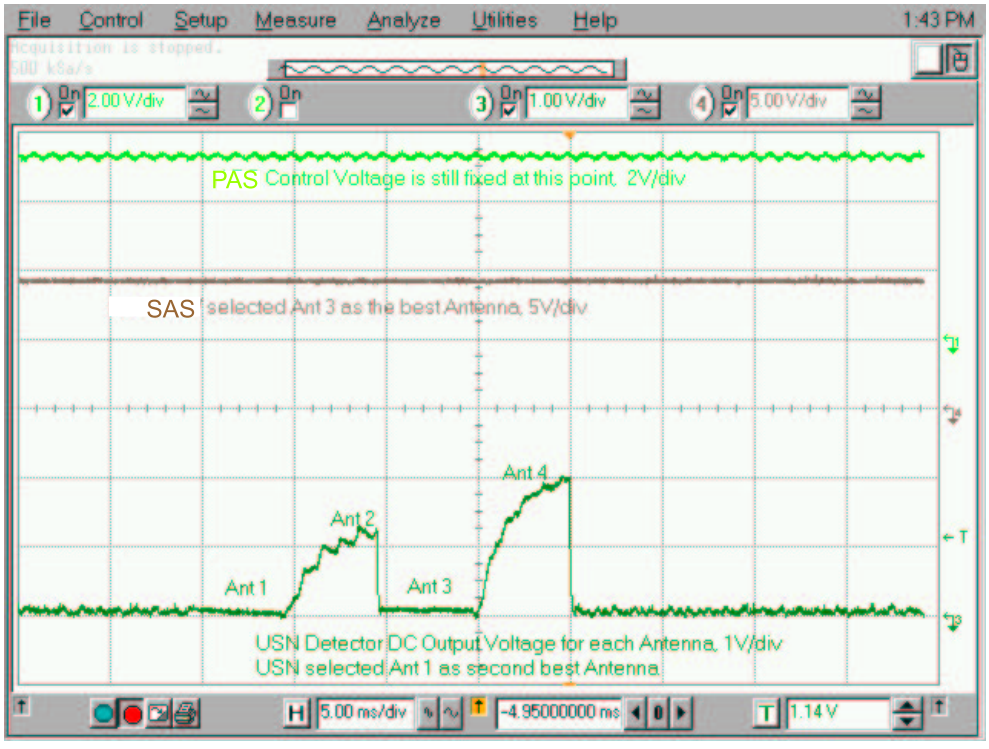

Figure 4.15: The System is ready to switch to PAS Mode

The $3dB$ loop bandwidth of the PAS is about $20Hz$ as described in Chapter 2. The SAS has very fast switching time (20 - $30\mu sec$) when it is compared to the PAS loop lock time ($50msec$). Therefore, it is necessary to provide PAS the time to lock and co-phase the two least distorted antennas. When SAS detects distortion in the FM demodulated sum of the PAS and switches to another antenna, the PAS must be turned off immediately and the system switches to SAS mode.

Figure 4.16 shows the system operating in PAS mode. The light green line, channel 1 at the top, is the PAS control voltage locked to the sum of Antenna 1 and Antenna 3. USN detector is off until SAS switches to another antenna.

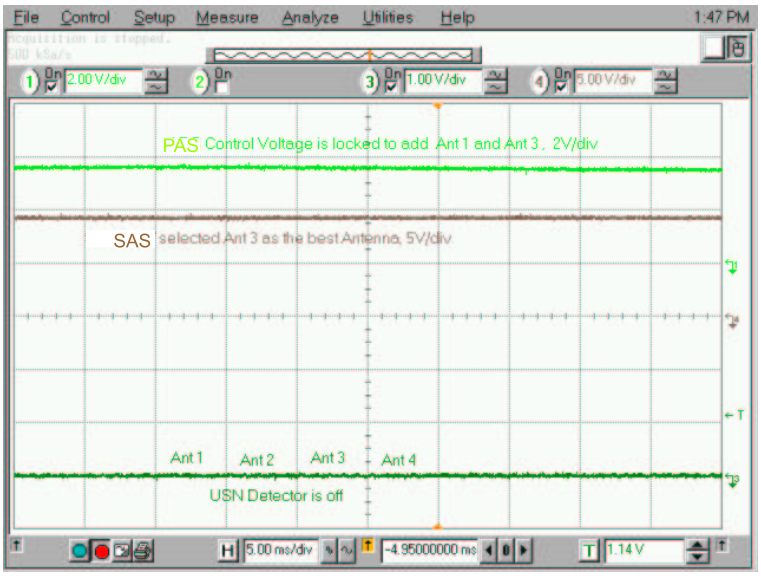

Figure 4.16: The System is in PAS Mode

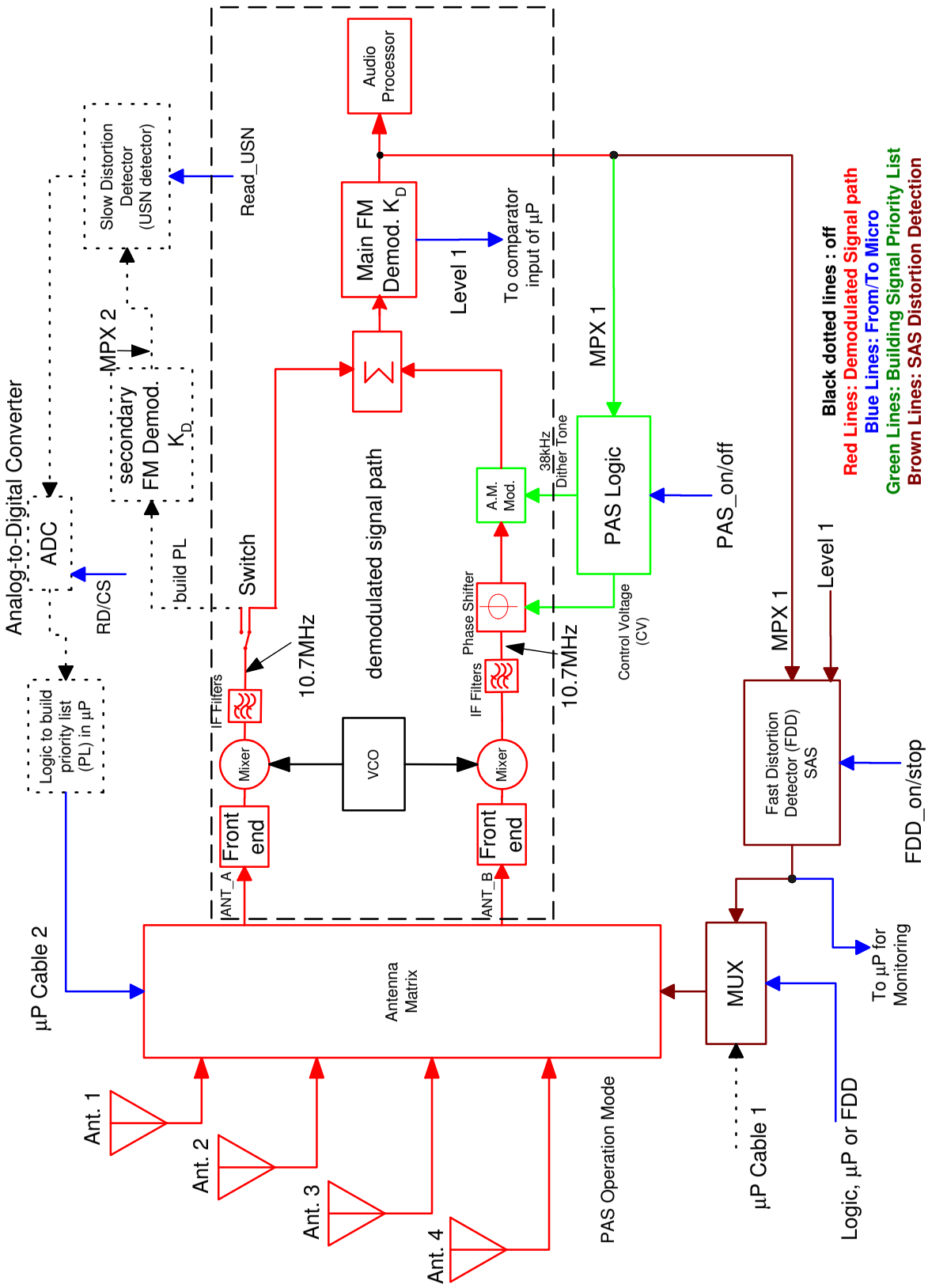

Figure 4.17: PAS Operation Mode Block Diagram

4.3.4 SPAS Software Flowchart

Simplified flowchart of the SPAS implemented software is shown in Figures 4.19 (A) and (B). The software uses an internal analog comparator to always monitor the voltage level 1 line of the main tuner in Figure 4.17. The main program always monitor SAS switching activities. The ACO is the output of the microprocessor comparator as shown in Figure 4.18. When level 1 voltage is above the reference level, ACO is high. The Reference voltage level corresponds to $25dB\mu V$ RF level. The buffer and the filter are used to filter out any undesired signal fluctuation in level 1 line. This insures smooth transition between ACO high/low states.

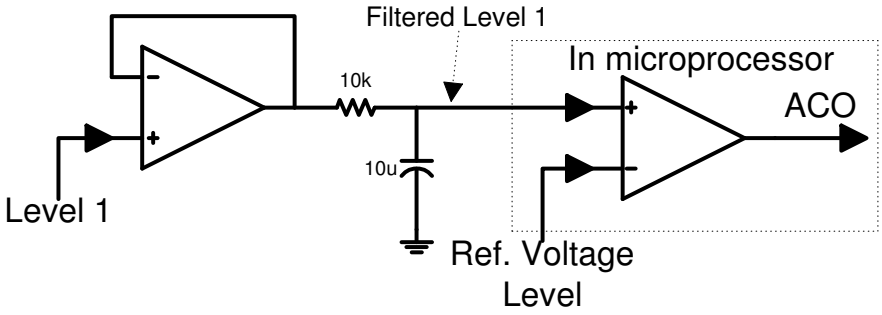

Figure 4.18: Level 1 voltage connection to the microprocessor comparator

The timer interrupt (TI) has higher priority than the analog interrupt. It is executed every $100msec$. The simplified TI algorithms is described in the following.
If the Analog comparator output (ACO) is low, the system is in USN mode. The USN detector function is to obtain the least (USNANT1) and second least (USNANT2) distorted antenna signals. The response time of the USN detector is $5msec$, therefore it evaluates each antenna for the same time via microprocessor Cable 2. The microprocessor Cable 1 controls the antenna matrix that provides ANT_B for the main tuner. When the level 1 voltage is above the reference level, the software passes control of the antenna matrix to SAS (FDD). The system is in SAS mode. If SAS stays on the same antenna (SASANT) for $500msec$, the system checks if PAS is on. If PAS is on, then exit the TI. If PAS is not on, call the USN detector to find out USNANT1 and USNANT2. If USNANT1 is equal to SASANT, then the system checks if USNANT2 USN value is less than $300mV$. If it is less, then the system turns on USNANT2 and PAS. If USNANT2 is equal to SASANT, then the system checks if USNANT1 USN value is less than $300mV$. When it is less then the system turns USNANT1 and PAS on.

A picture of the SPAS hardware prototype is shown in Figure 4.20. The system was developed at the University of the Bundeswehr Munich.

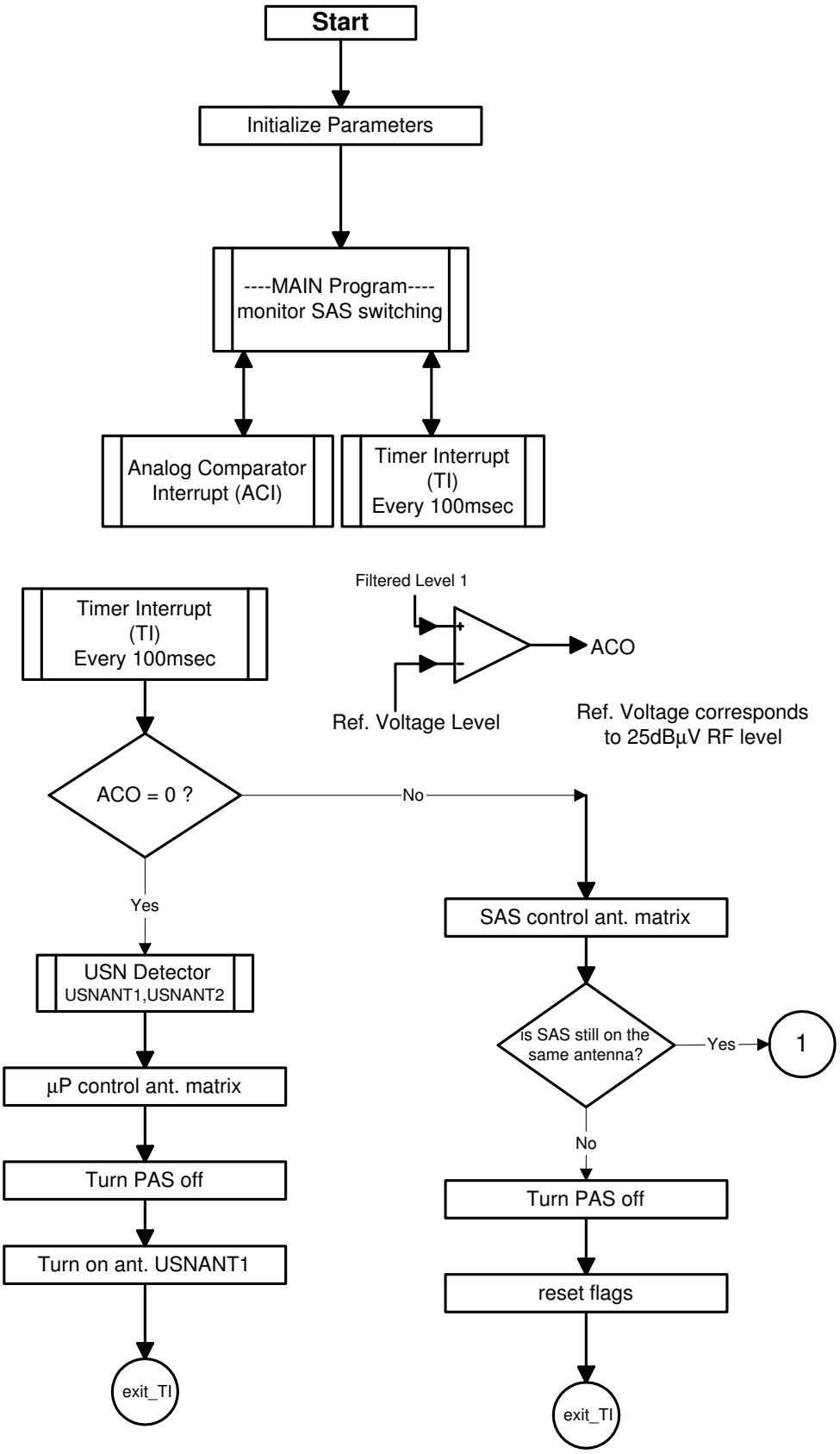

(A)

Figure 4.19: SPAS simplified software flow diagram (part A)

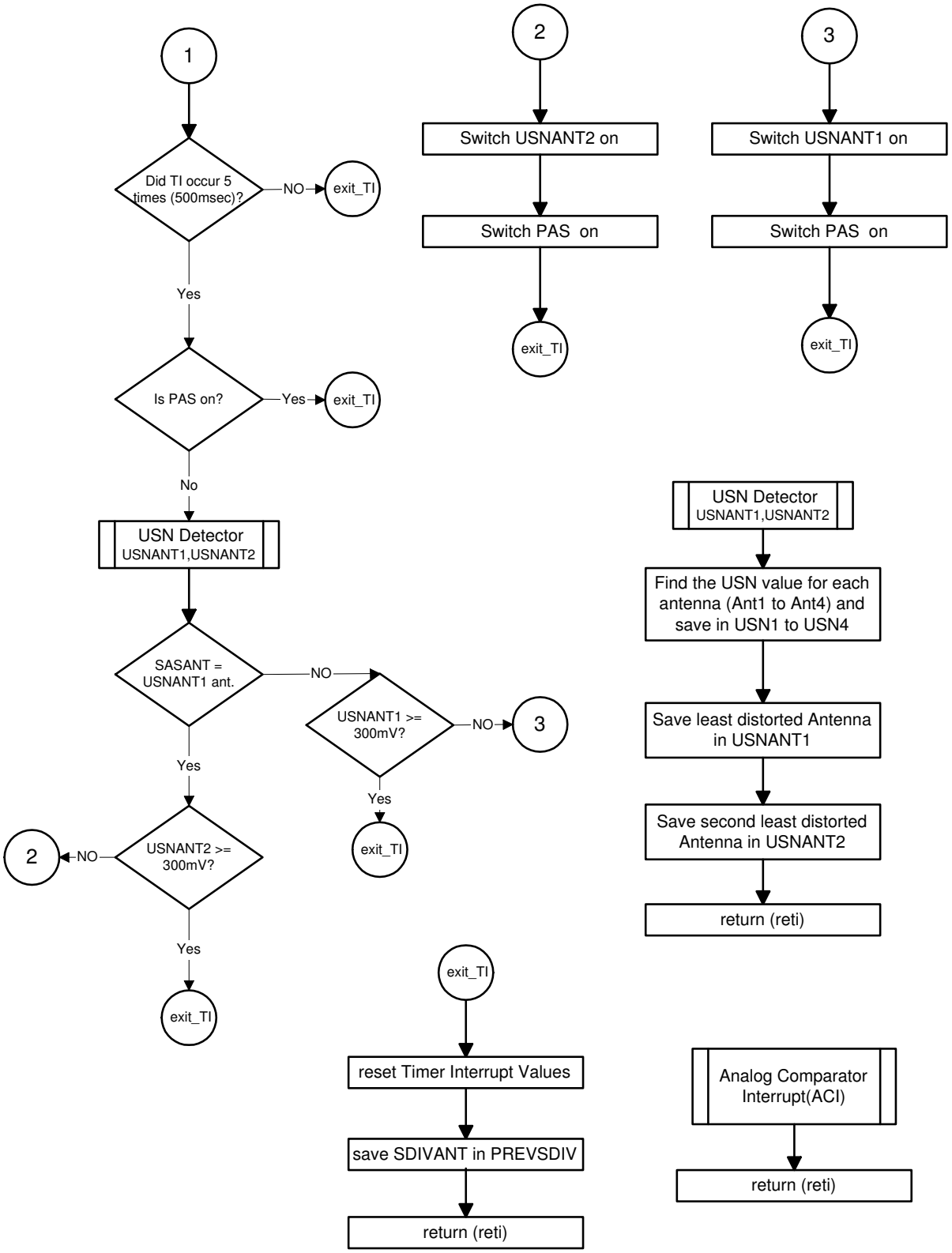

(B)

Continue... SPAS simplified software flow diagram (Part B)

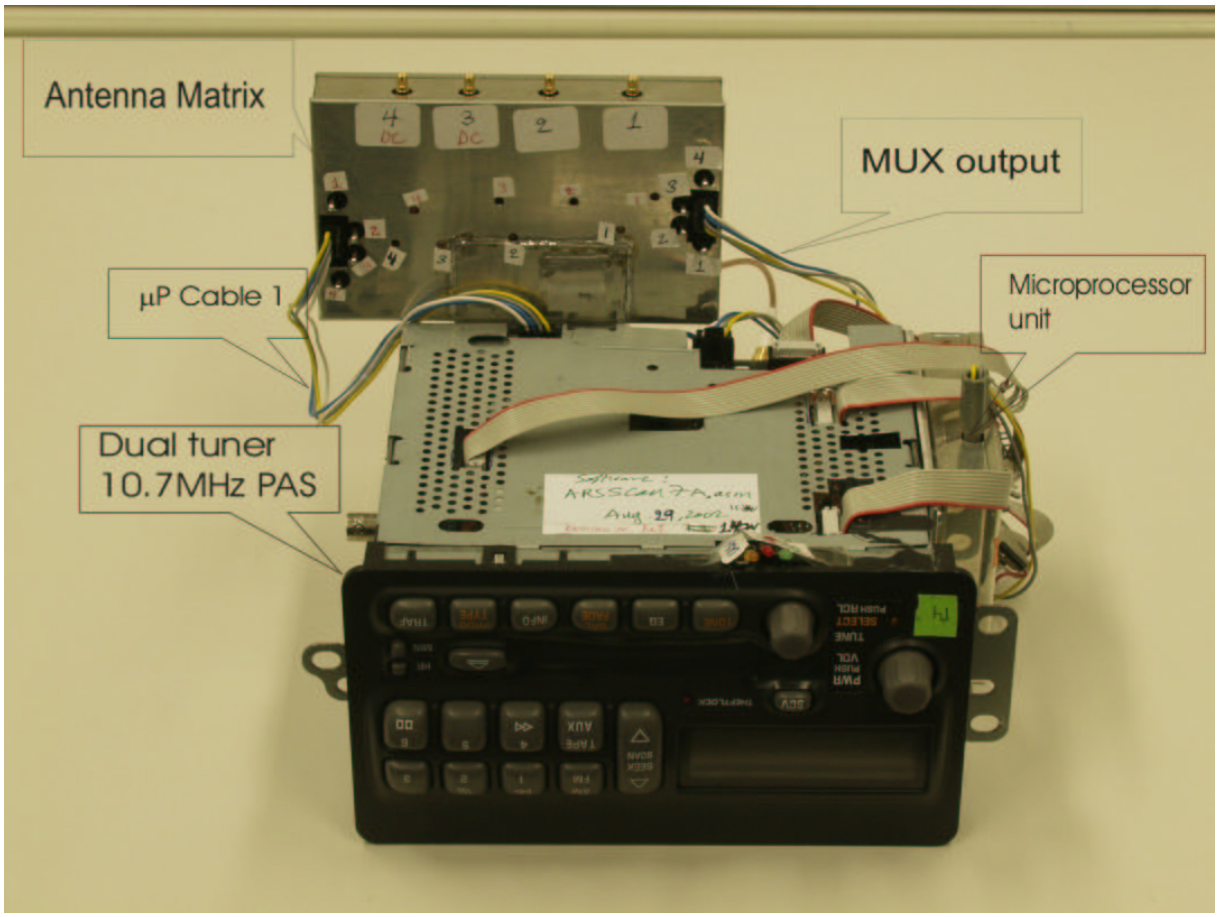

Figure 4.20: SPAS hardware prototype (picture was taken at the University of the Bundeswehr Munich)

Chapter 5

Diversity Testing System (DTS)

5.1 System Description

The Diversity Testing System (DTS) is a new system that has been developed and implemented to measure and record FM reception data/signals in the field. The main purpose of DTS is to test and optimize FM diversity systems in the lab by using the recorded signals from the field. The DTS consists of a receiver unit, a computer recording/playing unit, and transmitter unit. Figure 5.1 shows the basic structure of DTS. The FM signals are mixed down to baseband, via an I/Q demodulator, into in-phase and quadrature components. The in-phase and quadrature signals are digitized by the computer unit and saved on the hard drive.

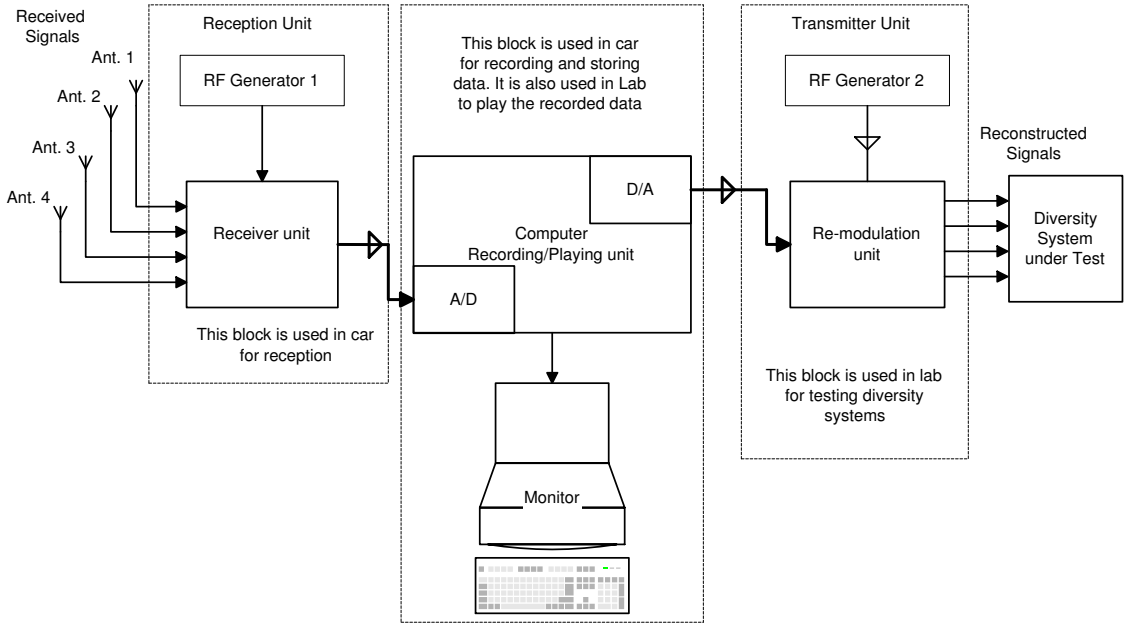

Figure 5.1: Diversity Testing System (DTS)

Traditionally, the radio designer would spent ample amount of time testing in the field to optimize the performance of a receiver. Furthermore, testing the radio in the lab with antenna dummy does not represent the actual antenna characteristics on the car. The most important advantage of using DTS is the amount of time saved in the design and testing of new FM diversity systems or even a single antenna FM receiver. Once we have recorded data from well known testing sites, it is saved in the recording unit and can be played

for more testing at any time in the lab. This configuration is able to measure maximum instantaneous RF level attenuation of $50dB$ in a Rayleigh field situation. It is also possible to generate a simulated FM data using the computer unit for various FM signal conditions and RF modulate it using the transmitter unit. Some of these FM conditions are co-channel, adjacent channel, Rayleigh field, and long delay multi-path. The following sections will explain in more details the hardware implementation of DTS.

5.1.1 Recording The Antenna Signals in the Field

Figure 5.2 shows the necessary components to record the antenna signals in the field. The antenna outputs must have 50 ohm output impedance to match the input receivers impedance. They can either be active or passive. The proper RF shielding must be done for the recording unit and it should be placed as far away as possible from the antennas to minimize the interference coupling. The RF cables that connect the antennas and the receiver unit must have the same length so that no extra RF delay is introduced to the system. In addition, the receiver unit should be completely shielded and placed close to the antennas to minimize the length of RF cables. This helps to minimize the interference coupling from the recording unit.

It is very important to measure the maximum RF signal level (using a reference antenna) in the desired driving area (or when driving in circles) before recording the antenna signals. This RF level is used to adjust the Programmable Gain Control (PGC) in all four I/Q demodulators to obtain the optimum signal-to-noise ratio (see Figure D.2).

The four received antenna signals are decoded by the receiver unit and recorded simultaneously by the computer. This has the advantage of including the coupling and correlation data between the antennas as well as multi-path information for the individual antenna signals.

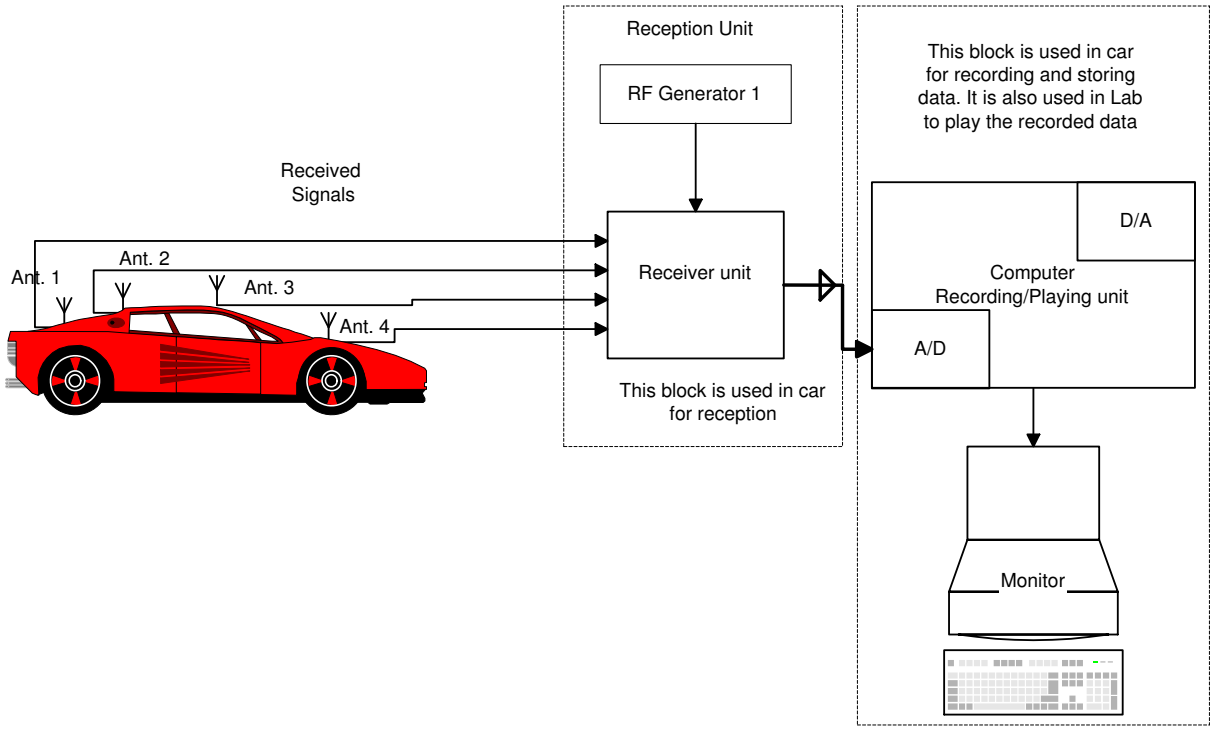

Figure 5.2: Recording Antenna Signals in the Field

5.1.2 Generating The Recorded Signals in the Lab

Figure 5.3 shows the necessary components to play the recorded antenna signals in the lab. It is necessary to adjust RF outputs of the Re-modulation unit when testing in the lab. This will insure accurate representation of the RF level of the recorded signals in the field. Adjusting RF levels can be done by using RF attenuators at each output.

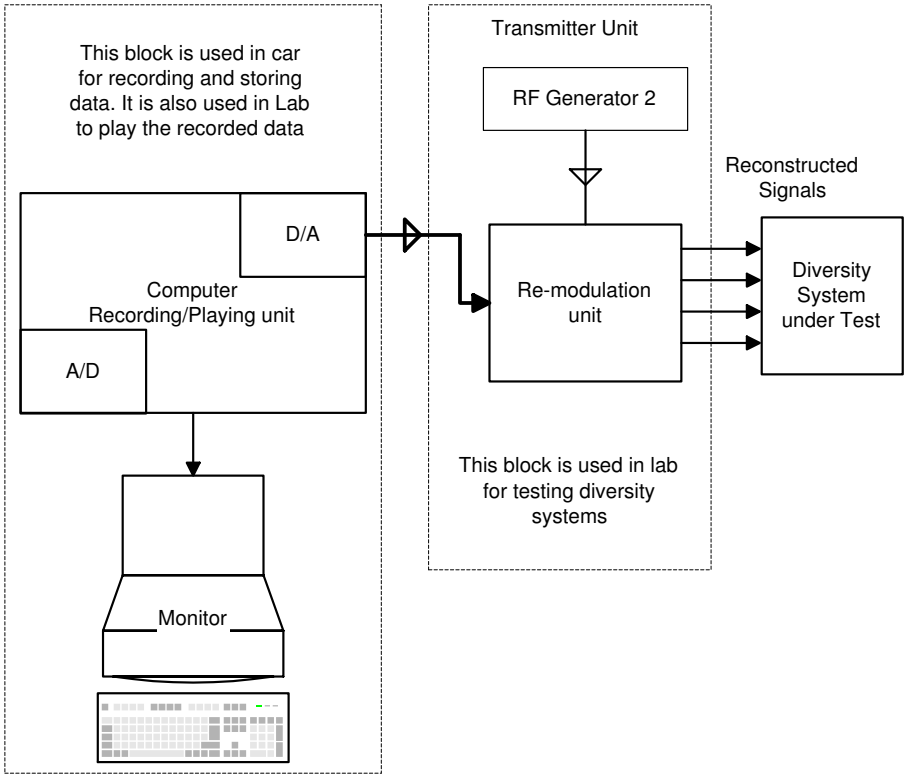

Figure 5.3: Playing Recorded Antenna Signals in the Lab

The DTS is able to test and optimize up to 4-antennas FM diversity systems. SAS, PAS as well as a single receiver are easily tested with this configuration. The playing unit can transmit the recorded data via the re-modulation unit in any number of antenna combinations. Therefore, diversity systems are easily compared with each other.

This system has also the capability to generate with the recording/playing unit a single test tone (i.e. 1kHz signal) along with multi-path data. The signal can have up to three multi-path signal reflections in addition to adjacent channel. Rayleigh fading field is easily generated with the desired car speed.

Figure 5.4 shows a picture of the implemented DTS that was taken at the University of the Bundeswehr, Munich Germany.

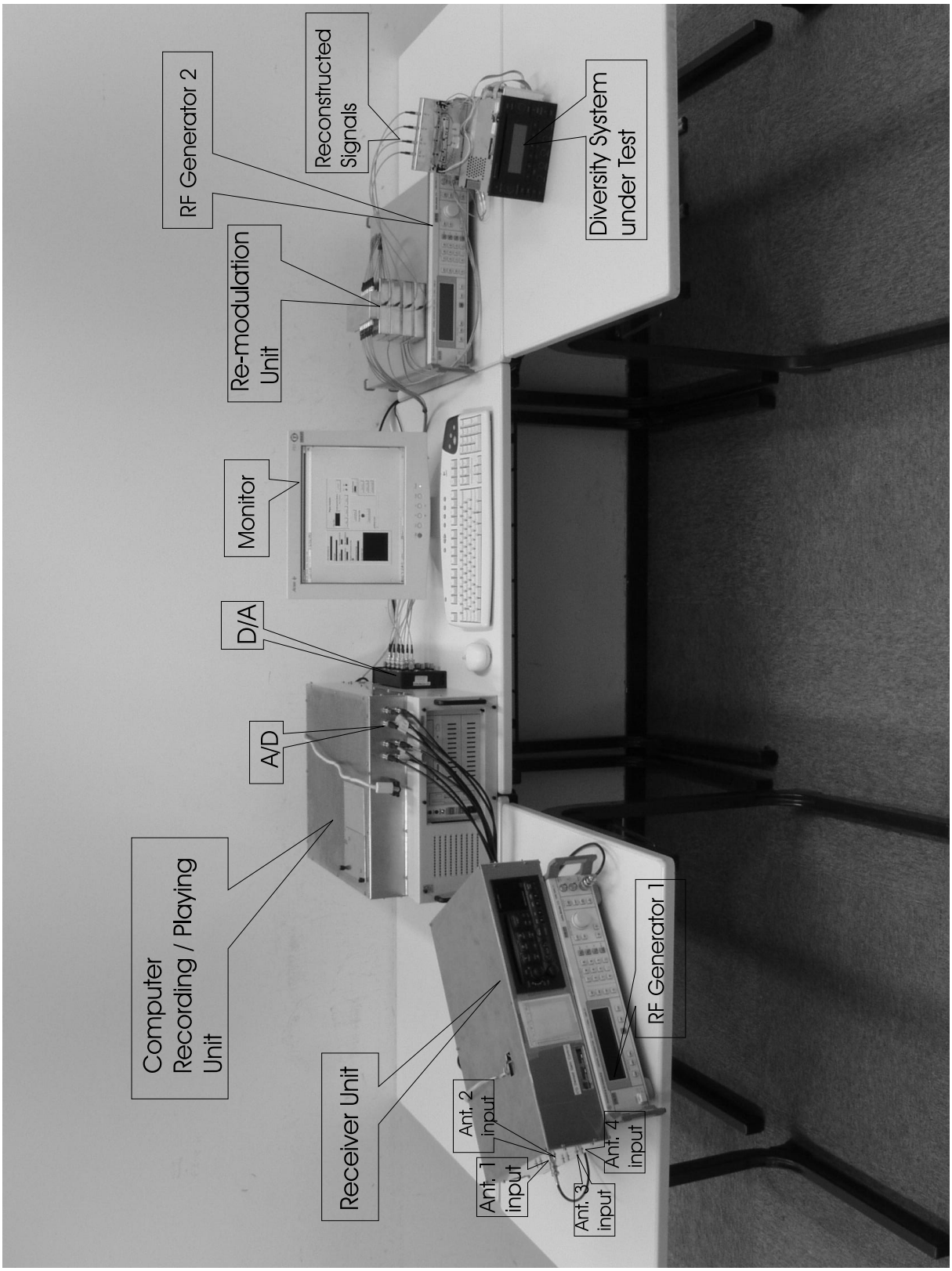

Figure 5.4: The implemented System

5.2 DTS Hardware Description

5.2.1 Receiver Unit

The system can utilize any four FM standard receivers as shown in Figure 5.5. The FM receivers must be synchronized to the same VCO frequency as shown in Figure 5.5. The four receivers are connected to four independent antennas in the vehicle. The required digital data to align each FM receiver must be loaded once before recording the antenna signals in the field. An output of f_{IF1} before the Intermediate Frequency (IF) limiter is taken from each receiver that is an input to an I/Q demodulator to produce I and Q baseband signals. The I/Q demodulator contains two mixers. The first mixer transfers the information of the f_{IF1}, i.e. $10.7MHz$ to a higher f_{IF2}, i.e. $246MHz$, which is required by the I/Q demodulator that is available commercially. It would be much easier if there is an I/Q demodulator available on the market that takes $10.7MHz$ directly. f_{o2} is generated from RF generator 1 as shown in Figure 5.1. The second mixer generates the I/Q baseband signals. The oscillator frequency f_{o3} is double of f_{IF2} frequency and is generated by filtering out the 5th harmonic of a $98.4MHz$ 5th overtone crystal. The differential baseband signals outputs of the I/Q demodulator are transformed to single I/Q outputs signals through differential amplifiers. These signals are the inputs to the recording system. Each I/Q demodulator has a Programmable Gain Control (PGC), a 16-bit shift register, to control f_{IF2} gain from -10dB to $70dB$ by $2dB$ steps. The recording computer system has two 12-bit 4 channels input A/D cards with $500kHz$ or $300kHz$ sampling frequency for recording the information from the I/Q demodulators.

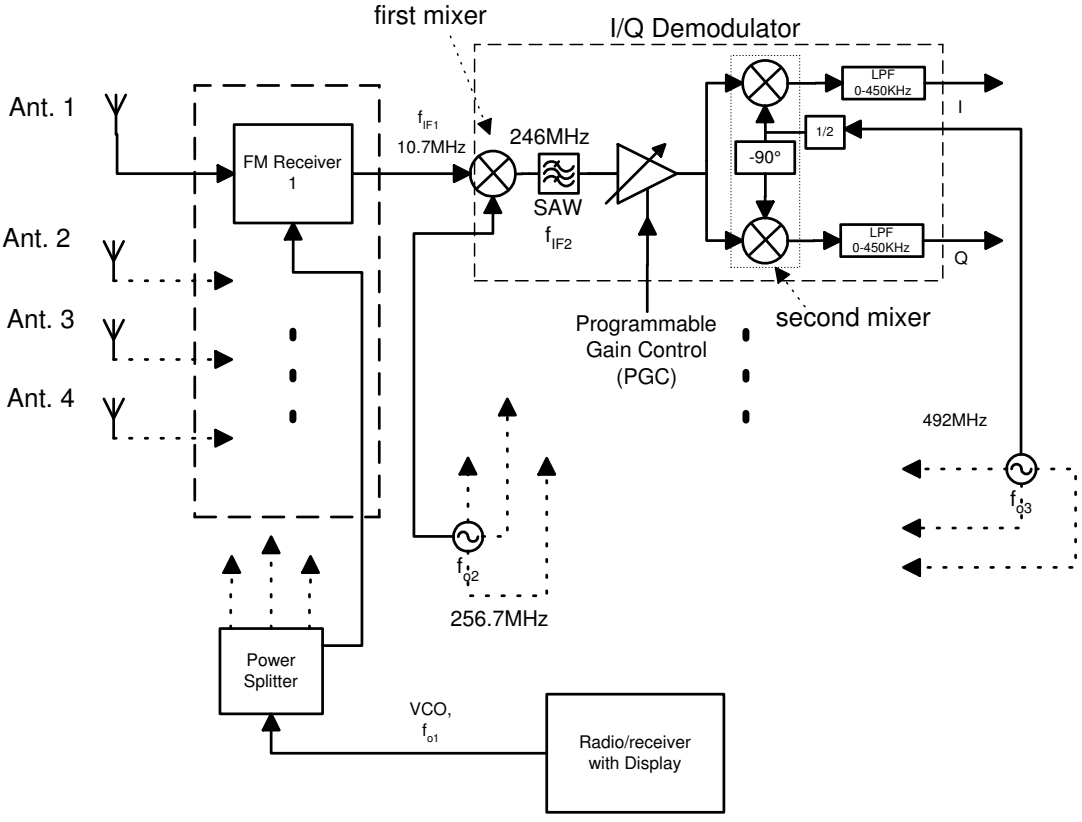

Figure 5.5: Receiver Unit

FM Receivers Characteristics

Each applied FM receiver (tuner) is of the superheterodyne type. The basic structure of such a receiver is shown in Figure 5.7. The front end is a variable bandpass filter which is tuned to the desired incoming radio-frequency (RF). The Voltage Controlled Oscillator (VCO) is automatically adjusted so that the mixer always produce the fixed IF. The VCO also serves in the tuning of the front end as it couples with the crystal oscillator in the tuning system. The IF section for this specific tuner has three IF filters that each has a bandwidth of $150kHz$. Each applied FM tuner has a Noise Figure (NF) of about $7dB$ and it outputs f_{IF1} $(10.7MHz)$ before the FM limiter to retain the multi-path information. Figure 5.6 shows the f_{IF1} output vs. RF input. Figure 5.6 also shows the wide band AM level voltage output in volts for the same RF input. The level line is proportional to the RF level and one of its functions is to serve the Automatic Gain Control (AGC) block. This is usually done for the purpose of not over-loading the receiver from strong RF signals. The measurements were taken at RF input frequency of $90.5MHz$ with no FM modulation. The $10.7MHz$ output is relatively linear for RF input of 1 to $64dB\mu V$ before it levels out due to AGC. The receiver has about $50dB$ of AGC range. This kind of receiver characteristics are adequate for recording multi-path signals in the field. The multi-path data of interest in the field usually has a range of amplitudes from $10dB\mu V$ to $50dB\mu V$. RF amplitudes above $60dB\mu V$ are considered strong signals.

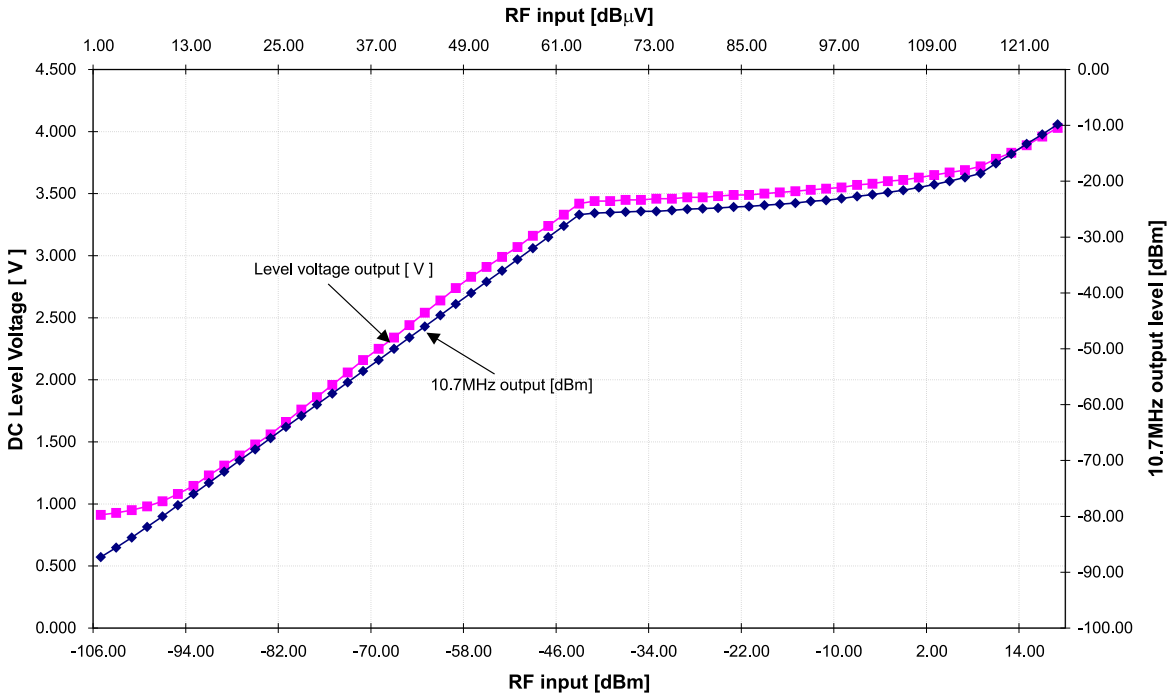

Figure 5.6: FM Receiver f_{IF1} $10.7MHz$ and level voltage outputs vs. RF input of the FM Antenna of Figure 5.7

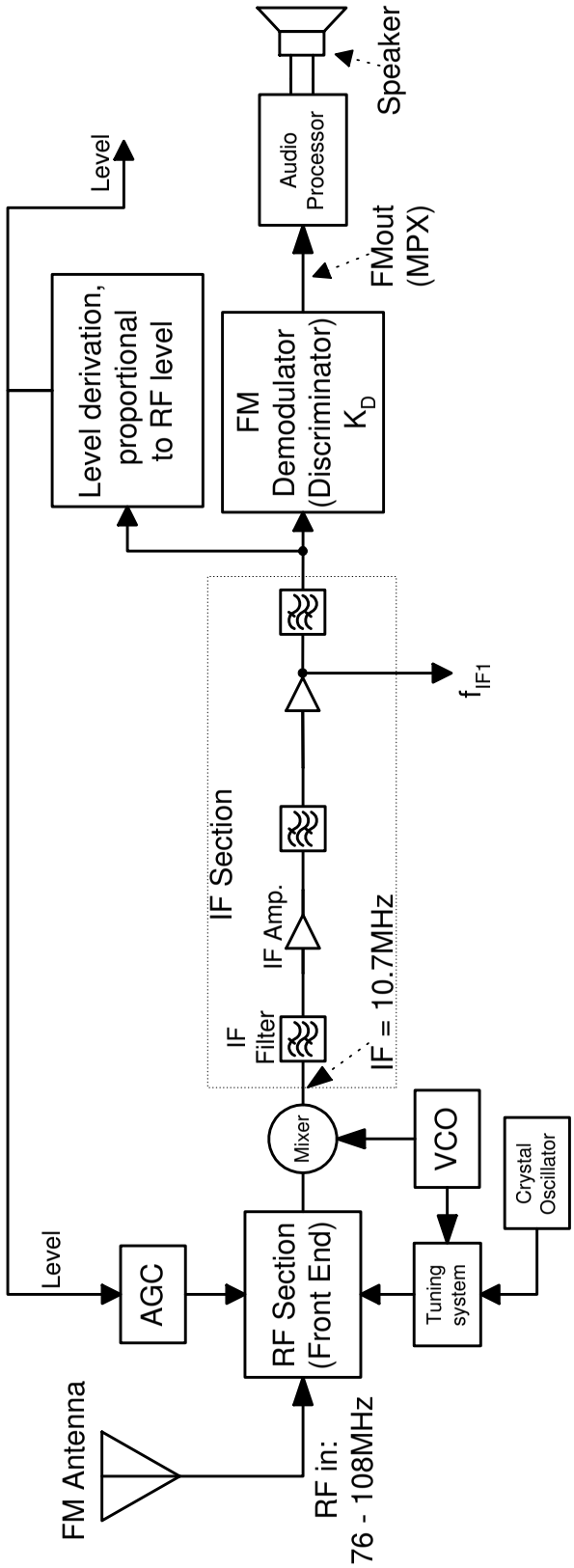

Figure 5.7: Superheterodyne Receiver structure

Figure 5.8 shows the output of $10.7MHz$ when the RF input frequency is 60% AM modulated with $40kHz$ signal and no FM modulation. This was done to show that the AM that would be produced due to multi-path is retained and the modulation coefficient would be kept constant with the increasing RF input level. The measurement was done with 50 Ohm-spectrum analyzer. The difference between the $10.7MHz$ peak and one of the $40kHz$-signal side band is measured in dB.

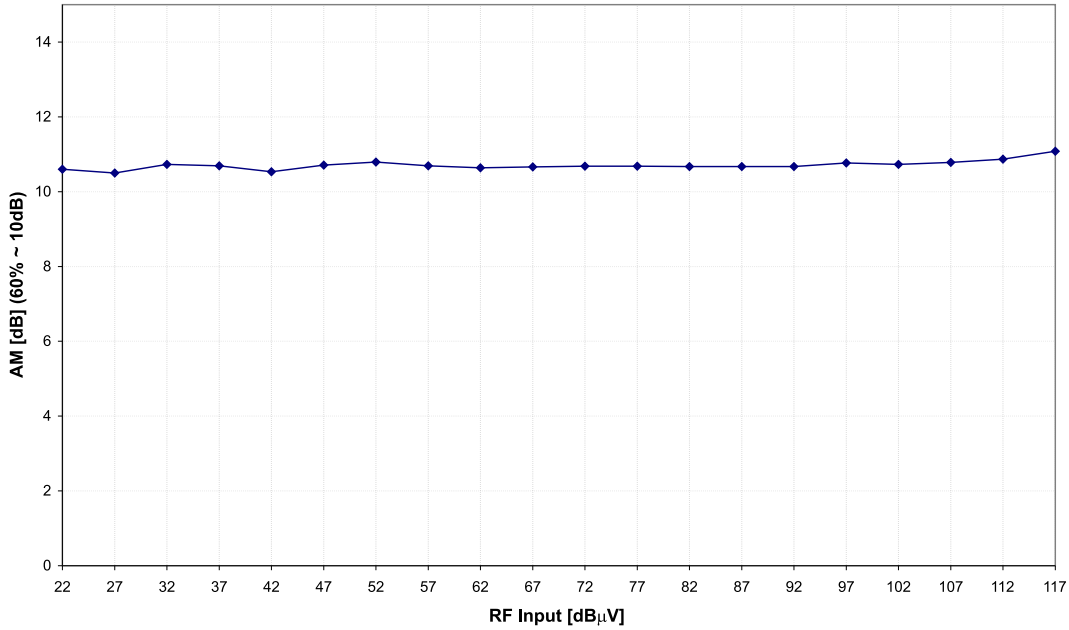

Figure 5.8: AM measurement at f_{IF1} $10.7MHz$ output of Figure 5.7

The First Mixer and I/Q Demodulator

The basic operation of the I/Q demodulator and the first mixer is shown in Figure 5.9. The input signal $V_{FM}(t)$ is converted to f_{IF1} by the first mixer. f_{IF1} gain can be controlled by PGC to obtain the maximum SNR before the signal is converted to $I(t)$ and $Q(t)$ components by the second mixer. The local oscillator (LO) generates the necessary quadrature signals $2\cos(\omega_{o3}t)$ and $2\sin(\omega_{o3}t)$ to produce $I(t)$ and $Q(t)$.

Assume PGC = 1 and the FM input signal $V_{FM}(t)$ to the first mixer is defined by the following

$$V_{FM}(t) = V_i \cos(\omega_{o1}t + \phi(t)) \tag{5.1}$$

where

$\omega_{o1} = 2\pi f_{IF1}$, V_i = Voltage Amplitude, $\phi(t)$ = FM modulation (see Equation 1.15)

The output of the first mixer is

$$V_{FM}(t) \cdot 2\cos(\omega_{o2}t) = V_i \cos((\omega_{o2} - \omega_{o1})t + \phi(t)) + V_i \cos((\omega_{o2} + \omega_{o1})t + \phi(t)) \tag{5.2}$$

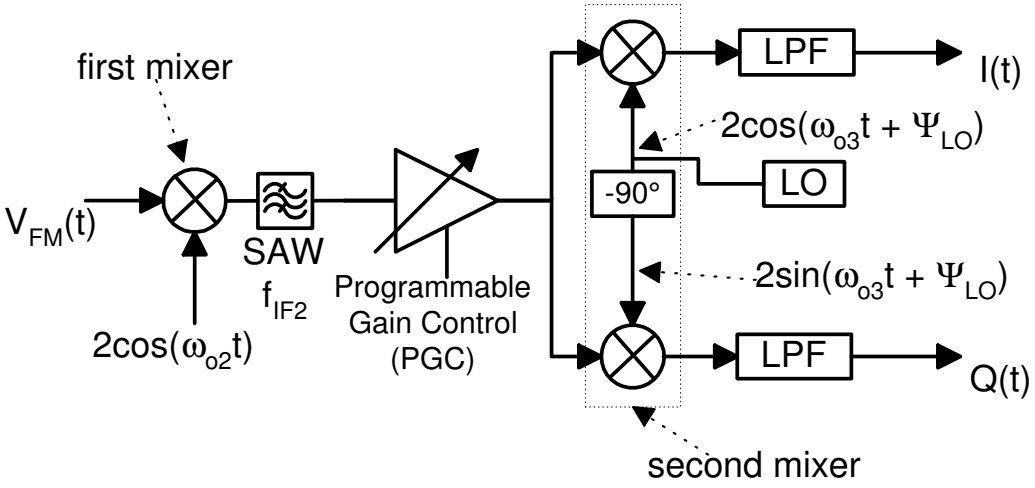

Figure 5.9: First mixer and I/Q demodulator

The SAW filter will filter out the up-converted component. The output of it will reduce to

$$V_i \cos((\omega_{o2} - \omega_{o1})t + \phi(t)) \tag{5.3}$$

where

$$\omega_{o2} - \omega_{o1} = 2\pi f_{IF2} = \omega_{o3}$$

The in-phase component $I(t)$ is

$$V_i \cos(\omega_{o3}t + \phi(t)) \cdot 2\cos(\omega_{o3}t + \Psi_{LO}) = V_i \cos(\Psi_{LO} - \phi(t)) + V_i \cos(2\omega_{o3}t + \phi(t)) \tag{5.4}$$

where Ψ_{LO} is assumed the local oscillator arbitrary constant phase.
The signal passes through the LPF, then we obtain

$$I(t) = V_i \cos(\Psi_{LO} - \phi(t)) \tag{5.5}$$

The quadrature component $Q(t)$ is

$$V_i \cos(\omega_{o3}t + \phi(t)) \cdot 2\sin(\omega_{o3}t + \Psi_{LO}) = V_i \sin(\Psi_{LO} - \phi(t)) + V_i \sin(2\omega_{o3}t + \phi(t)) \tag{5.6}$$

When the signal passes through the LPF, then we obtain

$$Q(t) = V_i \sin(\Psi_{LO} - \phi(t)) \tag{5.7}$$

The local oscillator is not phased locked and its generated from a crystal oscillator. The phase of the local oscillator constant phase Ψ_{LO} does not influence the FM signals because the information lies in the time derivative of the phase $\phi(t)$. Therefore, we can assume $\Psi_{LO} = 0$. It is necessary to adjust f_{IF2} gain so that the baseband signal levels are set to a maximum possible linear output as the RF input level changes. The f_{IF2} gain can be adjusted from -10 to 70dB by 2dB steps through a 16-bit shift register. When recording data in the field, the f_{IF2} can be set to a fixed gain to get the maximum signal-to-noise value to a measured average RF level in testing area. Section 5.3 describes the signal-to-noise performance of the DTS.

The SAW filter has about 248kHz 3-dB bandwidth as shown in Figure 5.10. This is adequate for FM reception.

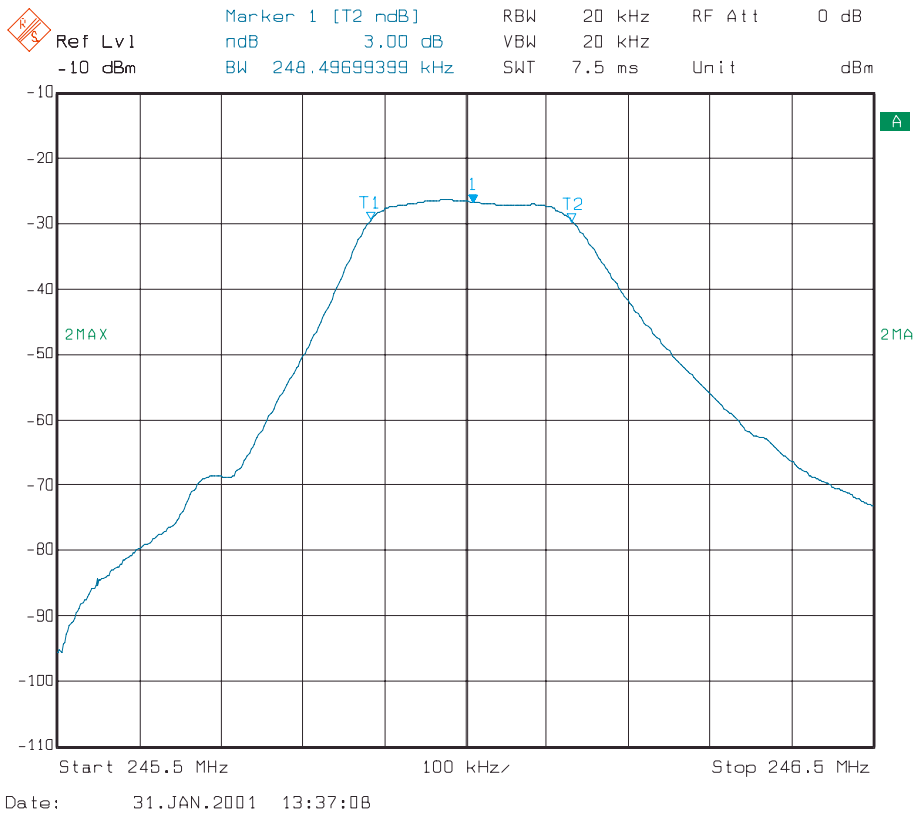

Figure 5.10: SAW filter measured frequency response

5.2.2 Transmitter Unit

The main function of the transmitter unit is to reproduce the recorded signals from the field. In addition, this unit should not introduce intolerable distortions to the recorded FM signals. The output from the computer recording system will drive the I/Q modulators as shown in Figure 5.1. The transmitter unit consists of four I/Q modulators and only used in the laboratory to replay the recorded signals and to test up to 4 antennas diversity systems. RF generator 2 is set to the desired RF frequency f_c in playing mode.

Ideal Operation of the I/Q Modulator

The quadrature modulator is a basic building block in many of wireless mobile communication products. It can be found in Global System for Mobile Communications (GSM), Personal Communications System (PCS) and many other systems. The basic operation of the I/Q modulator is shown in Figure 5.11. The input signals $I(t)$ and $Q(t)$ are directed to separate mixers. The LO generates the necessary quadrature signals to multiply them by the input signals to produce the in-phase and quadrature components. The resulting output signal V_{out} is the sum of the in-phase and quadrature components.

$I(t)$ and $Q(t)$ are defined by Equations 5.5 and 5.7, respectively. Assume $\Psi_{LO} = 0$. The in-phase component is

$$V_i \cos(\phi(t)) \cdot \cos(\omega_c t) = \frac{V_i}{2} \cos(\omega_c t + \phi(t)) + \frac{V_i}{2} \cos(\omega_c t - \phi(t)) \tag{5.8}$$

and the Quadrature component is

$$-V_i \sin(\phi(t)) \cdot (\sin(\omega_c t)) = -\frac{V_i}{2} \cos(\omega_c t - \phi(t)) + \frac{V_i}{2} \cos(\omega_c t + \phi(t)) \tag{5.9}$$

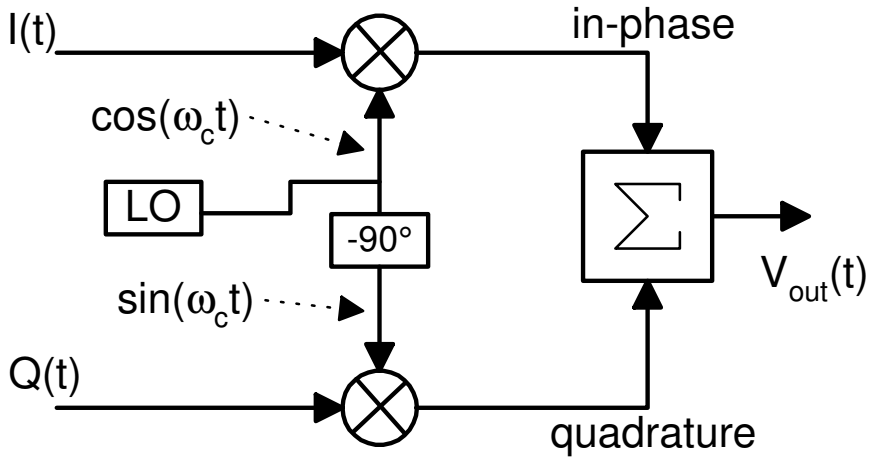

Figure 5.11: Basic operation of the I/Q Modulator

The sum of equations 5.8 and 5.9 yields the output signal $V_{out}(t)$ of the I/Q modulator

$$V_{out}(t) = V_i \cos(\omega_c t + \phi(t)) \tag{5.10}$$

Evaluating the I/Q Modulator

There are many book references that discuss the I/Q modulator basic concepts [16] [34] [33]. R. Umstattd [16] describes the associated linear errors in evaluating an I/Q modulator. Umstattd also includes test setups and mathematical equations that represents the linear errors due to amplitude imbalance, phase imbalance, and DC offsets of the carrier and modulating signals. Carrier suppression and the undesired sideband information can be obtained by the single sideband (SSB) test as shown in the hardware setup in Figure 5.12. It includes a two wave generator (provides $V_i \cos(2\pi f_m t)$ and $V_i \sin(2\pi f_m t)$ single tones), I/Q modulator, LO generator, and spectrum analyzer. In addition, the I/Q modulator input modulating signals are DC coupled and the offset is adjusted in the modulator and in the computer of the recording/playing unit. Let the computer provide sinusoidal signal $f_m = 1kHz$. The output spectrum of $V_{ssb}(t)$ (Figure 5.13) shows that the carrier suppression is about $62dB$ and the undesired sideband is about $50dB$ down from the desired sideband. The undesired sideband suppression mainly depends on the amplitude and phase balance between the modulation signals. Such I/Q modulator spectrum response (sideband and carrier suppression) should not degrade the overall SNR of the recorded FM signals and it should not add any significant distortion. This is discussed further in section 5.3. Such I/Q modulator characteristics are acceptable to re-modulate the FM signals.

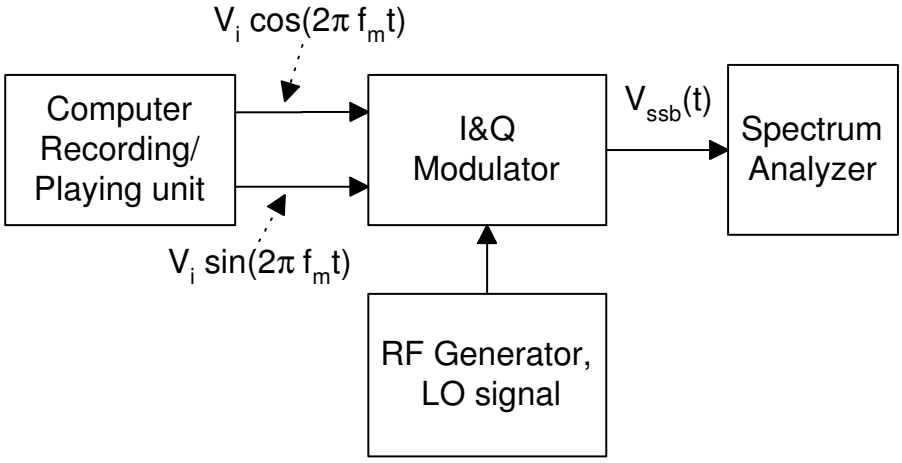

Figure 5.12: SSB Hardware Test Setup

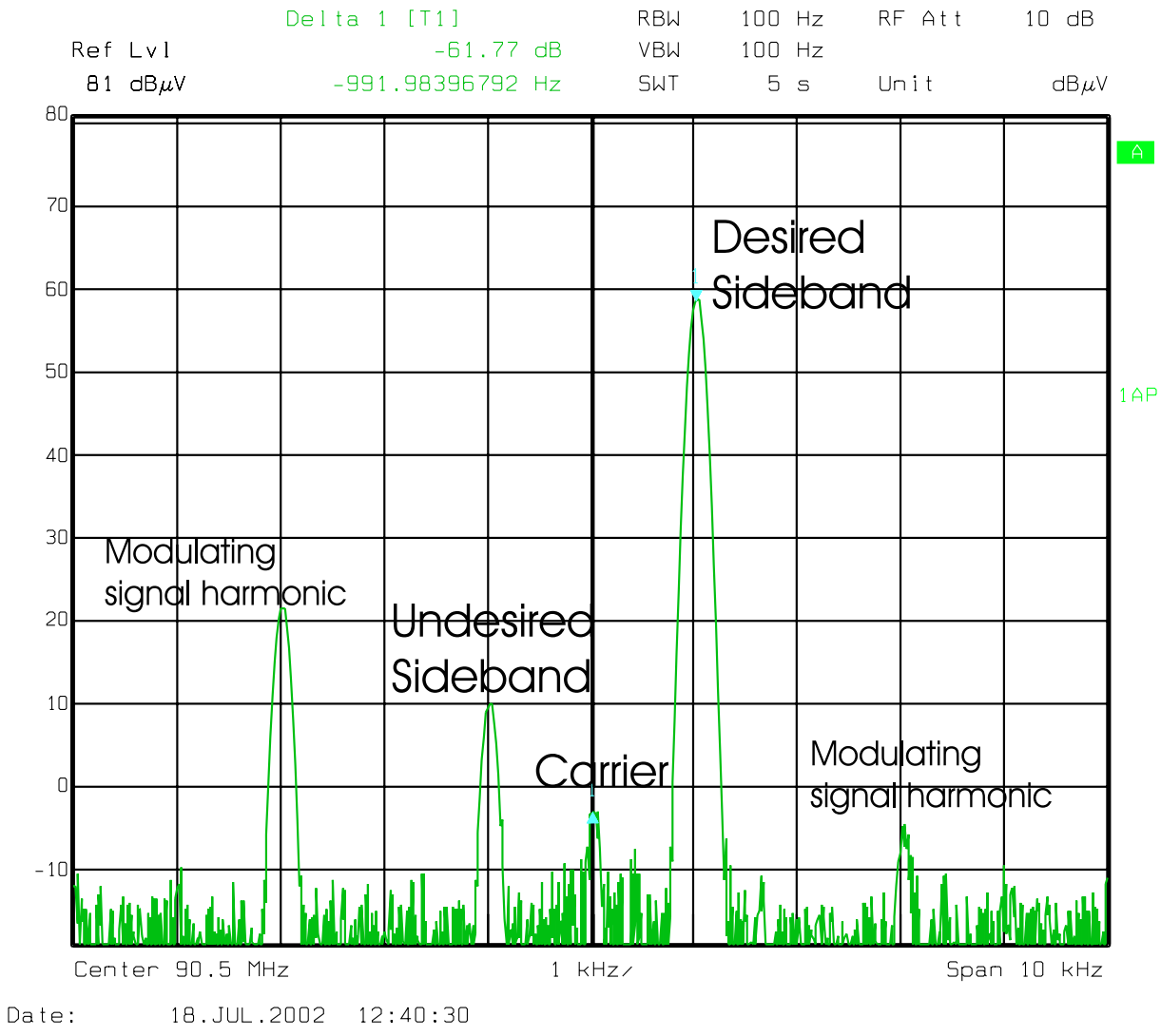

Figure 5.13: I/Q Modulator SSB Test Spectrum Output

The main purpose of using the I/Q modulator is to re-modulate FM signals whether they are recorded in the field or generated by the computer. Let the computer of the recording/playing unit generates the $I(t)$ and $Q(t)$ signals of a single tone FM baseband signal (1kHz) as shown in Figure 5.14. The $I(t)$ and $Q(t)$ baseband signals are up-converted by the I/Q modulator to the desired RF carrier. The RF carrier is demodulated by the FM receiver to produce the recovered signal FMout. The AMout is the level voltage that corresponds to the RF level input. FMout and AMout are monitored by the digital scope along with the original single tone. The output signals are shown in Figure 5.15 and it shows no evidence of significant distortions (see Appendix C) introduced by the I/Q modulator.

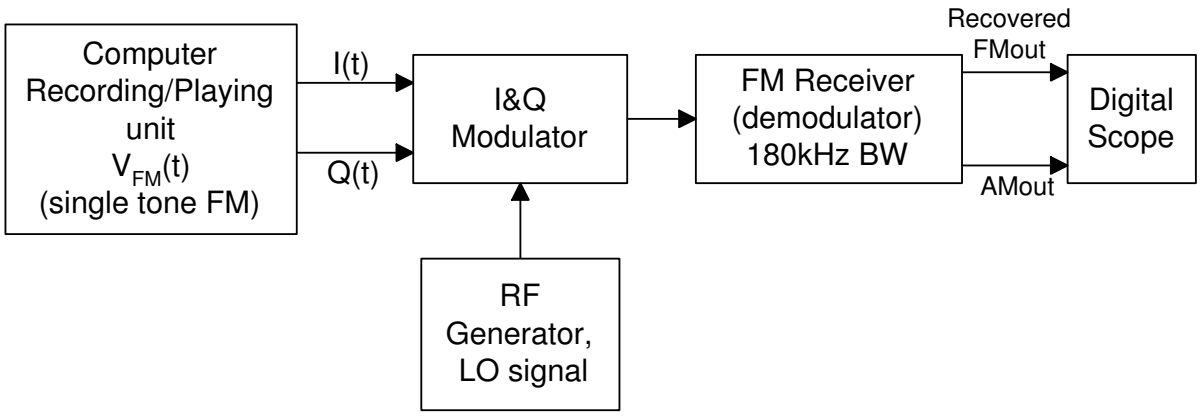

Figure 5.14: Hardware Test Setup to Recover FM modulating signal

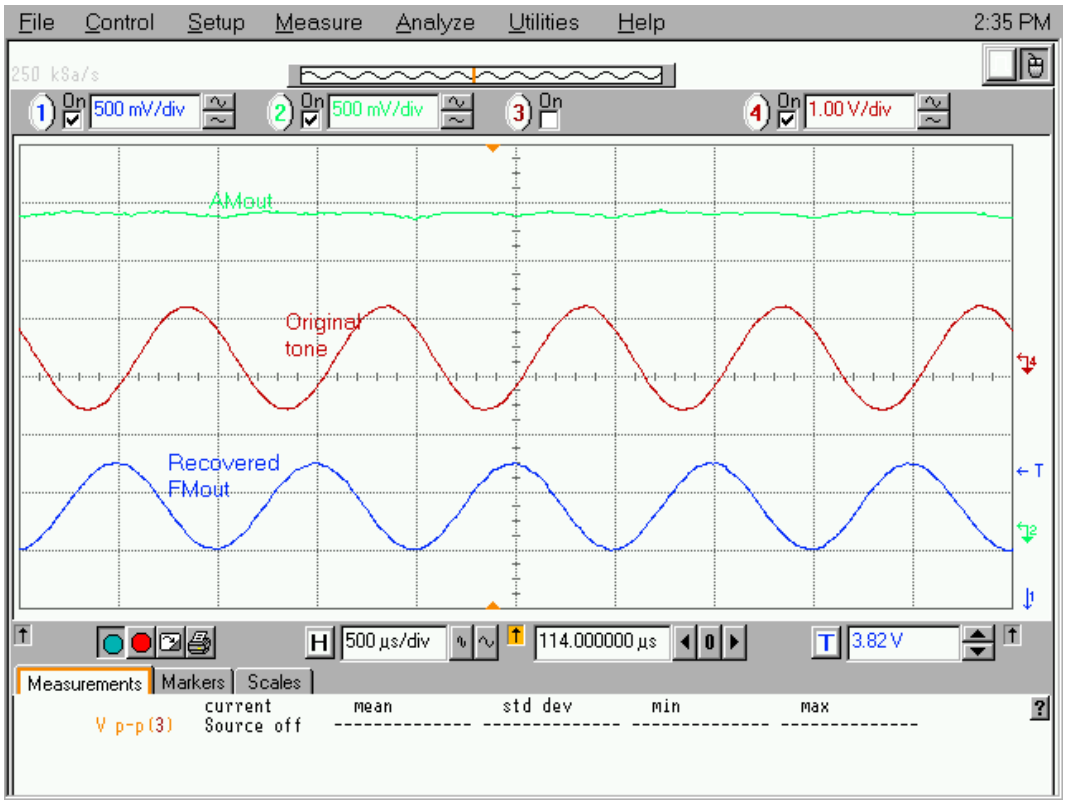

Figure 5.15: Recovered FMout (1kHz), Original Tone and AMout (level voltage). Parameters: $f_m = 1kHz$ tone, $f_d = 50kHz$ FM deviation, and $30dB\mu V$ RF level

AC Coupling of $I(t)$ and $Q(t)$ and the Effect on the Recovered FM Spectrum

Due to the fact that the signals $I(t)$ and $Q(t)$ are baseband signals, we can not block (by means of AC coupling) the DC component of the FM spectrum. The FM spectrum in traditional FM receiver is down-converted to the IF stage (typically $10.7MHz$) before demodulation. The DC component is shifted to the IF and the FM spectrum would not be degraded due to proper AC coupling. In case of DTS, the I/Q demodulator shifts the FM spectrum to baseband before it is saved in the computer and it can be transmitted again by using the I/Q modulators as shown in Figure 5.16. When the I/Q signal path is AC coupled, the DC component of the FM spectrum is eliminated. This causes audible and visible distortions in the demodulated FM signal FMout (MPX) as shown in Figure 5.17.

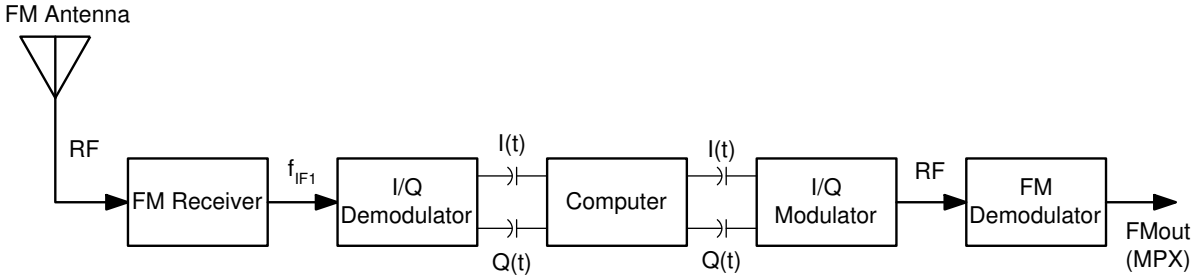

Figure 5.16: Simplified diagram of AC coupled I/Q signal path

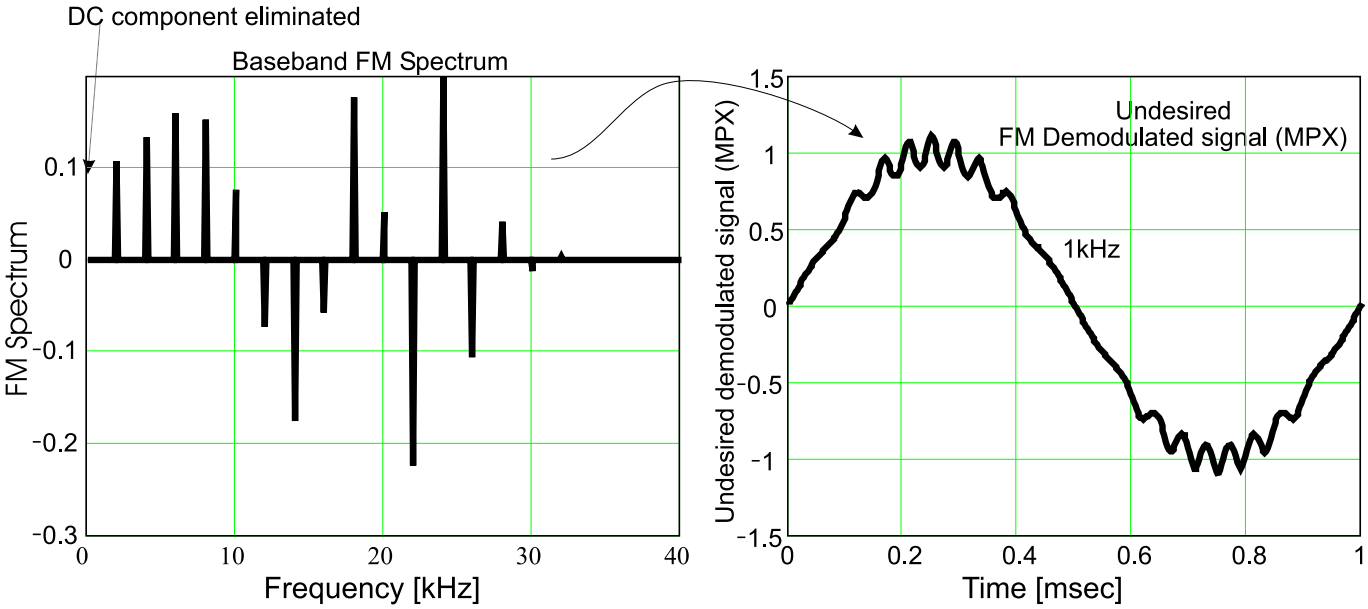

Figure 5.17: Undesired FM spectrum and demodulated MPX with AC coupling. Parameters: $f_d = 25kHz$, $f_m = 1kHz$, ideal FM demodulator, no filters.

The resulting distortion from such signals is a function of the frequency deviation f_d and modulating frequency f_m as shown Figure 5.18. The distortions were calculated from the demodulated signal MPX spectrum with no filters. It is obvious that the worst distortions occur at low frequency deviations (i.e. 1kHz to 20kHz). The distortion for the undesired signal in Figure 5.17 is about 6.8% (1.9% with $15kHz$ digital (ideal) low-pass filter).

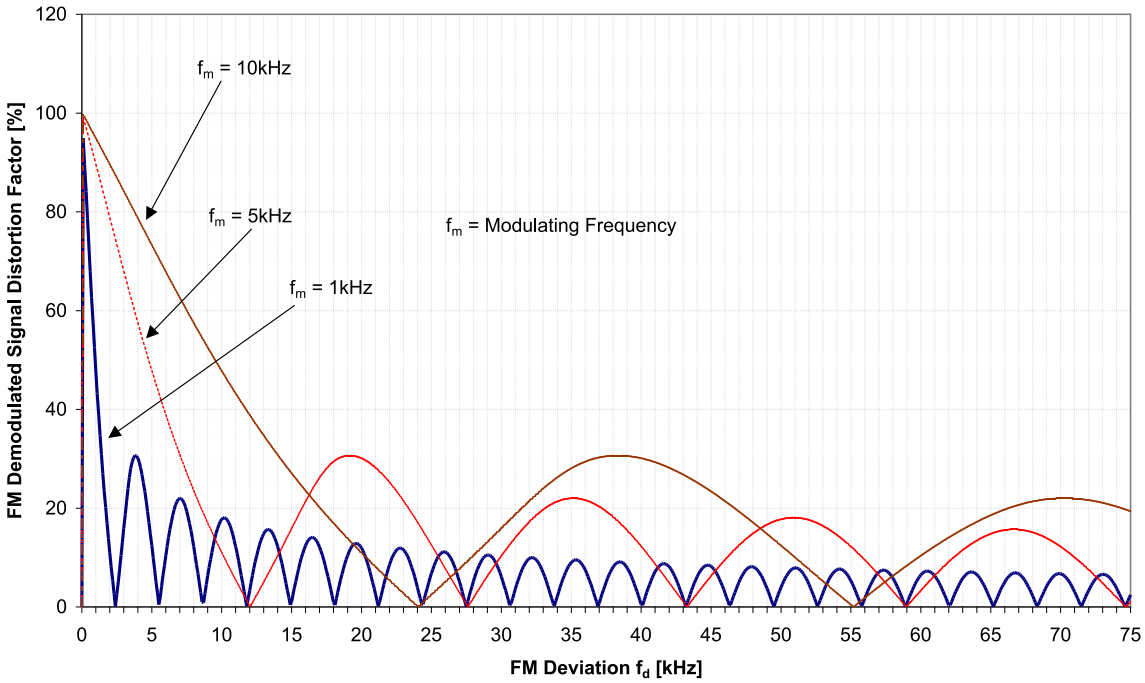

Figure 5.18: Undesired signal (MPX) distortion as a function of FM deviation. Parameters: ideal FM demodulator and no filters.

The above problem can be eliminated by replacing the capacitors in Figure 5.16 with direct coupling and adjusting the offsets of the modulating signals in the I/Q demodulator and modulator. The desired FM spectrum and the demodulated signal are shown in Figure 5.19.

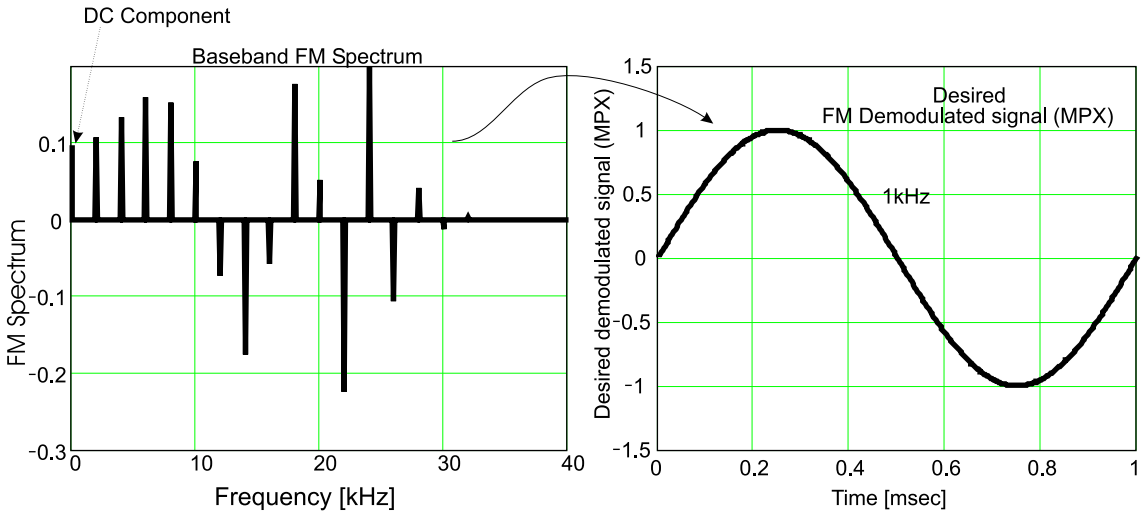

Figure 5.19: Desired FM spectrum and demodulated MPX with DC coupling. Parameters: $f_d = 25kHz$, $f_m = 1kHz$, ideal FM demodulator, no filters.

5.2.3 The Recording/Playing Unit

The 12-bit A/D cards, that are used to record data from the field, will provide a Signal-to-Quantization Noise Ratio (SQNR) [15] for a sinusoidal signal according to the following formula

$$\sqrt{SQNR} = \sqrt{\frac{3}{2}} 2^b \tag{5.11}$$

where b is quantizer bits.

Solving the above equation for SQNR in dB will give us

$$SQNR(dB) = 10 \log_{10} \frac{3}{2} + 20b \log_{10} 2 \tag{5.12}$$

A 12-bit A/D system will yield SQNR of 74dB in theory.

The computer system will record and save the measured data from the antennas on the vehicle. It will be possible to play the data to test diversity systems in the laboratory via a 12-bit D/A card as mentioned before. In addition, it is possible to generate multi-path data with a mathematical software and feed it into the device under test via the I/Q modulators [35].

5.3 Signal-to-Noise Ratio of DTS

It is necessary to determine the overall Signal-to-Noise Ratio (SNR) of the DTS because the system should not introduce extra significant distortions or degrade the SNR of the recorded signals. Distortions introduced by the DTS could cause false testing of an FM diversity system or a single antenna radio. Therefore, DTS SNR performance must be investigated and compared to a known reference.

The signal path of importance is the I/Q modulating FM baseband signals directed from the computer to the I/Q modulator. We assume that the signals from the computer add no extra distortions in this analysis. The model we use to investigate the resulting FM SNR and distortion of the due to the I/Q modulator is shown in Figure 5.21. The FM baseband signal $V_{FM}(t)$ and the Gaussian additive white noise $n(t)$ are split to the in-phase $I(t)$ and the quadrature $Q(t)$ components. Let $I(t)$ be

$$I(t) = A_i \cdot Re\{(V_{FM}(t) + \frac{n(t)}{\sqrt{C/N}}) \cdot e^{j \cdot \theta off}\} + Dc_i \tag{5.13}$$

and

$$Q(t) = A_q Im\{V_{FM}(t) + \frac{n(t)}{\sqrt{C/N}}\} \tag{5.14}$$

where C/N is the Carrier-to-Noise. The noise $n(t)$ is a zero-mean Gaussian white noise and

is represented by [36]

$$n(t) = \sum_{m=1}^{M} \cos(2\pi \frac{m}{N} t + \phi_m) \tag{5.15}$$

where $M = \frac{(N-1)}{2}$ and sequence length $N = 4096$. ϕ_m is uniformly randomly distributed between $[0, 2\pi]$. The mean is zero and the standard deviation is 0.26. Figures 5.20 (A) and (B) show the normalized noise distribution and the noise signal in time domain, respectively.

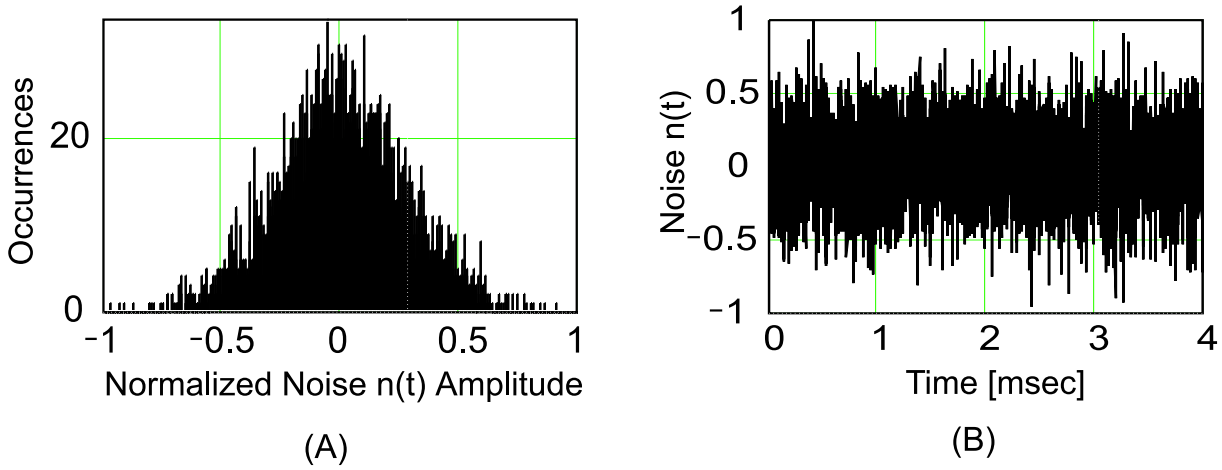

Figure 5.20: (A) Gaussian distributed Noise (B) Noise signal in time domain

The amplitude offset, phase offset and DC offset between $I(t)$ and $Q(t)$ are represented by A_i - A_q, θoff, and Dc_i, respectively. Assume no offsets with the carrier LO signals. The I/Q modulator output drives the FM demodulator followed by $150kHz$ low-pass filter. The calculations of the FM SNR and distortion are done for $1kHz$ modulating frequency f_m , $25kHz$ frequency deviation f_d. The above I/Q signals offsets are set to result in $50dB$ sideband suppression and $60dB$ carrier suppression (see Appendix C) as shown in the output response of the ssb test shown in Figure 5.13. Amplitude offset A_i - A_q is $5mV$, phase offset θoff is 0.25°, and Dc_i is $1mV$. The calculated SNR and distortion factor percentage at the output of the low-pass filter, as a function of the C/N, are shown in Figure 5.22. The red solid line (used as reference) in both Figures 5.22 (A) and (B) represents the FM demodulator SNR and distortion factor to the direct input of the FM baseband signal $V_{FM}(t)$. The black dotted line represents the SNR and distortion factor of the FM signal path shown in Figure 5.21. We can see that when the C/N is above $40dB$, the black dotted curve is limited to maximum SNR value of $48dB$ due to the above offsets of the I/Q modulator. When setting all offsets to zero, the black dotted line follows the red solid line. This maximum distortion contributed by the I/Q modulator in this case is about 0.5%. Obviously the SNR and distortion factor improve when using a $15kHz$ low-pass filter instead of $150kHz$ and eventually will follow the same curve characteristics (Figure 5.22) but at a higher C/N values. See Appendix D for the measured SNR curve of the DTS system. Finally, the threshold effects [31] [33] of the FM demodulator are obvious when the C/N is below $2dB$ in this case .

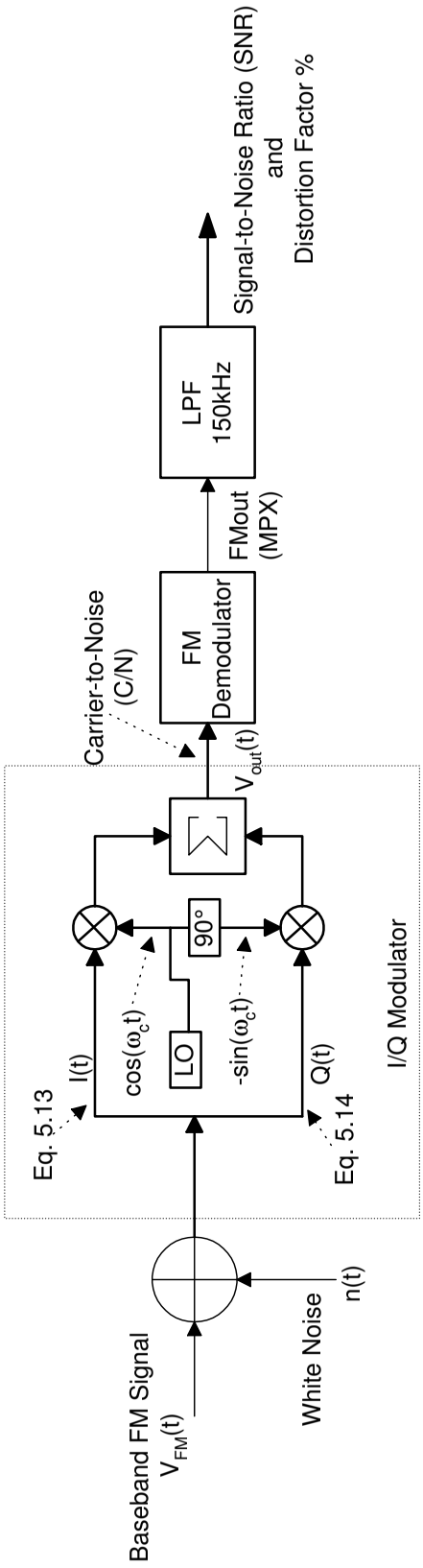

Figure 5.21: I/Q Modulator and FM demodulator Model to calculate FM SNR and Distortion

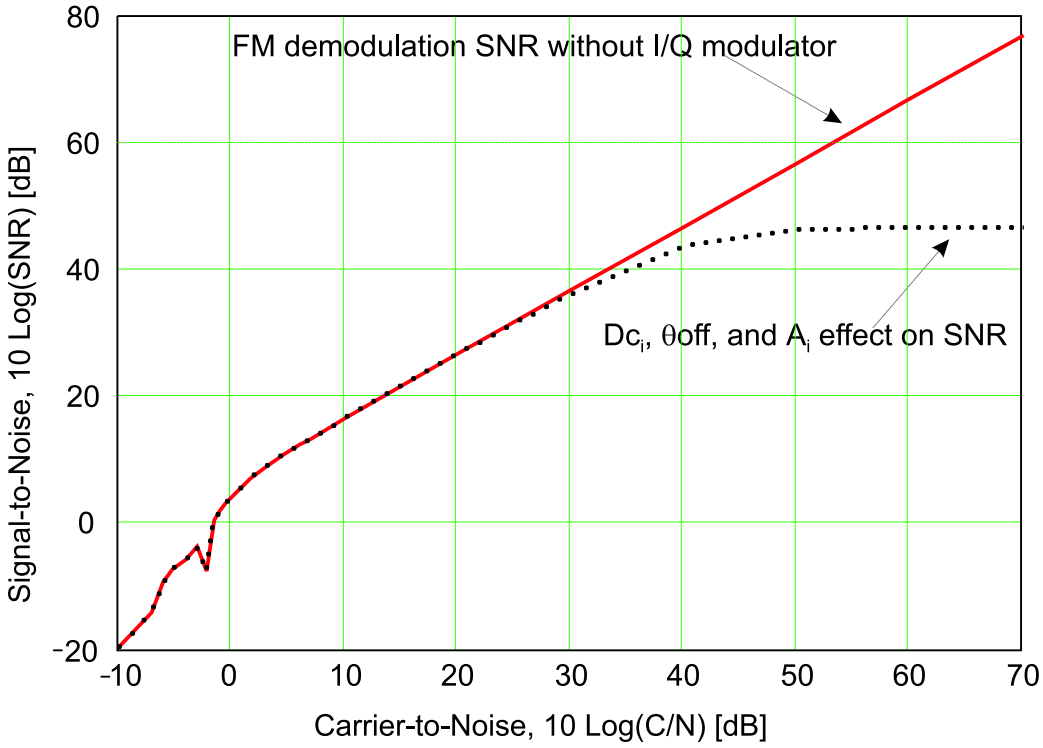

(A)

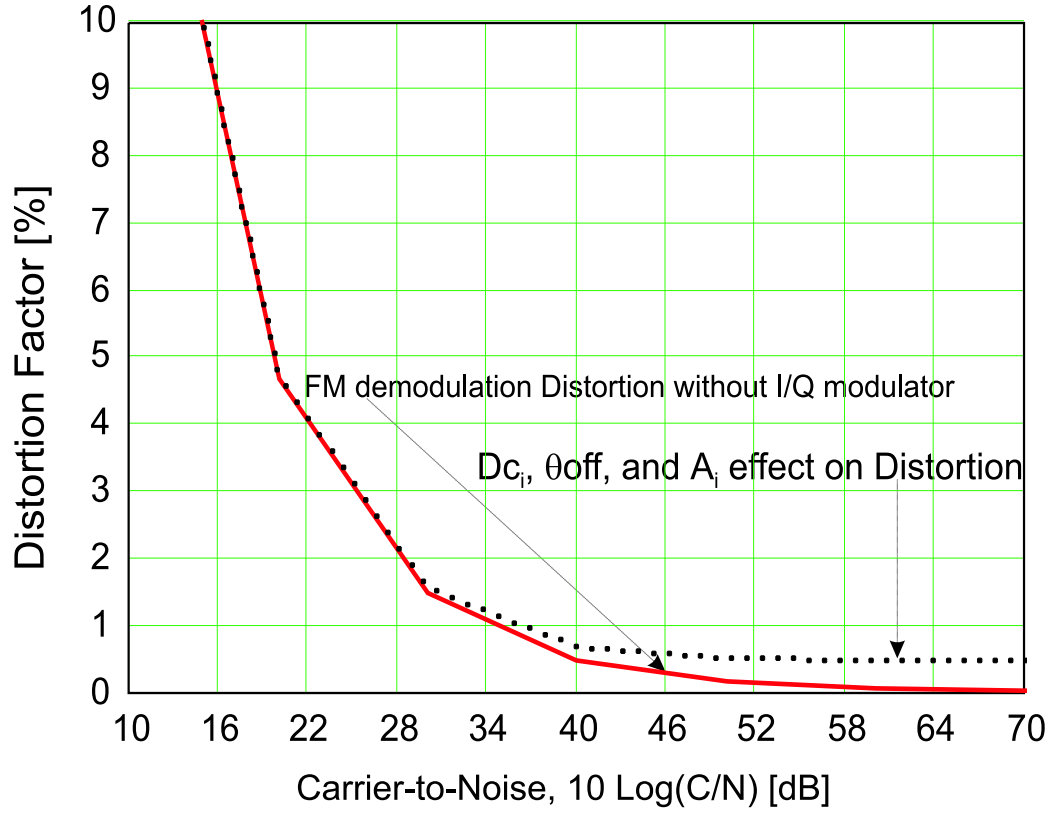

(B)

Figure 5.22: (A) SNR vs. C/N (B) Distortion Factor % vs. C/N

5.4 Dynamic Range of Amplitude Fades in Rayleigh Field

The DTS must be able to record multi-path Rayleigh signals such the one shown in Figure 1.7. Rayleigh fading was described in details in chapter 1.
A second hardware setup was necessary to observe the capability of the overall system to measure the maximum amplitude fades in a Rayleigh environment. Figure 5.24 shows the necessary hardware setup. The RF input was AM modulated with a 1kHz square wave using double balanced mixer as shown in Figure 5.24. The square wave was used to simulate the situation where the carrier amplitude fades due to multi-path propagation. The double balanced mixer is usually used to overcome nonlinearities of the RF generator when using external modulation.

The result in Figure 5.23 shows the capability of the system to record fades of approximately $50dB$. It can be seen that we have max amplitude when the square wave is high and $50dB$ of attenuation when the square wave is low.
The input RF signal is AM modulated with $10kHz$ and no FM modulation to guarantee that the AM is affected by the field attenuation. The system displays acceptable performance to measure FM signals in a multi-path propagation field.

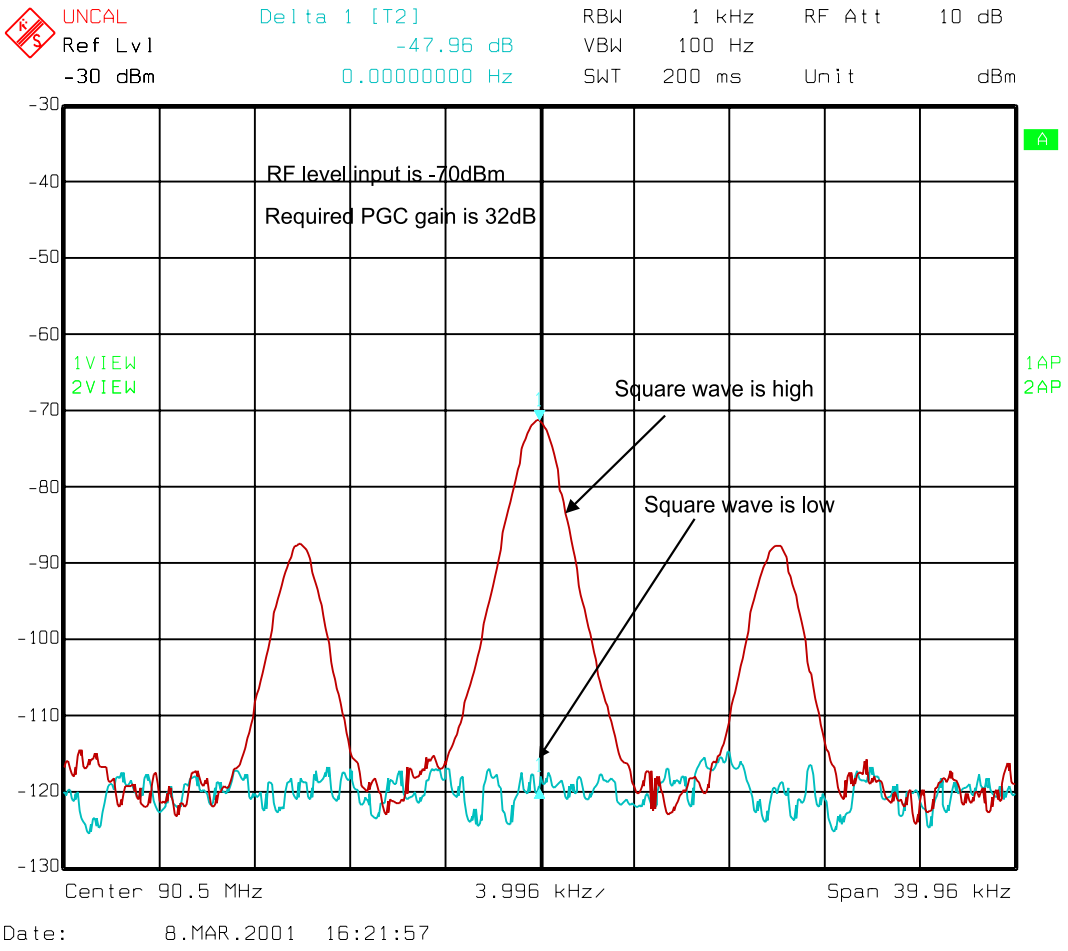

Figure 5.23: Measuring maximum fade with 30% AM Modulated RF input of -70dBm

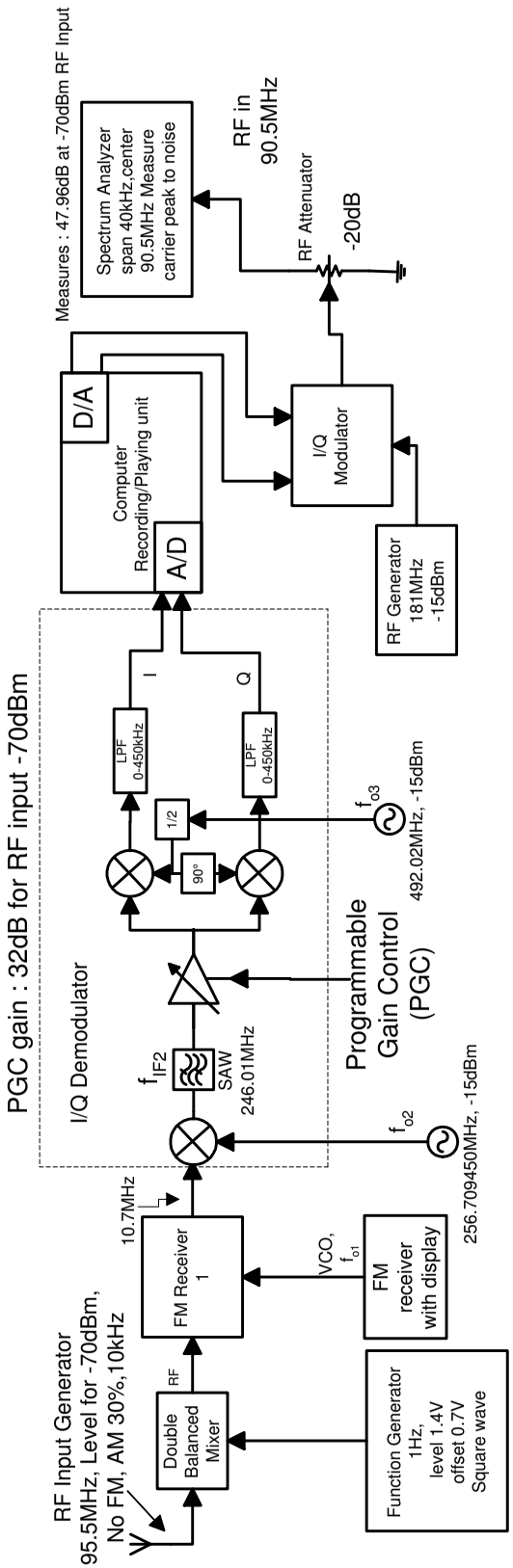

Figure 5.24: Hardware setup to measure maximum possible fades amplitude in a Rayleigh field

Appendix A

Acronyms

PAS	Phase Alignment System. Co-phase two antenna signals
SAS	Switching Antenna System
FDD	Fast distortion Detector (SAS is FDD)
SPAS	Scanning Phasing Antenna System
USN	Ultrasonic Noise Detector (slow detector)
DTS	Diversity Testing System
LPF	Low-pass Filter
PGC	Programmable Gain Control
IF	Intermediate Frequency
VCO	Voltage Controlled Oscillator
A/D	Analog to Digital Converter
D/A	Digital to Analog Converter
RF	Radio Frequency
AGC	Automatic Gain Control
SAW	Surface Acoustic Wave
LO	Local Oscillator
MPX	FM demodulator output

SNR	Signal-to-Noise Ratio
SQNR	Signal-to-Quantization Noise Ratio
C/N	Carrier-to-Noise Ratio

Appendix B

Important Variable Definitions

Chapter 1

v	Voltage envelope received by a mobile antenna
$p(v)$	Probability density function (pdf). Defines the expected narrow range for voltage level to be found around a given level
$P(v)$	Cumulative density function or probability (cdf). Defines the percent of time the voltage lies below the given level
$E\{\cdot\}$	Expected value operator or mean
$E\{v^2\} = \overline{V^2}$	Mean-square of v
λ	Wavelength
β	Phase constant
$\underline{V}(x)$	The received complex voltage sum of direct and reflected signals
Φ_t	Resulting phase of $\underline{V}(x)$
L	Total travelling distance
T	Total time of travelling distance
Δt	Time steps or Delta time
ν	Vehicle speed
f_c	Carrier frequency
f_D	Doppler frequency
$V(t)$	FM signal

$\phi(t)$	Phase or angle of $V(t)$ (FM modulation)
f_d	FM Frequency deviation
f_m	FM modulation frequency
$D_{FM}(t)$	Ideal FM demodulator
K_D	FM demodulator constant [V/Hz]

Chapter 2

θ_e	PAS error angle
m	AM modulation index
ω_r	PAS dither frequency
$T(s)$	PAS closed loop transfer function
K_p	Phase shifter constant
K_f	Gain constant
K_s	Synchronous detector constant
K_i	Integrator constant
$\Delta\phi(t)$	Erroneous angle deviation

Chapter 3

n	Diversity effectiveness
N	Number of ideally uncorrelated antennas
P_d	Probability that all antennas have signal-to-distortion less than a given threshold in diversity mode
P_s	Probability of single antenna that its signal-to-distortion less than a given threshold
i_f	Improvement factor
q	Signal quality

Γ	Reflection coefficient
Z_L	Load impedance
Z_o	Characteristic impedance, 50Ω
$[\underline{A}]$	Received waves matrix (complex)
$[\underline{B}]$	Reflected waves matrix (complex)
$[\underline{S_p}]$	Complex S-parameters matrix
$[\underline{S_t}]$	Transmission complex matrix (antenna gain pattern)

Chapter 5

$I(t)$	In-phase Component
$Q(t)$	Quadrature Component
V_{FM}	FM signal
Ψ_{LO}	Local Oscillator arbitrary phase
$n(t)$	Zero-mean gaussian distributed noise

Appendix C

I/Q Modulator Offsets Effect on FM Distortion

Consider the I/Q modulator model that is shown in Figure C.1. The in-phase component $I(t)$ has amplitude A_i, phase θoff, and DC Dc_i offsets relative to the quadrature $Q(t)$ component.
We use single tone sinusoidal signal $\omega_m(t)$ for sideband and carrier suppression calculations. Let $I(t)$ be

$$I(t) = A_i \cos(\omega_m t + \theta off) + Dc_i \tag{C.1}$$

and

$$Q(t) = A_q \sin(\omega_m t) \tag{C.2}$$

Assume no offsets with the LO signals.

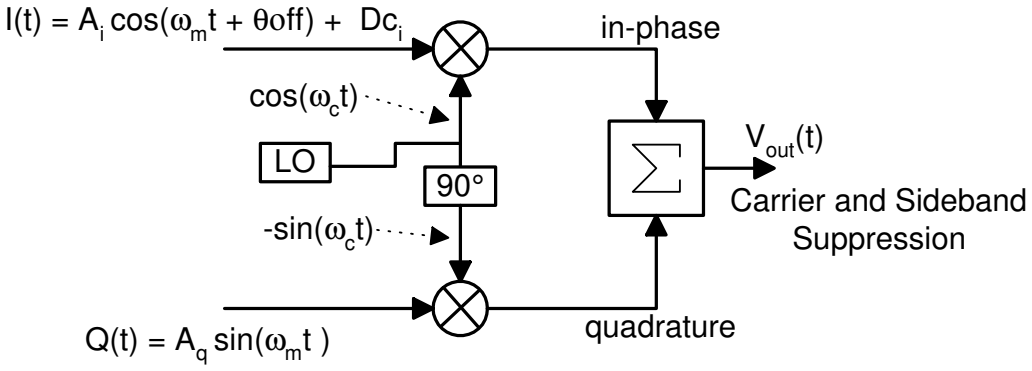

Figure C.1: I/Q Modulator with amplitude, phase and DC offsets

We need to compute $V_{out}(t)$ to be able to calculate the sideband and carrier suppressions due to offsets. $V_{out}(t)$ is given by

$$V_{out}(t) = \cos(\omega_c) \cdot (A_i \cos(\omega_m t + \theta off) + Dc_i) - \sin(\omega_c) \cdot A_q \sin(\omega_m t) \tag{C.3}$$

Simplifying further yields

$$\begin{aligned} V_{out}(t) = \quad & \tfrac{1}{2}(A_i\cos(\theta off) + A_q)\cdot\cos(\omega_c t + \omega_m t) \\ & -\tfrac{1}{2}A_i\sin(\theta off)\cdot\sin(\omega_c t + \omega_m t) \\ & +\tfrac{1}{2}(A_i\cos(\theta off) - A_q)\cdot\sin(\omega_c t - \omega_m t) \\ & +\tfrac{1}{2}A_i\sin(\theta off)\cdot\sin(\omega_c t - \omega_m t) \\ & +Dc_i\cos(\omega_c t) \end{aligned} \tag{C.4}$$

The upper sideband with the term $(\omega_c t + \omega_m t)$ is desired. The sideband suppression is

$$sideband\ suppression = 20\log\left|\sqrt{\frac{(A_i(\cos(\theta off) - \sin(\theta off)) + A_q)^2}{(A_i(\cos(\theta off) + \sin(\theta off)) - A_q)^2}}\right| \tag{C.5}$$

and the carrier suppression is

$$carrier\ suppression = 20\log\left|\sqrt{\frac{(A_i(\cos(\theta off) - \sin(\theta off)) + A_q)^2}{(2\cdot Dc_i)^2}}\right| \tag{C.6}$$

The sideband suppression mainly effected by the amplitude and phase offsets as shown in Figure C.2 (A) and (B), respectively. The DC offset Dc_i mainly effects the carrier suppression as shown in Figure C.2 (C).

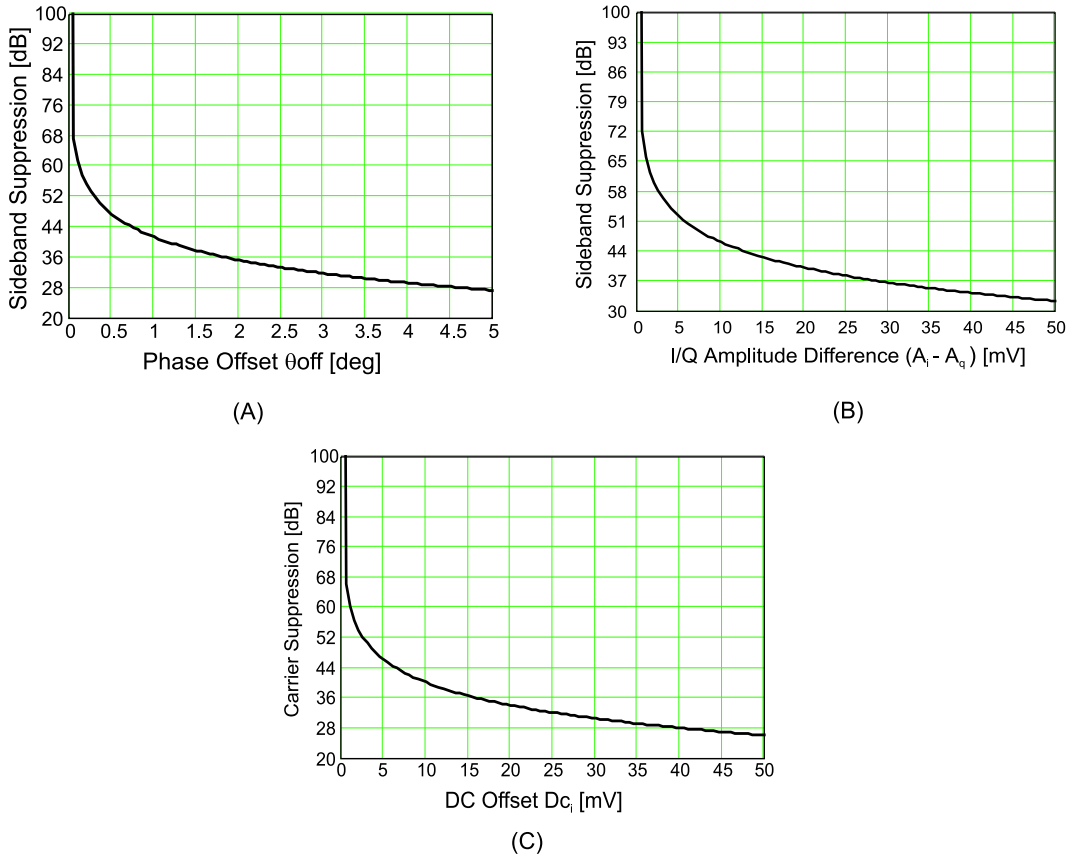

Figure C.2: (A) Sideband Suppression vs. θoff (B) Sideband Suppression vs. A_i - A_q (C) Carrier Suppression vs. DC_i

Now consider the FM signal $V_{FM}(t)$ as the input to the above I/Q modulator. The output of the I/Q modulator is then followed by an ideal FM demodulator and $150kHz$ low-pass as shown in Figure C.3. Let the modulation frequency $f_m = 1kHz$, $f_d = 25kHz$. The resulting distortion factor (see Equation 1.27) from each the above offsets is shown in Figure C.4 (A) through (C). Phase offset of 0.25° results in $53dB$ of sideband suppression and about 0.4% of FM distortion factor.

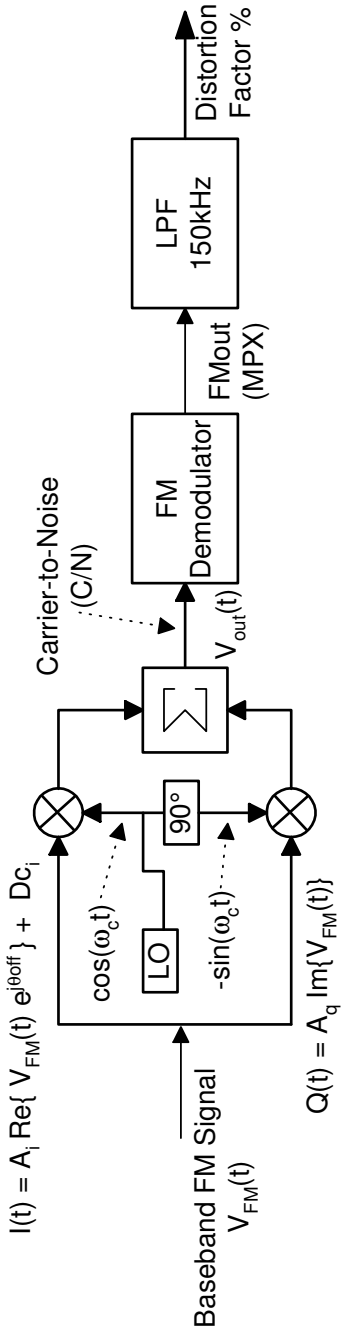

Figure C.3: FM signal as an input to the I/Q modulator followed by ideal FM demodulator

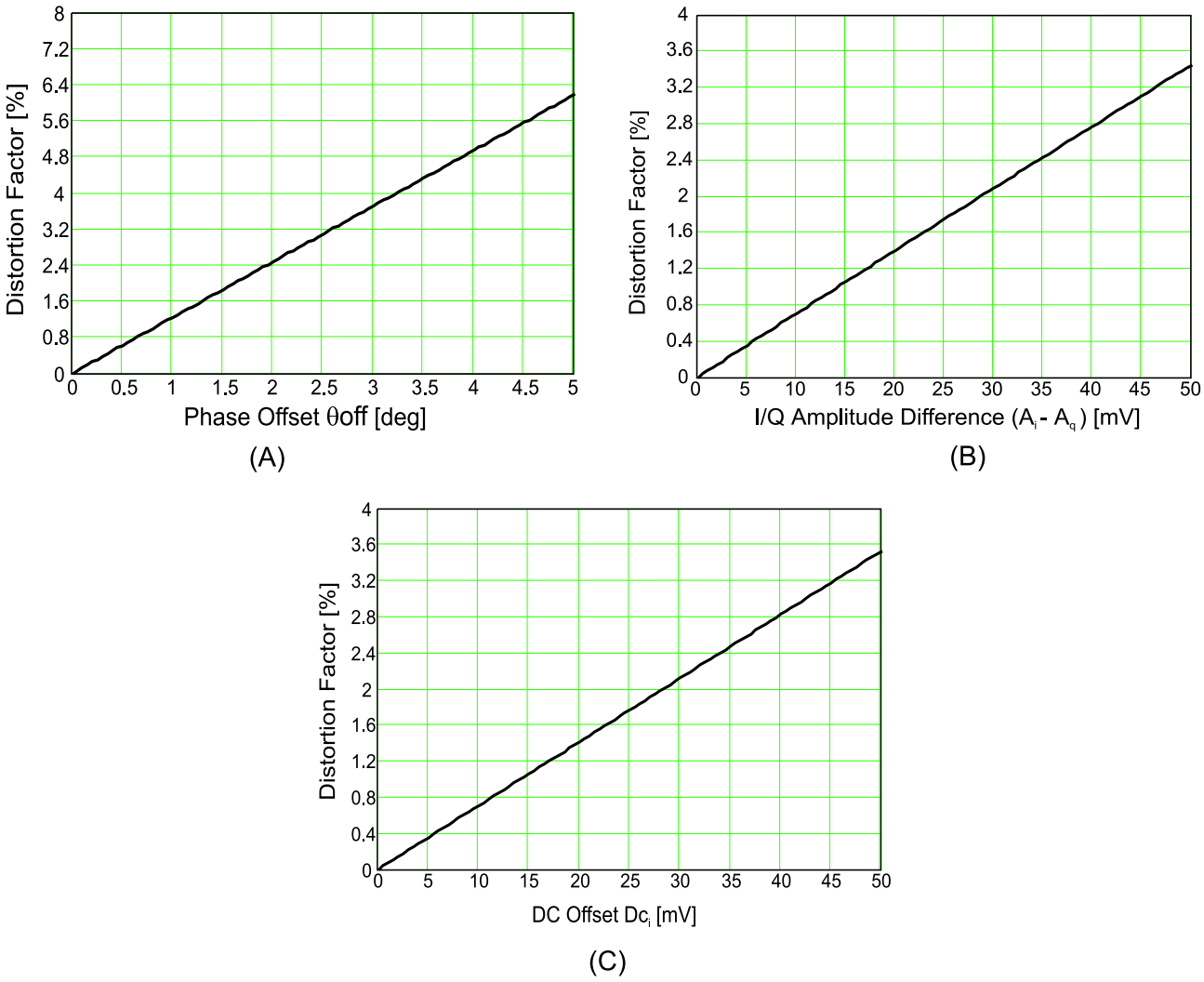

Figure C.4: FM Distortion factor %

Appendix D

Measured DTS Signal-to-Noise Ratio

The necessary hardware setup to evaluate the overall system SNR performance is shown in Figure D.1. The RF input level was varied from -116dBm($-9dB\mu V$) to 16dBm($123dB\mu V$) at 95.5MHz with 25kHz FM deviation and 1kHz signal tone. First, the SNR of the reference receiver was measured alone at the audio level (15kHz low-pass filter) with the spectrum analyzer as shown in top of Figure D.1. The second measurement was done after one section of the DTS was inserted in between the RF generator and reference receiver as shown in Figure D.1. f_{o2} can be controlled by 1Hz steps with an external RF generator to avoid frequency offsets at baseband level between all three oscillators. RF generator 2 must be set to double of the desired RF input because the I/Q modulator has a divide by two function.

It can be seen in Figure D.2 that the overall DTS SNR is almost similar (1 to $2dB$ less) to that of the reference receiver. The reason that the DTS SNR curve does not follow the curve shown in Figure 5.22 because of the $15kHz$ filter and the AGC system in the reference receiver. The AGC system limits the C/N that is presented to the FM demodulator. Therefore, the SNR of DTS stays constant for high RF inputs. Adjusting f_{IF2} gain insures maximum linear output voltage of baseband signals to maintain optimum SNR of the overall system.

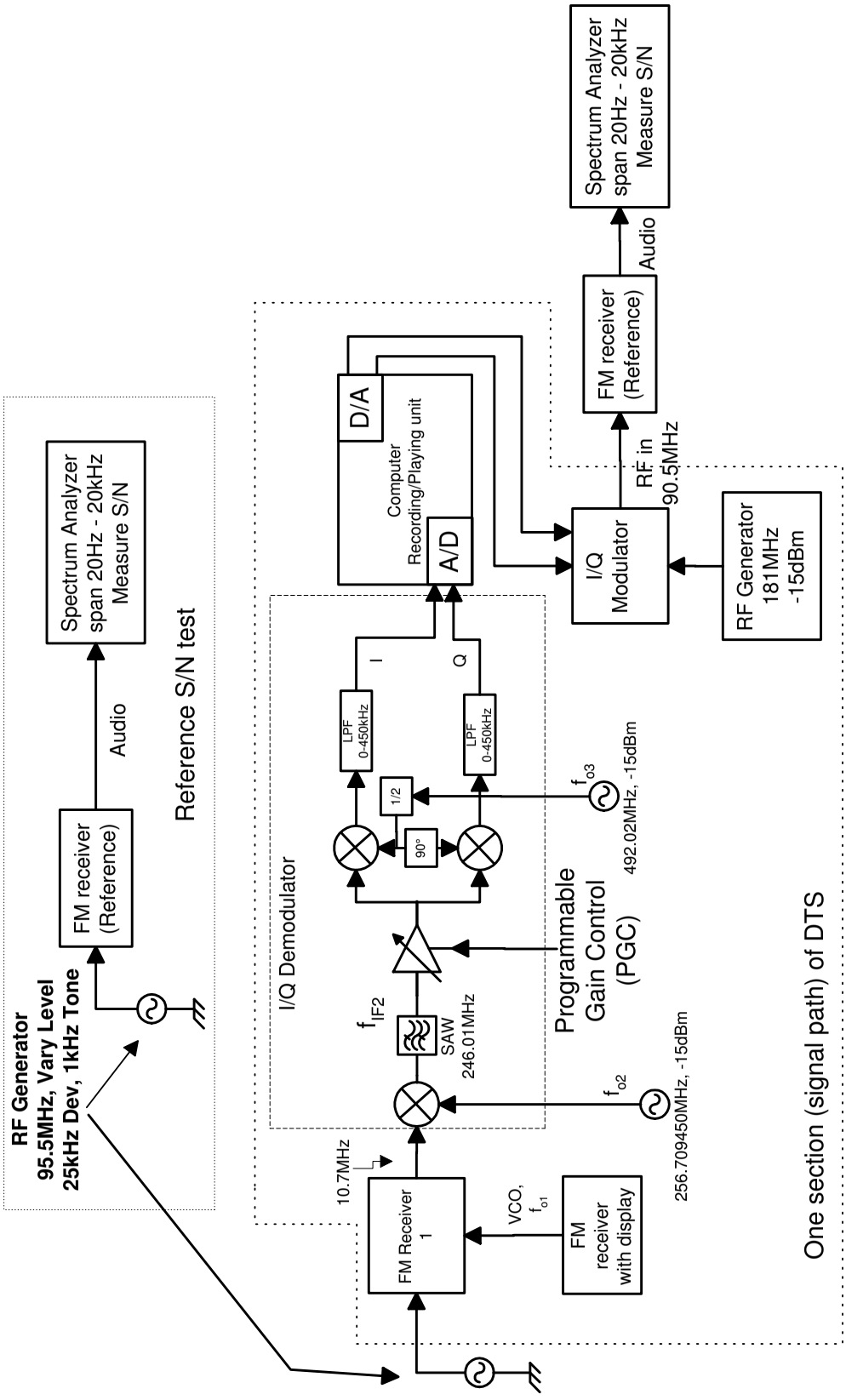

Figure D.1: Hardware setup to measure SNR

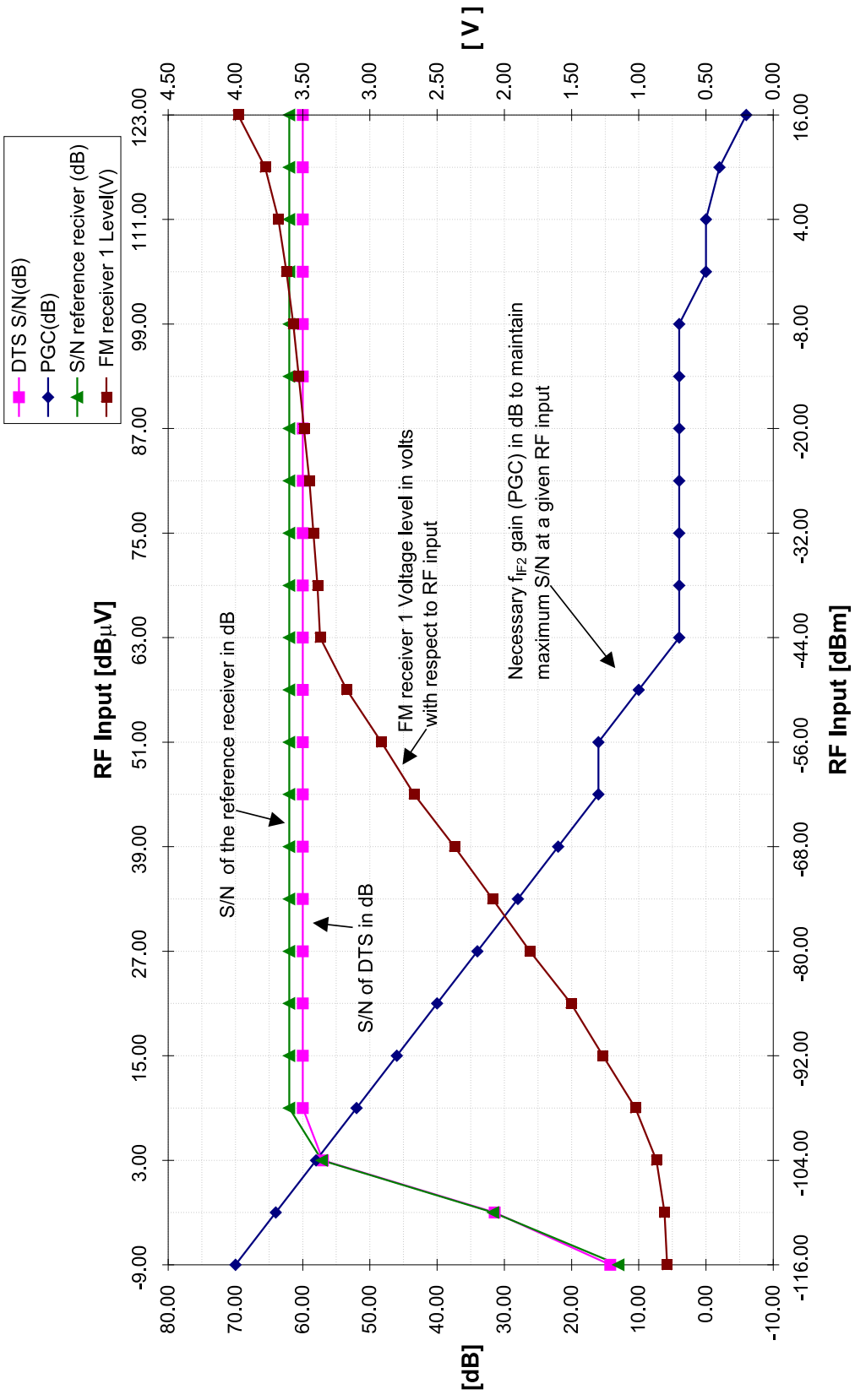

Figure D.2: SNR Ratio Measurement and Necessary f_{IF2} Gain Setting

Appendix E

FM Demodulator output of PAS

The resulting phase of PAS mathematical model (Equation 2.8) is repeated here for convenience

$$\phi_3 = \arctan\left(\frac{(\frac{A_1}{A_2})(1 + m\cos(\omega_r t))\sin(\theta_e)}{1 + (\frac{A_1}{A_2})(1 + m\cos(\omega_r t))\cos(\theta_e)}\right) \tag{E.1}$$

To show the exact derivation of Equation 2.10, let

$$y(t) = (\frac{A_1}{A_2})(1 + m\cos(\omega_r t))\cos(\theta_e) \tag{E.2}$$

and

$$z(t) = (\frac{A_1}{A_2})(1 + m\cos(\omega_r t))\sin(\theta_e) \tag{E.3}$$

Substitute Equation E.2 and E.3 into Equation E.1

$$\phi_3 = \arctan(\frac{z(t)}{1 + y(t)}) \tag{E.4}$$

The derivative of ϕ_3 is

$$\frac{\partial\phi_3}{\partial t} = \frac{1}{1 + \frac{z^2(t)}{(1+y(t))^2}} \cdot \frac{z'(t)\cdot(1 + y(t)) - z(t)\cdot(1 + y(t))'}{(1 + y(t))^2} \tag{E.5}$$

where $'$ denotes derivative with respect to t. Simplifying E.5 yields

$$\frac{\partial\phi_3}{\partial t} = \frac{z'(t)\cdot(1 + y(t)) - z(t)\cdot(1 + y(t))'}{z^2(t) + (1 + y(t))^2} \tag{E.6}$$

Taking the derivatives of Equation E.2 and E.3 yield

$$y'(t) = -(\frac{A_1}{A_2})\cdot m\cdot\omega_r\cdot\sin(\omega_r t)\cdot\cos(\theta_e) \tag{E.7}$$

and

$$z'(t) = -(\frac{A_1}{A_2})\cdot m\cdot\omega_r\cdot\sin(\omega_r t)\cdot\sin(\theta_e) \tag{E.8}$$

Now substitute Equation E.2, E.3, E.7, and E.8 into Equation E.6 then factor out the term $-(\frac{A_1}{A_2})\cdot m\cdot\omega_r\cdot\sin(\omega_r t)\cdot\sin(\theta_e)$

$$\frac{\partial \phi_3}{\partial t} = -(\tfrac{A_1}{A_2}) \cdot m \cdot \omega_r \cdot \sin(\omega_r t) \cdot \sin(\theta_e) \cdot \frac{(1+(\frac{A_1}{A_2})(1+m\cos(\omega_r t))\cos(\theta_e)) - (\frac{A_1}{A_2})(1+m\cos(\omega_r t))\cos(\theta_e)}{(\frac{A_1}{A_2})^2(1+m\cos(\omega_r t))^2\sin^2(\theta_e) + (1+(\frac{A_1}{A_2})(1+m\cos(\omega_r t))\cos(\theta_e))^2} \tag{E.9}$$

Equation E.9 simplifies to the following

$$\frac{\partial \phi_3}{\partial t} = -\frac{1}{R(t)} \cdot (\frac{A_1}{A_2}) \cdot m \cdot \omega_r \cdot \sin(\omega_r t) \cdot \sin(\theta_e) \tag{E.10}$$

This is the desired result that is shown in section 2.1.2 where

$$R(t) = 1 + 2 \cdot (\frac{A_1}{A_2})(1 + m\cos(\omega_r t))\cos(\theta_e) + (\frac{A_1}{A_2})^2(1 + m\cos(\omega_r t))^2 \tag{E.11}$$

Bibliography

[1] Harald Bochmann, and Kurt Wiedemann, *"FM - Receiver with Adaptive Antenna,"* Blaupunkt Werke GmbH, Germany 1988.

[2] Widrow B., Mantey P. E., Griffiths L. J., and Goode B. B., *"Adaptive Antenna Systems"*, Proceedings of IEEE,Vol. 55, pp.2143-2159, December 1967.

[3] Parsons J. D., Henze M., and Ratliff P. A., *"Single-Receiver Diversity Systems"*, IEEE Trans. on Communications, Vol. Com 21, No. 11, 1973.

[4] Shortall W. E., *"A Switched Diversity Receiving System for Mobile Radio"*, IEEE Trans. on Communications, Vol. Com 21 No. 11, 1973.

[5] Brennan, D. G., *"Linear Diversity Combining Techniques"*, Proceedings of the IRE,Vol. 47, pp.1075-1102, June 1959.

[6] Parsons, J. D., and Ratliff, P. A., *"Self-Phasing Aerial Array for FM Communication Links"*, Electronic Letters, Vol.7 No.13, pp.380-1, 1 July 1971.

[7] Lewin, L., *"Diversity Reception and Automatic Phase Correction"*, Proceedings of IEEE: Paper No. 3584 E, Vol.109 Part B, No.46, pp.295-304, July 1962.

[8] Parsons, J. D., Ratliff, P. A., and Shearman, E. D. R., *"Space Diversity Reception for VHF Mobile Radio"*, Electronic Letters, Vol.7, No.22, pp.655-6, 4 November 1971.

[9] Kock, B. and Kennedy, R., *"Diversity receiver for FM stereo utilizing a pilot tone multiple for phase alignment of received signals"*, Delphi Delco Electronics patent, 1996.

[10] Marrah, J., Kennedy, R., Shatara, R. *"Adaptive Reception System (ARS)"*, Delphi Delco Electronics internal paper, 1999.

[11] Delphi Delco Electronics Systems *"USN Detector Schematic"*, Delphi Delco Electronics internal documentation, 1996.

[12] Kahn, L., *"Ratio Squarer"*, Proceedings of the IRE(Correspondence),Vol. 42, pp. 1074, November 1954.

[13] Theodore S. Rappaport, *"Wireless Communications"*, Prentice-Hall, Inc., 1996, ISBN 0-13-375536-3.

[14] Dorf R. C., Bishop R. H., *"Modern Control System"*, Addison-Wesley Publishing, Seventh Edition 1995.

[15] Proakis J. G, Manolakis D.G., *"Digital Signal Processing"*, Third Edition, Printice-Hall, Inc. 1996.

[16] Umstattd R., *"Operating and Evaluating Quadrature Modulators for Personal Communication Systems"*, Application Note 899, National Semiconductor, Wireless Communication, October 1993.

[17] Philips Semiconductors, *"New In Car Entertainment (NICE)IC"*, Data sheet, July 12, 1999.

[18] Delphi Delco Electronics Systems, *"Generation 4 FM Receivers"*, RF building Block, Gen 4 design team.

[19] Johnson E. L., Karim M. A., *"Digital Design"*, PWS Publishers 1987.

[20] Ernst Manner , *"Stoerungen und Ihre Beseitigung durch Mehrantennendiversity beim Frequenzmodulierten Funkempfang im Auto"*, Doctor Thesis, University of the Bundeswehr Munich, 1985.

[21] Reiter, Leopold, *"Mobile Rundfunkempfangstechnik"*, Habilitationsschrift zur Erteilung der Lehrbefugnis in der Fakultaet fuer Elektrotechnik der Universitaet der Bundeswehr Muenchen, February 1995.

[22] Lee W. C. Y., *"Mobile Communication Engineering"*, McGraw-Hill, Second Edition 1998.

[23] Jakes, C. William, *"Microwave Mobile Communications"*, IEEE Press, Reissued Edition 1994 (original edition 1974).

[24] Kronberger R., Lindenmeier H., Reiter L., Hopf J., *"Far Field Antenna Measurement System For Advanced Car Antenna Development"*, Institute for High Frequency Techniques, University of the Bundeswehr Munich, ISA 2000.

[25] Lindenmeier H., Reiter L., Hopf J., Brose J., University of the Bundeswehr Munich, Germany; Kronberger R., Fuba Automotive, Bad Salzdetfurth *"Electronic Systems for Vehicles"*, VDI Berichte Nr. 1547, 2000.

[26] Lindenmeier H. K., Manner E. J., University of the Bundeswehr Munich, Germany; Sessink F., Philips Car Audio Development in Eindhoven/Holland, *"FM Antenna Diversity Experiments in Philips Car Radios in Theory and Practice"*, Society of Automotive Engineers, Inc. 1986 Nr. 850021. H.

[27] Lindenmeier, J. Hopf, L. Reiter, University of the Bundeswehr Munich; B. Leinwetter, Fuba Automotive, Bad Salzdetfurth *"Integrated Backlite Antenna System for AM/FM and TV Broadcast Reception and for Mobile Telephone"*, February 28 - March 3, 1994, Detroit, Michigan, USA, SAE Technical paper series: 940264.

[28] Lindenmeier, H. K., Hopf, J. F., Reiter, L. M., *"Diversity-Effectiveness and Programmable Device for Self-Testing of Operating Functions in Complex OEM-AM/FM/TV-Car-Antenna Systems"*,. International SAE Conference, February 1998, Detroit, Michigan, USA, SAE Technical paper series: 981147.

[29] Lindenmeier, H. K., Reiter, L.M., Kronberger, R.P., Hopf, J.F., *"Terrestrial Television-Reception in Fast Moving Cars by Means of Antenna Diversity Techniques"*, SAE Technical Paper series 1999-01-0259; ISSN 0148-7191, Society of Automotive Engineers, International Congress and Exposition, Detroit, Michigan, USA, March 1-4, 1999, 9 pages.

[30] Lindenmeier, H. K., *"Internal document to prove independence of* $\mathbf{n}$ *from the statistical distribution of* P_s*"*, University of the Bundeswehr Munich, Germany.

[31] Ziemer R. E., Tranter W. H. *"Principles of Communications Systems, Modulation, and Noise"*, John Wiley & Sons, Inc., Fourth Edition 1995.

[32] Papoulis, A., *"Probability, Random Variables, and Stochastic Processes "*, McGraw-Hill, Third Edition 1991.

[33] Haykin, S., *"An Introduction to Analog and Digital Communications"*, Wiley 1989.

[34] Carson, S. Ralph, *"Radio Concepts, Analog"*, John Wiley & Son, Inc. 1990.

[35] Bauer, G. Klaus, C., *"Erstellung eines Simulationsprogramms fuer Mehrwegeempfangsgestoerte FM-signale"*, Diplomarbeit, Universitaet der Bundeswehr Muenchen April 2002.

[36] Kafadar, Karen, *"Gaussian White-Noise Generation for Digital Signal Synthesis"*, IEEE Transactions on Instrumentation and Measurement, Vol. IM-35 No.4, 1986.